PRECISION MEASUREMENT OF X-RAY SPECTRA WITH APPLICATION TO THE L X-RAY SPECTRA OF URANIUM, NEPTUNIUM, PLUTONIUM, AND AMERICIUM

Thesis by

John Jay Merrill

In Partial Fulfillment of the Requirements

For the Degree of

Doctor of Philosophy

California Institute of Technology

Pasadena, California

1960

ACKNOWLEDGMENTS

The author has profited in many ways from his association with Professor J. W. M. DuMond, who suggested this problem and provided much of the motivation and inspiration needed to bring it to a successful conclusion.

Several others have rendered valuable assistance. Among these are included Dr. J. C. Wallman, who supervised the preparation of the small samples of Np, Pu and Am at the University of California Radiation Laboratory. Dr. George L. Rogosa, of the Atomic Energy Commission, was instrumental in obtaining the loan of these elements. Machlett Laboratories, Inc. produced the U target X-ray tubes under the direction of Mr. T. H. Rogers. Finally, Mr. F. M. Trapnell, Mr. John C. Everitt, and Mr. Warren Teitelman assisted in the taking of data.

The author was supported, during this investigation, by the generous terms of the Howard Hughes Fellowship, and the experimental work was supported by the U. S. Atomic Energy Commission.

This work is a continuation of the work initiated by Dr. Robert L. Shacklett, and the extent to which the present work is dependent upon his results will be obvious from the frequent reference to his Ph.D. thesis. In addition, Dr. Shacklett has made several suggestions which have proved valuable in the present research.

ABSTRACT

Techniques for the precision measurement of X-ray lines using the two-crystal spectrometer are discussed, and then applied to measurement of the L X-ray spectra of the trans-uranic elements uranium, neptunium, plutonium and americium. In all, 52 emission lines and 4 L_{III} absorption edges were measured, all of them with higher precision than has heretofore been obtained and many of them for the first time. Using these data, the binding energies of the electrons for these atoms were computed. The L_{II}-L_{III} level splitting was computed and compared with theory and it was found that current theory is not sufficient to account quantitatively for the observed data. Certain features of the emission line widths are discussed and given qualitative explanations in terms of the Coster-Kronig transition L_{II}-$L_{III}M_V$ and hyperfine structure. The observed hyperfine structure is due to the large magnetic moment of Np^{237} which leads to increased widths of certain of the Np lines. It is believed that this is the first experimental observation of hyperfine structure in X-ray spectra.

TABLE OF CONTENTS

LIST OF TABLES

LIST OF FIGURES

PART I

INTRODUCTION

X-Ray spectra have for some time been one of our important sources of information regarding atomic processes and energy levels, and considerable effort has been directed toward the precision measurement of the emission and absorption spectra of the elements. The purpose of the present investigation was to improve, if possible, the techniques used in these measurements as applied to the two-crystal spectrometer, to develop methods whereby this instrument could be used when only small amounts of the element being studied could be obtained and, finally, to apply these techniques in the investigation of spectra which have not previously been measured with high precision.

This research was undertaken as a continuation of the work of Shacklett and DuMond (1,2), who were mainly interested in the L_{II}-L_{III} energy level difference of heavy elements and the effects of nuclear size and quantum electrodynamics on this splitting. These problems are reviewed in Parts V-B and V-C of this report, together with some revisions to take into account the new data of the present investigation as well as recent work of other investigations.

In all, some 52 emission lines and 4 absorption edges were measured in this research, all of them with higher precision than has heretofore been attained and many of them for the first time. Many of these lines were extremely weak, and

only by taking every precaution to ensure stability of the apparatus were the measurements possible at all.

The transuranic elements were chosen for this work mainly because of the availability of these elements in suitable form for the first time.

The availability of a commercial, sealed-off U target X-ray tube permitted the study of the U spectrum using the high intensity of the characteristic spectrum. It was impossible to obtain other transuranic elements in suitable form for the target of such a tube, and so the other spectra were investigated using fluorescent radiation excited by a W target tube. The 5g source of metallic Pu used by Shacklett made possible the first precision measurement of this spectrum using the techniques developed in the work of Shacklett and DuMond. When it became known that samples of Np and Am could be made available in milligram amounts, the techniques for using these samples were developed, and the fluorescent emission spectra of these elements, as well as the absorption spectra of all four elements, were studied using 50 mg samples of the elements in oxide form.

The transuranic region is particularly interesting, since the atomic electrons of these elements are expected to be significantly affected by the size of the nucleus. Furthermore, the strong fields surrounding these nuclei are expected to introduce significant changes due to effects predicted by quantum electrodynamics. It is shown in Part V that theory is not sufficiently well developed to explain all of the

observed deviations, and so the present work must serve not to verify theoretical predictions, but to point out areas wherein the theory is incomplete and might be improved.

The data of this investigation will also be of value to nuclear spectroscopists, who have previously been forced to rely upon extrapolated values for the binding energies of the electrons in these atoms. These values are important in correcting the results of conversion electron measurements, and are computed in this report using the experimental data, together with a few extrapolations of small differences as described in Part V-A.

Part II of this report is a brief resume of the theory of the two-crystal spectrometer, with special emphasis on the properties of this instrument which lead to its high accuracy and resolving power, together with a discussion of the corrections needed in order to compensate for imperfections in the instrument.

In Part III the experimental apparatus is described, again with special attention to the features and adjustments which ensure the full use of the capabilities of the instrument.

Part IV is a description of the experimental techniques used in the actual measurements, together with a presentation of the experimental results.

Finally, Part V is a discussion of the results with a comparison of them with the applicable theory.

PART II

RESUME OF THE THEORY OF THE TWO-CRYSTAL SPECTROMETER

The principal instrument used in this investigation was the precision two-crystal, or double, spectrometer designed and built by DuMond and Marlow (3). The most important components of this instrument are two calcite crystals which rotate about axes passing through the crystal face parallel to each other and to the reflecting (cleavage) planes of the crystals. The intensity of the X-ray beam after being successively reflected (usually in the same order) from each of the two crystals is measured as a function of the dihedral angle between the crystal faces. Obviously the intensity of the primary source of X-rays must be either monitored or maintained constant. This arrangement can be shown to give an extremely high resolving power, the spectrometer transmission window being the same order of magnitude in angular width as the crystal diffraction pattern itself, practically independent of any auxiliary slits used to define the beam to be studied. Thus, the two-crystal spectrometer closely approximates the highest resolving power possible in any spectrometer using crystals as the only dispersive element.

The two-crystal spectrometer has been used extensively to study the reflecting properties of crystals since about 1917, and has become a most important tool in the study of X-ray spectra. Its resolving power is high enough to permit a detailed study of the shape of spectral lines, and all of

our data concerning the width of X-ray lines have been obtained with this instrument. The high resolving power is obtained at the sacrifice of luminosity, and for this reason the instrument has not been used extensively to investigate all lines of complex spectra. Most investigators prefer photographic, single crystal instruments in which the primary source intensity need not be monitored and the wavelengths of numerous lines can be simultaneously measured more easily though perhaps less accurately.

The theory of X-ray reflection by crystals has been treated by numerous authors, and a few of them have extended the theory to successive reflections by two crystals. Most of this work is consolidated and presented in the textbook of Compton and Allison (4). These authors have, however, given somewhat more emphasis to the use of the instrument in the study of the reflecting properties of crystals than to the problem of precision wavelength measurements. Shacklett (2) has considered this latter problem in considerable detail, and his thesis is probably the best reference available for this work. Since the analytical details are contained in the literature, only a brief resume will be included here in order to rationalize the various corrections which must be applied to the observed data before it can be made physically significant.

Since the single crystal diffraction pattern determines the window of the instrument, its theory will be briefly reviewed. This will be followed by a simplified discussion

of the two-crystal instrument, which will finally be expanded to include the perturbations and imperfections of the actual spectrometer as used in the laboratory.

A. X-Ray Reflection from a Single Crystal

If a plane, polarized, monochromatic beam of radiation is incident upon the surface of a crystal whose atomic reflecting planes are parallel to the crystal surface, the ratio of reflected to incident intensity, as derived by Prins (5), is given by*

$$I_\sigma(\ell) = \left| \frac{(D+iB)\,\delta}{\ell - i\beta/\delta \pm \left\{(\ell - i\beta/\delta)^2 - [(D+iB)/\delta]^2\right\}^{1/2}} \right|^2 \qquad (2.1)$$

if the electric vector of the incident radiation is parallel to the reflecting planes. The quantities appearing in this expression are defined as follows: the variable ℓ is proportional to the difference between the angle of reflection ψ (as measured from the plane of the crystal) and the corrected Bragg angle Θ and is given by

$$\ell = (\psi - \Theta)\,\frac{\sin 2\Theta}{2} \qquad (2.2)$$

where $\delta = 1-\mu$ is the unit difference of the refractive index. "The corrected Bragg angle," Θ, is the Bragg angle which has

---

*The notation is that of Compton and Allison.

been corrected for index of refraction effects, namely

$$\theta = \sin^{-1}\left\{\frac{n}{2d}\left[1 - \frac{4d^2\delta}{n^2\lambda^2}\right]^{-1}\right\} \quad * \qquad (2.3)$$

where d = actual grating space of the crystal

n = order of reflection

λ = wavelength of incident radiation.

Coming back to equation 2.1, the quantity β is given by

$$\beta = (\lambda/4\pi)\mu_\ell \qquad (2.4)$$

where μ_ℓ is the linear absorption coefficient for the crystal, and finally

$$D+iB = (\delta+i\beta)F/Z \qquad (2.5)$$

where Z represents the number of electrons in the unit cell of the crystal and F is the crystal structure factor, defined as the ratio of the amplitude scattered by the unit cell in the direction θ to the amplitude scattered by a single, free electron in the same direction. Thus F takes into consideration the phase differences of the waves scattered from the various electrons of the unit cell, and is a function of and θ. F/Z is always less than or equal to unity, and for the cleavage planes of calcite at λ= 0.708 Angstrom units,

---

*In this equation δ can be shown to be proportional to λ^2, so that the index of refraction correction is independent of λ.

$F/Z = 0.516$. $Z = 100$ for these planes.

If the absorption is negligible ($\beta \approx 0$), equation 2.1 reduces to the form first derived by Darwin (6), namely

$$I^D(\ell) = \left| \frac{F/Z}{\ell \pm \sqrt{\ell^2 - F^2/Z^2}} \right|^2 \qquad (2.6)$$

where the sign of the radical is taken to be the same as that of ℓ. This expression is much easier to work with than equation 2.1, and is in many cases sufficiently adequate to demonstrate the important features of the diffraction pattern. $I^D(\ell)$ is shown in figure 1 for calcite at $\lambda = 0.708$ Angstroms. A scale of $\psi - \theta_o$ expressed in seconds of arc is placed immediately below the ℓ axis, where θ_o is the uncorrected Bragg angle. The effect of the index of refraction term in equation 2.3 can be clearly seen, in the separation between the two points $\psi = \theta_o$ and $\psi = \theta$.

An important feature of this pattern is the small angular region of width $\Delta\ell = 2F/Z$ over which the crystal reflects all of the incident radiation. Another feature is the steepness of the sides, the width at half-maximum being only about 6 percent greater than the region of total reflection. The area under the wings, in fact, can be shown to be 1/4 of the total area. It is also interesting to note that because of the strong constructive interference in the direction of the reflected beam at the Bragg angle, the radiation does not penetrate as far into the crystal as at other angles. In

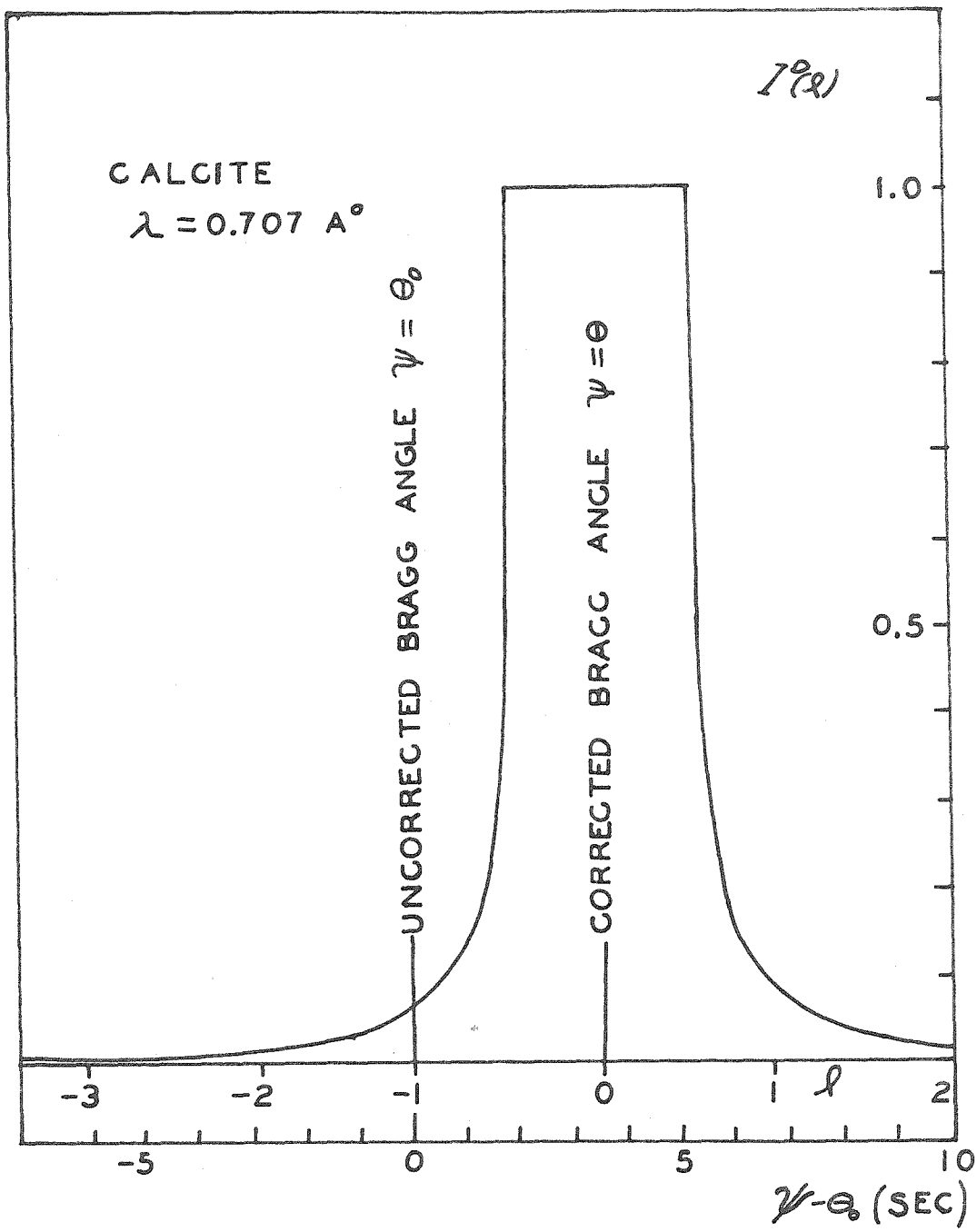

Figure 1. Darwin diffraction pattern as given by equation 2.6.

fact, it can be shown that the intensity of the incident radiation decays with an "extinction" coefficient which may be orders of magnitude larger than the usual linear absorption coefficient. Furthermore, the extinction coefficient can be shown to be directly proportional to F.

Since the number of crystal planes contributing significantly to the reflection is roughly inversely proportional to the extinction coefficient, and hence inversely proportional to F, the width of the totally reflecting portion of the diffraction pattern (equal to 2F/Z) is roughly inversely proportional to the number of crystal planes contributing to the reflection. This is exactly analogous to the dependence of the resolving power of an optical grating on the number of participating lines.

The effect of the absorption terms in equation 2.1 is shown in figure 2, taken from reference 7. The most important change is that the diffraction pattern is now asymmetric, a fact which will be shown to introduce a small error into the measurement of any spectral line. The longest wavelength studied in the present investigation was about one angstrom, so that the absorption can almost, but not quite, be ignored. Another interesting feature of figure 2 is that the maximum reflection is no longer 100 percent, as would be expected merely from the fact that part of the incident beam is lost in the absorption processes.

All of the above is based on the assumption that the incident beam is polarized with its electric vector parallel

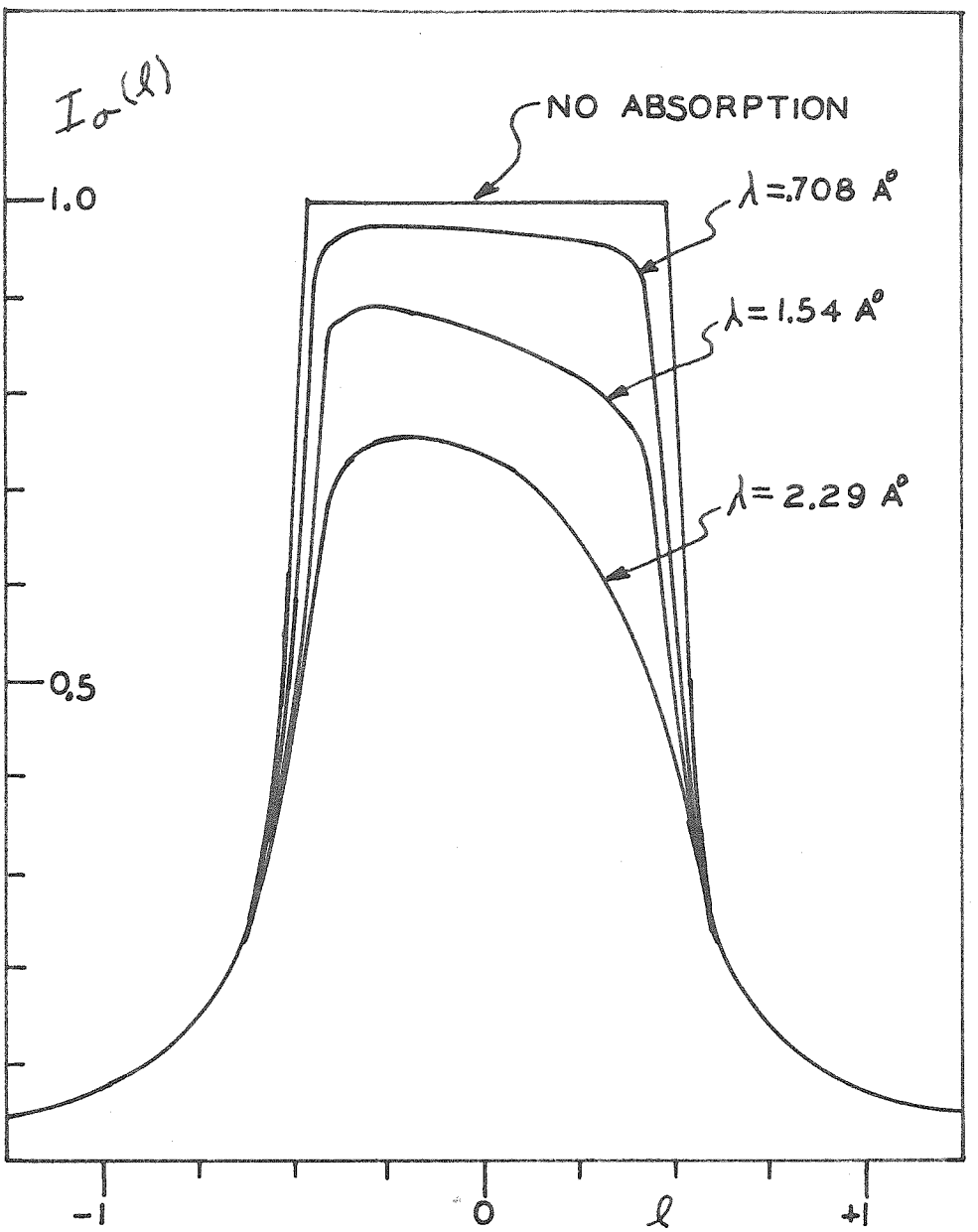

Figure 2. Diffraction pattern of calcite for various wavelengths as given by equation 2.1 (taken from reference 7).

to the crystal reflecting planes (σ - polarization). Another possibility is that the electric vector lies in the "plane of incidence," defined by the incoming ray and the normal to the reflecting planes. This is called π-polarization. It is evident that only the component of the incident electric vector perpendicular to the reflected beam will produce radiation in that direction. Therefore F/Z must be replaced by $(F/Z)\cos 2\theta_o$ wherever it appears in equations 2.1 and 2.6. The effect of introducing this term is shown in figure 3, taken from reference 8.

Completely unpolarized radiation can be resolved into these two components, each with an intensity equal to half the total intensity of the incident beam. Therefore, the diffraction pattern for unpolarized radiation would be given by

$$I(\ell) = \frac{1}{2} I_{\sigma}(\ell) + \frac{1}{2} I_{\pi}(\ell) \ . \qquad (2.7)$$

This is also shown in figure 3.

B. The Two-Crystal Spectrometer

As previously stated, the two-crystal spectrometer consists of two crystals which rotate about axes which are parallel to each other and to the reflecting planes of the crystals. In order to reach the detector,* a beam must be

---

*This treatment is restricted to first order reflection, since multiple orders were not used in this investigation.

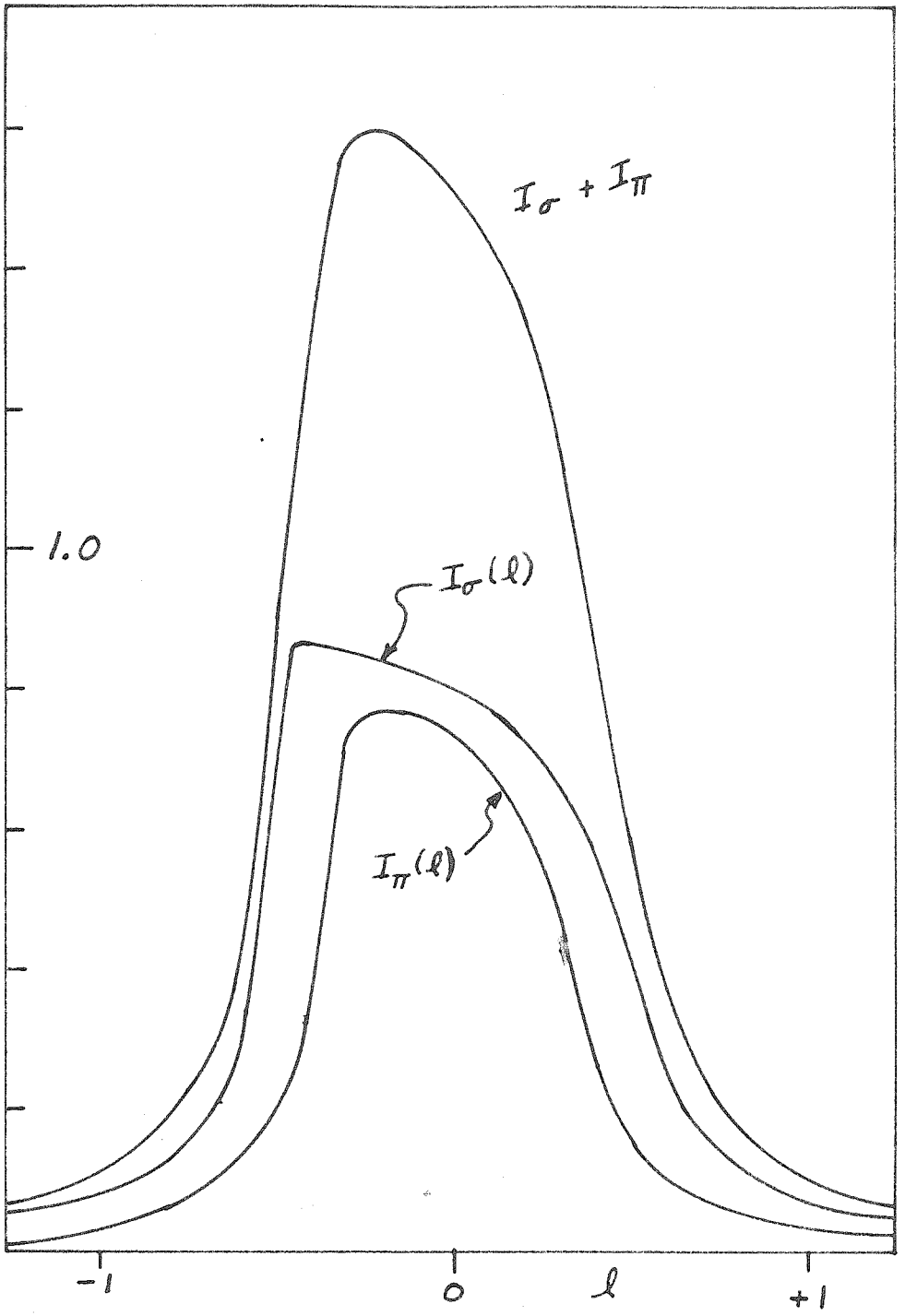

Figure 3. Effect of polarization on the diffraction pattern of calcite at λ = 2.3 A° (taken from reference 8).

reflected by each crystal in turn, and thus must be incident upon each crystal at or near the Bragg angle. Actually, the important consideration is that it must leave the first crystal (usually referred to as crystal A) and arrive at the second (crystal B) at this angle. Thus, the only factor which determines whether a beam will be able to pass through the instrument is the dihedral angle between the two sets of crystal planes.

Restricting attention to first order reflection, there are evidently two relative positions of the crystals which satisfy this condition, namely when the crystal planes are parallel (this is called the parallel position), and when the dihedral angle is $180°-2\theta$ (the antiparallel position). These positions are illustrated in figure 4. DuMond (9) has invented a graphical method of illustrating the operation of this instrument in these two positions. The ratio of reflected to incident intensity for a single crystal is regarded as a function of incident angle and wavelength. Rather than resorting to a three-dimensional graph, this may be illustrated by a two-dimensional graph whose "transparency" is given by the single crystal diffraction pattern. In other words, the graph is practically transparent near the locus $\lambda = 2d\sin\theta$ and nearly opaque elsewhere. If we now imagine a light, whose intensity is proportional to the intensity of the radiation incident upon the crystal face (again as a function of wavelength and angle), placed behind this graph, then the total transmitted light intensity is

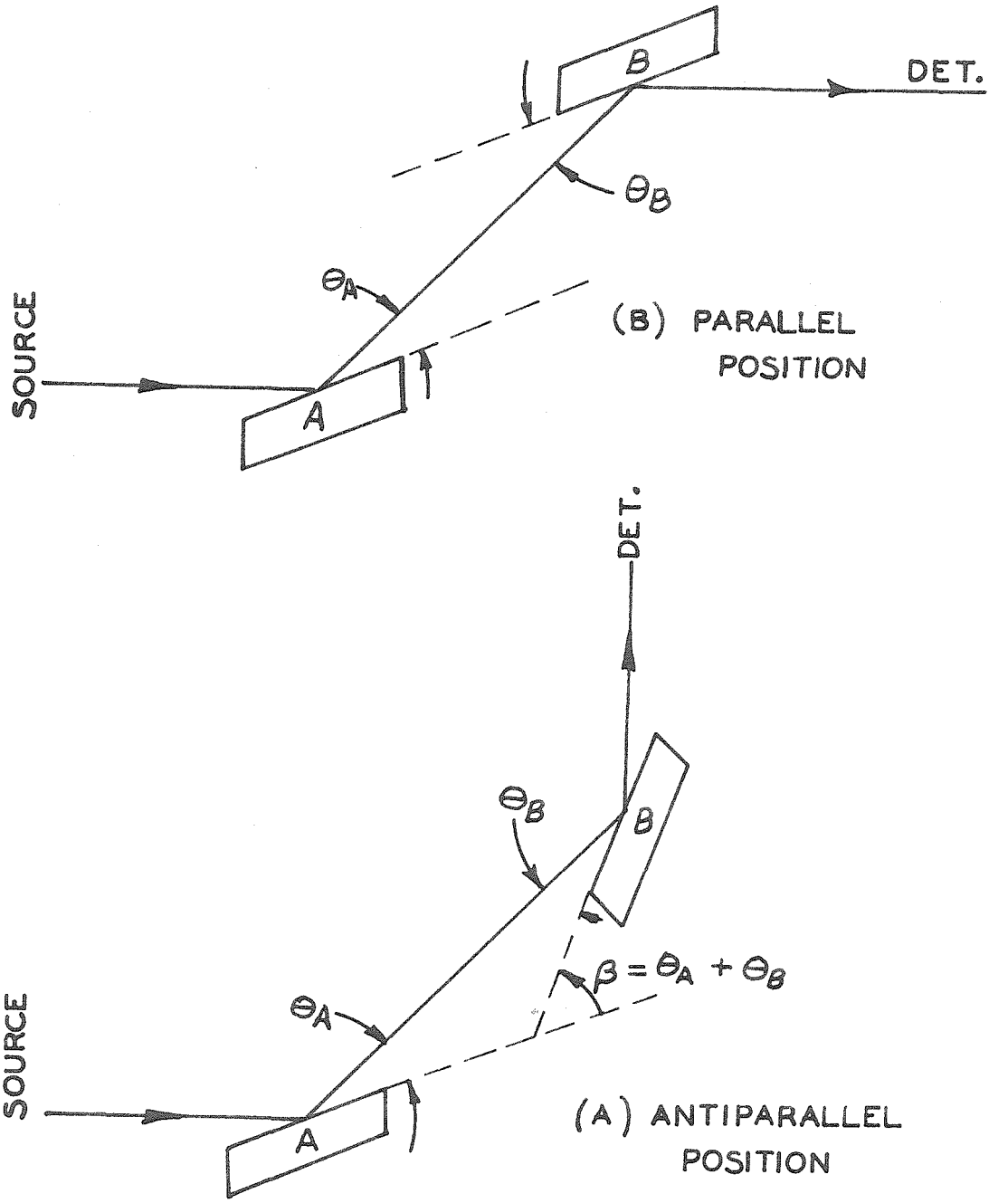

Figure 4. Basic arrangement of the two-crystal spectrometer showing crystal B in the parallel and in the antiparallel positions.

proportional to the total X-ray intensity reflected by the crystal. Such a diagram is illustrated in figure 5.

A second crystal may be included in this demonstration by placing its transparency diagram over the first so that their angular scales overlap indicating the angle at which radiation reflected from crystal A is incident upon crystal B. Now the light can only pass through areas where both diagrams are transparent. For the antiparallel position, it can be seen from figure 4a that $\Theta_A + \Theta_B$ is constant for a fixed dihedral angle. Thus, the two transparency diagrams must be superimposed with their angular scales oppositely directed, as shown in figure 6a. The "window" of the two-crystal spectrometer is the small region where the two transparency regions overlap. As the dihedral angle, β, is changed (by sliding one transparency diagram relative to the other) this window moves up and down the wavelength scale thus exploring the spectral distribution of the heterogeneous incident radiation. The appropriate shape of the window is the response that would be obtained as a function of β for monochromatic incident radiation. From figure 6a it can be seen that this will be slightly asymmetrical, due to the asymmetry in the Prins diffraction pattern. The window has been analyzed by Allison (10) by performing numerically the appropriate integrations, and his result for $\lambda = 1.54$ Å is shown in figure 7. The asymmetry of this curve is not pronounced, even at this wavelength, as can be seen by com-

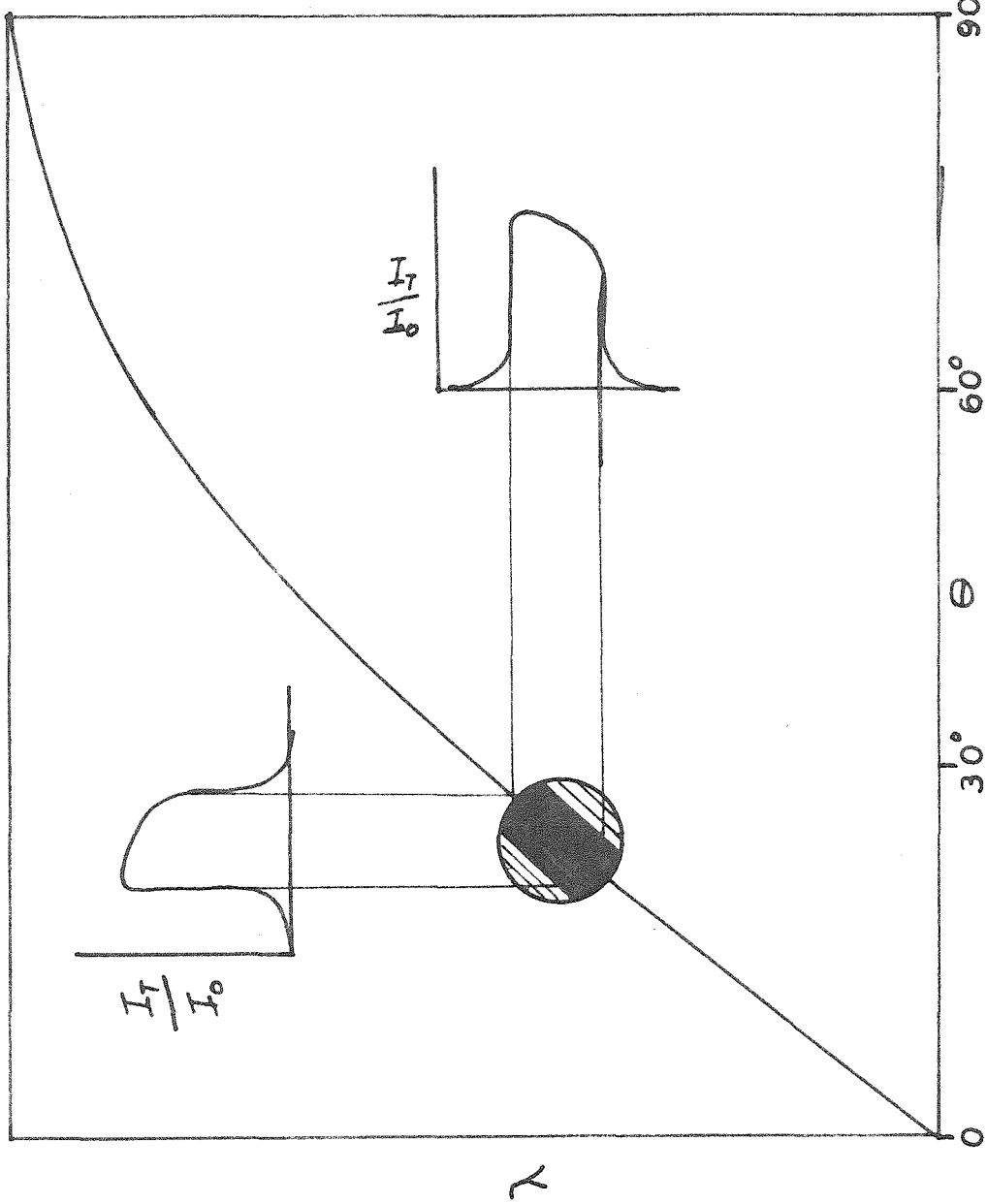

Figure 5. Transparency diagram for a single crystal. The diffraction pattern, including absorption, is shown both in terms of incident Bragg angle and incident wavelength so that the direction of the asymmetry may be clearly seen.

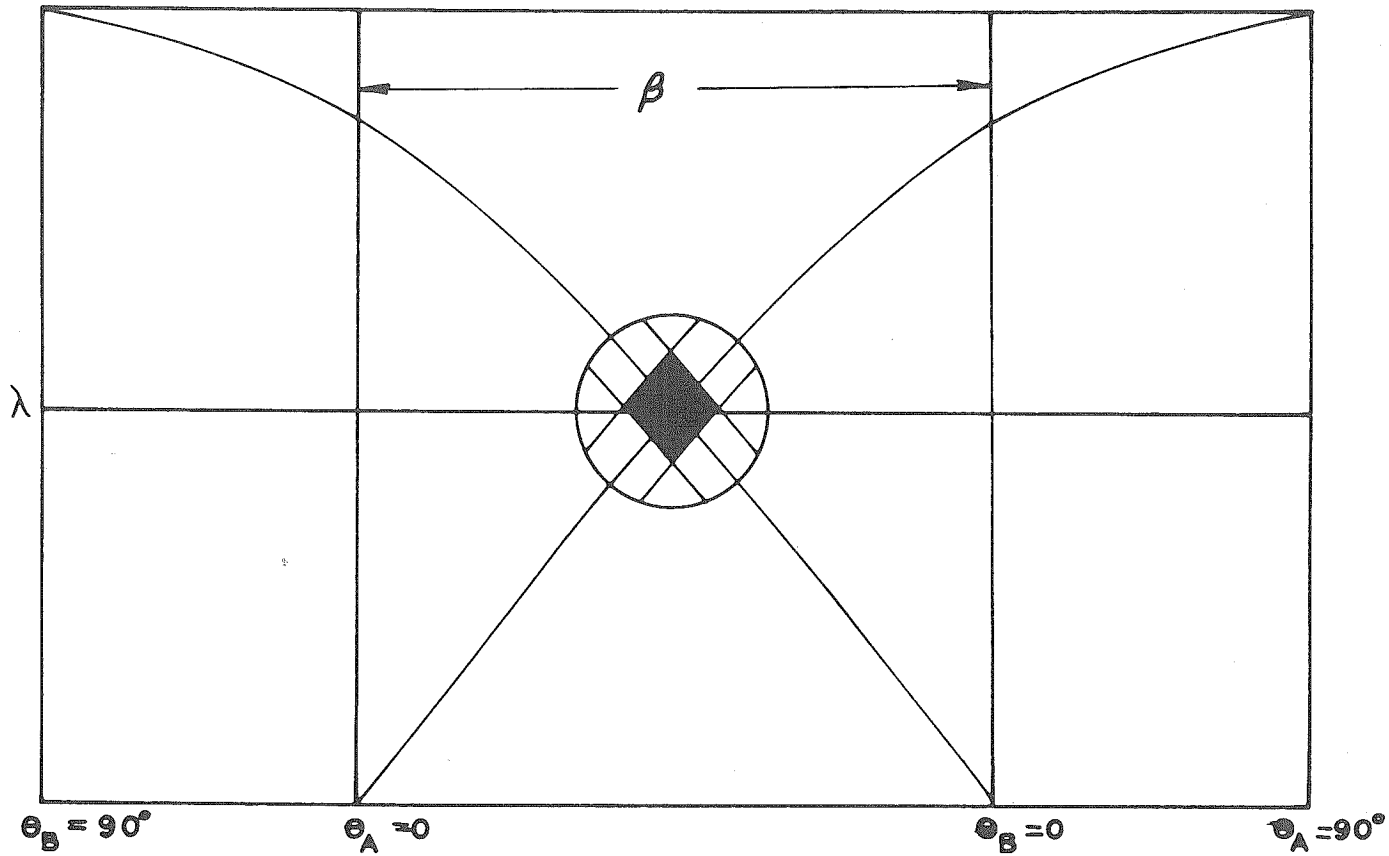

Figure 6a. Transparency diagrams in position to illustrate the antiparallel position. Only in the parallelogram-shaped region will radiation be transmitted through both diagrams. As the dihedral angle, β, is changed this window will move up or down the wavelength scale, analyzing the input radiation represented here by a monochromatic line of wavelength . By comparing this diagram with figure 5 it can be seen that the low wavelength side of the window is slightly more transparent than the high wavelength side, due to the asymmetry of the diffraction pattern. Thus, the spectrometer response for monochromatic radiation will be slightly asymmetric, being shifted slightly towards smaller values of β.

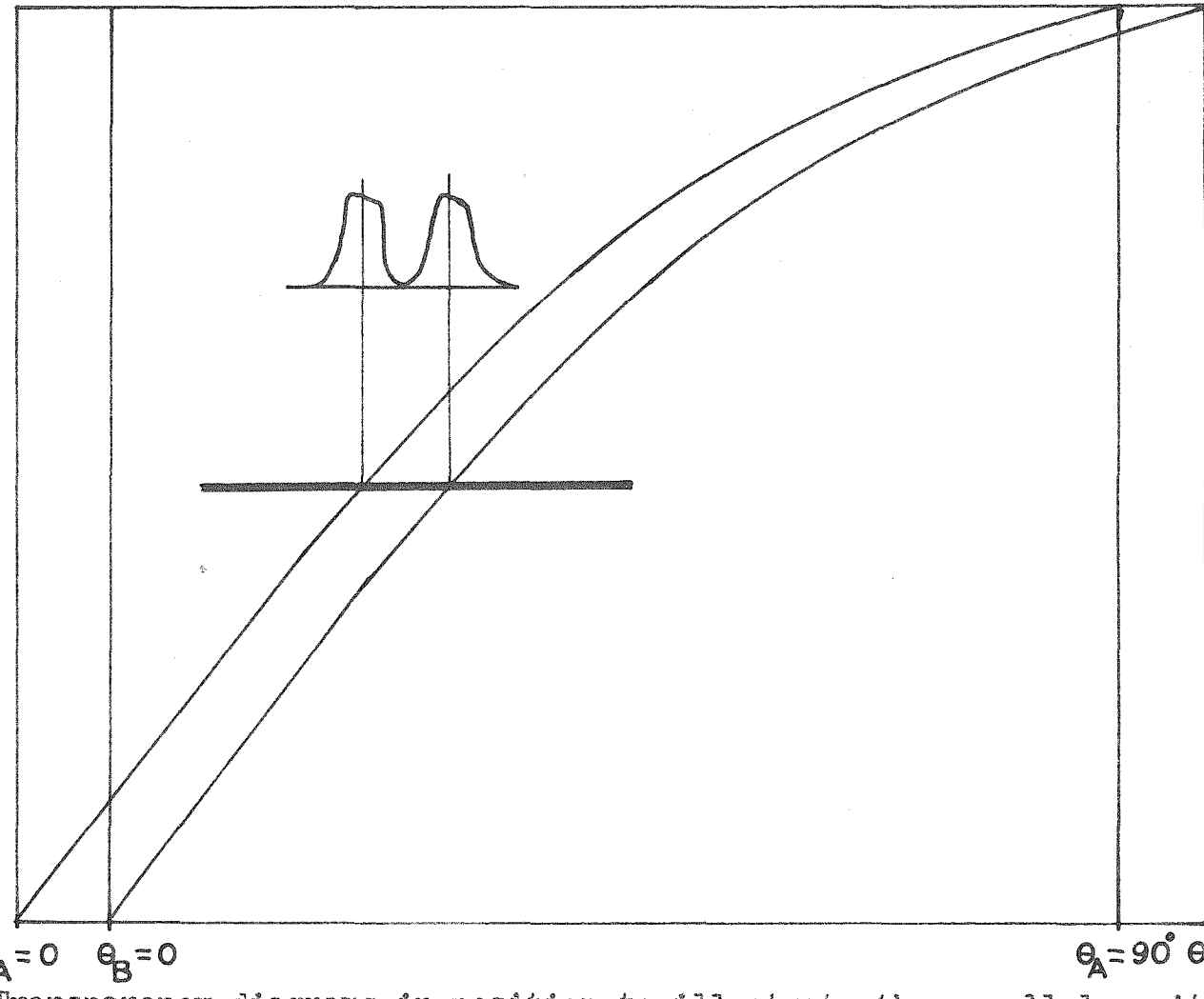

Figure 6b. Transparency diagrams in position to illustrate the parallel position. Note that the relative position of the crystals is given by $\theta_A - \theta_B$ and that the illustration is symmetrical around $\theta_A - \theta_B = 0$. Thus the parallel rocking curve is symmetrical. Furthermore, the shape of the response is the fold into itself of the diffraction pattern and not by the shape of the line comprising the incident radiation.

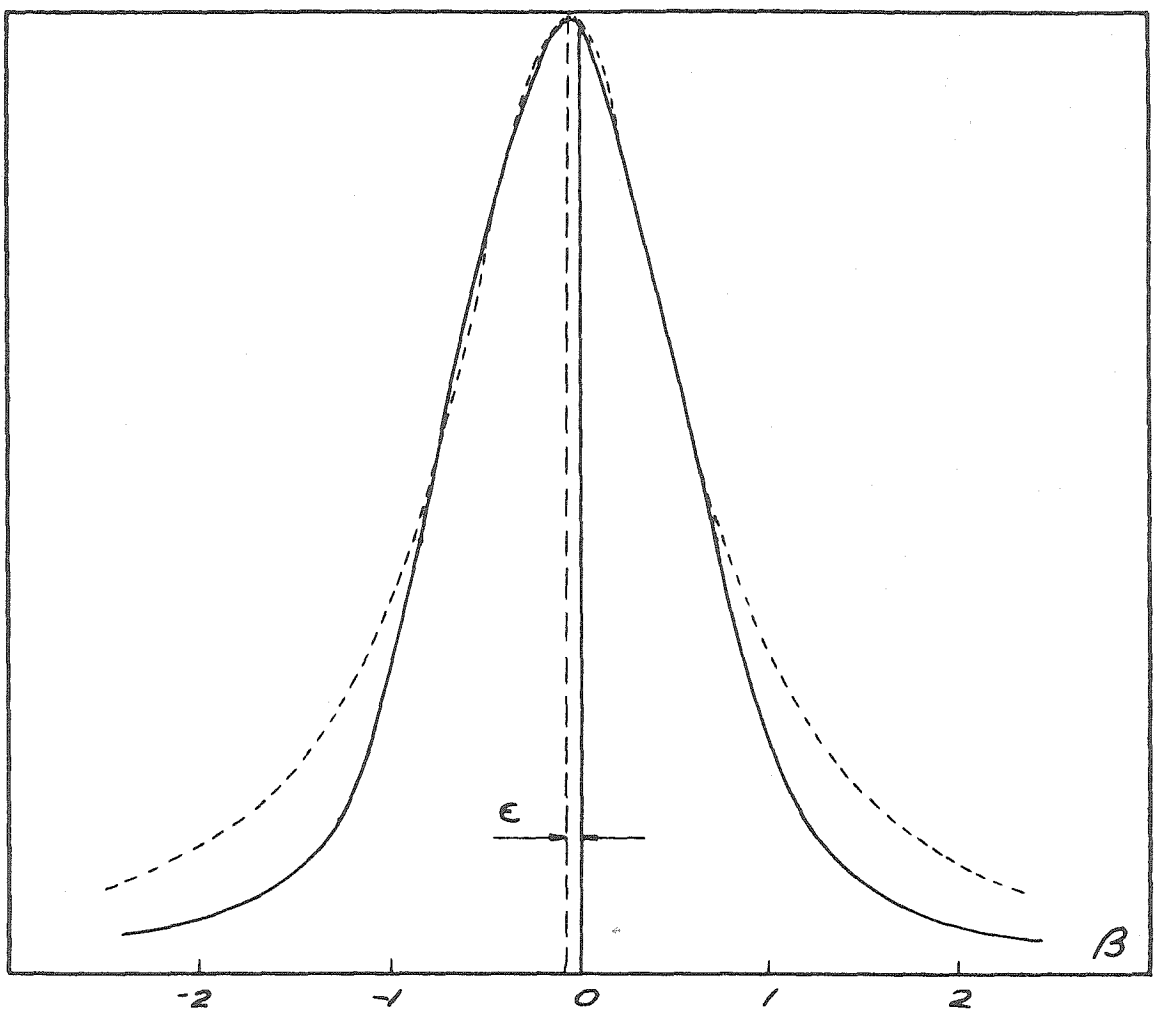

Figure 7. Antiparallel "monochromatic" curve as obtained by Allison for 1.537 Å. The dashed curve is a witch having the same half-width. The axis of symmetry of the witch is shown at $\beta = -\varepsilon$.

paring it with the symmetrical witch with the same width at half maximum* whose center is displaced by an angular displacement ϵ towards negative β from the point satisfying the Bragg law. Shacklett (2) has shown that ϵ is given approximately by

$$\epsilon = 0.2\ \lambda^2 \text{ seconds } (\lambda \text{ in } A^\circ) . \qquad (2.8)$$

This will be seen to introduce a correction into the precision measurement of wavelength using this instrument. The width of this window will be discussed shortly.

If the incident radiation is that of a symmetrical spectral line, which several investigators (11) have shown in particular cases to be well approximated out to a few half-widths by the shape of a witch, the output of the spectrometer as a function of dihedral angle may be computed by folding the monochromatic profile into the curve of incident radiation vs dihedral angle. This may be done conveniently by the method outlined in Appendix A, wherein the monochromatic profile is approximated by a witch, chosen to have the same asymptotic behavior at large values of β, plus a correction function which has significant values only near $\beta = 0$. The folding process may then be accomplished in two parts, the major contribution coming from the fold of the

---

*The witch, or Cauchy distribution, sometimes also called a "Lorentzian," has the formula

$$y = (1+x^2/a^2)^{-1} .$$

two witches which may be done analytically, and the second coming from the fold of the correction function into the spectral line. This latter fold must be done by numerical integration which, fortunately, need extend over a small region about the center of the monochromatic profile. Such calculations show that the spectrometer output, under these conditions and for spectral lines whose widths at half maximum height are at least three times as large as the corresponding width of the monochromatic window, may be accurately approximated out to about two half-widths by a witch whose center is displaced toward smaller Bragg angles by an approximate amount ε from the value computed from the Bragg law for the central wavelength of the spectral line. The width at half maximum height of this output curve is represented by figure 8, where the difference, ΔW_o, between the widths of the output curve and the spectral line, normalized to the width, W_m, at half maximum height of the monochromatic curve, is plotted as a function of the width, W_o, of the output curve, again normalized to W_m.

In analyzing the parallel position, using the transparency diagrams, it is apparent from figure 4a that for fixed crystals the difference between Θ_A and Θ_B must be constant. Therefore, the two transparency diagrams must be superimposed with their angular scales going the same way, as in figure 6b.

It is apparent from the diagram that the profile (as a function of β) of the spectrometer output in this position

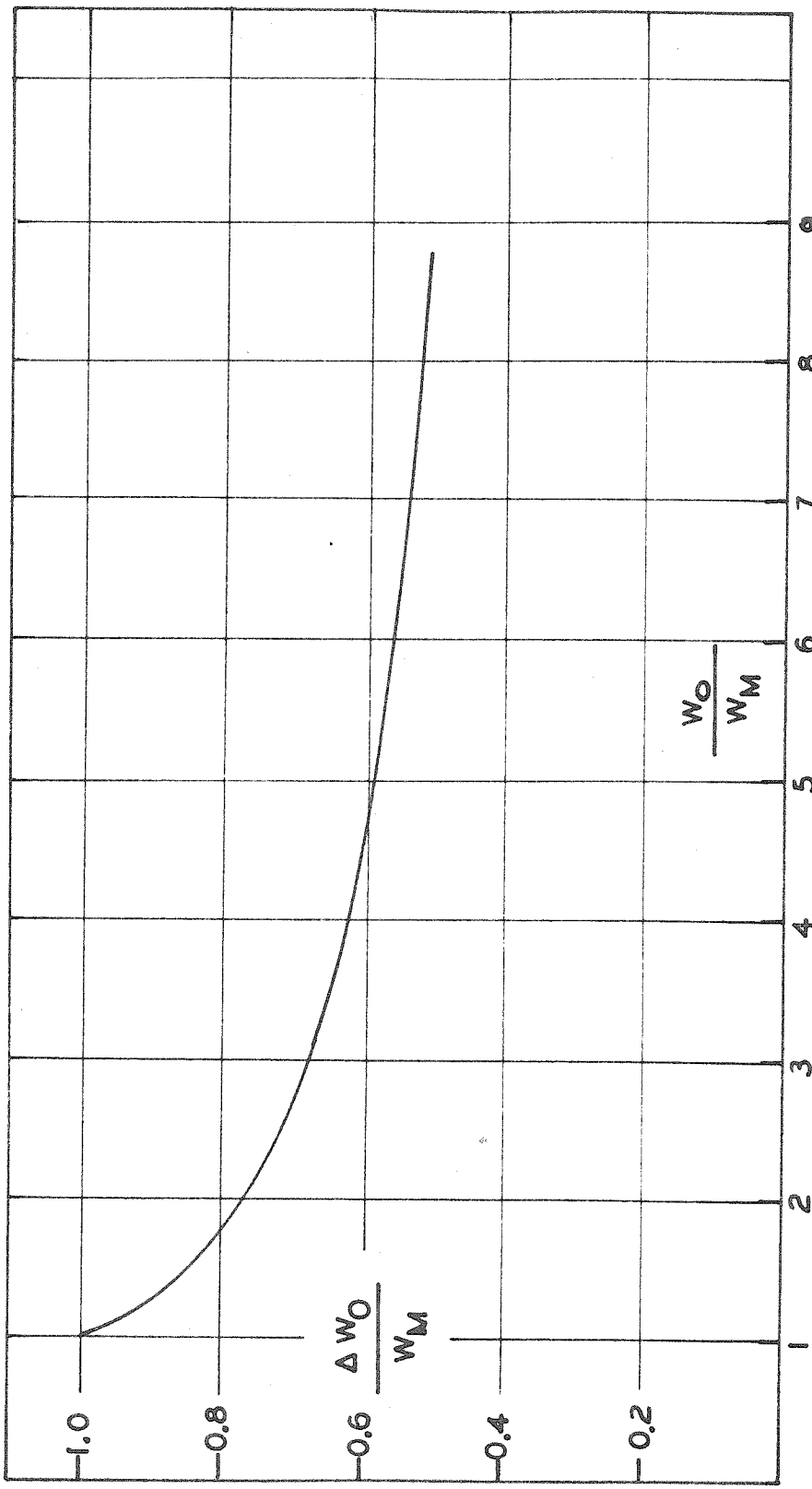

Figure 8. The difference, ΔW_o between the widths at half maximum height of the spectrometer output curve and incident spectral line vs the width, W_o, of the output curve. The normalizing factor, W_m, is the width at half maximum height of the antiparallel monochromatic output curve.

is the fold into itself of the crystal diffraction pattern and is not affected by the shape of the line comprising the incident radiation. Indeed, it can be shown that, for the symmetrical diffraction pattern of Darwin in the case of negligible absorption, the profile of this "parallel rocking curve" is identical to that of the two-crystal monochromatic response curve in the anti-parallel position. The parallel response, furthermore is symmetrical, independent of the absorption, as can be seen by considering the transparency diagram.

The width of the parallel rocking curve for perfect calcite crystals has been calculated by Allison for several wavelengths, with the result shown in figure 10, Part III. On the same graph are shown some of the values actually measured in this experiment and the work of Shacklett which preceded it. It can be seen that the experimental values are somewhat higher than the theoretical. This is probably fortunate, since it improves the luminosity of the instrument without reducing the resolving power below a usable value.

In actual practice, the dihedral angle is changed, and thus the response curves examined, by rotating crystal B with crystal A held fixed. Typical response curves, showing the various features described above, are shown in figures 13, 14 and 15, Part IV. The angular rotation between the centers of symmetry of the two curves is thus $180°+2\theta$, where θ is

the Bragg angle of the central wavelength of the spectral line. To this value of Θ must be added several corrections, which will be described in the next section.

C. Perturbations and Corrections to the Response Curves

In order to achieve the highest accuracy with the two-crystal spectrometer, it is necessary to investigate several perturbations of the ideal instrument described in the previous section. Fortunately, these are all quite small in the spectral region covered by this investigation, so that they can be treated separately in applying the appropriate corrections.

The largest and most obvious correction is that due to the effect of temperature on the crystal spacing. The usual practice is to correct all measured Bragg angles to their value at 18°C and this may be done by applying the correction

$$\Delta\theta_t = + 2.10(T-18°)\tan\theta \text{ seconds}, \qquad (2.9)$$

calculated from the Bragg law and the coefficient of thermal expansion of calcite.*

Another correction is due to the displacement of the line caused by the asymmetry of the Prins diffraction pattern, as discussed in the previous section. This may be compensated for by applying to the observed Bragg angle a

---

*Compton and Allison, op. cit., p. 682.

correction given by

$$\Delta\theta_a = \frac{\epsilon}{2} = 0.1\,\lambda^2 \text{ seconds } (\lambda \text{ in } \text{Å}) \,. \qquad (2.10)$$

In the discussion of section II-B it was implicitly assumed that the incident radiation consists of rays lying in a plane perpendicular to the (mutually parallel) axes of rotation of the crystals, and that the crystal planes are parallel to said axes of rotation. In actual practice it is fairly easy in a well-designed spectrometer to get the axes of rotation parallel and vertical within about 10 to 15 seconds of arc. It is somewhat more difficult to get the crystal reflecting planes parallel to the axes of rotation. The angle which incoming rays may make with a horizontal plane (the so-called angle of vertical divergence) and still be accepted after two successive crystal reflections by the detector, is limited by the slits used to define the beam and the geometrical distribution of the source. In many cases it is impractical to accept the sacrifice in intensity resulting from limiting this vertical divergence angle to extremely low values. Furthermore, it is fairly obvious that the dihedral angle formed by the reflecting planes of the two crystals which will permit a vertically divergent ray to be reflected from crystal A and be incident upon crystal B at the Bragg angle is different from the corresponding dihedral angle for a horizontal ray. This introduces a further correction term, which will now be considered.

In Appendix B it is shown that successive Bragg reflection from the two crystals is possible only if the angle β of figure 4 is, to second order,

$$\beta_a = 2\theta+\phi^2\tan\theta+\phi\left[\frac{\delta_1-\delta_2-4\delta_1\sin^2\theta}{\cos\theta}\right] + \tan\theta[2\delta_1\delta_2-\delta_2^2+2\delta^2\sin^2\theta] \tag{2.11}$$

for the antiparallel position, or

$$\beta p = \pi+\frac{(\delta_1+\delta_2)}{\cos\theta}\phi - \tan\theta(\delta_1+\delta_2)^2 \tag{2.12}$$

in the parallel case. In these expressions ϕ is the angle of vertical divergence, δ_1 and δ_2 are the angles between a horizontal plane and unit normals to the reflecting planes of crystal A and crystal B, respectively, and $\delta^2 = \delta_1^2 + \delta_2^2$. If the incident radiation is distributed symmetrically with respect to ϕ around $\phi = 0$, the terms in equations 2.11 and 2.12 which are linear in ϕ will contribute no net displacement of the center of an observed line profile in either position. They will, however, broaden the spectrometer window in both positions, and this can be used to align the crystals as discussed in section III-A. The terms which are quadratic in the δ's will displace, but not broaden, the profiles in both positions. The δ's are usually made as close to zero as possible in aligning the spectrometer, and any residual misalignment will introduce a corresponding

uncertainty in the Bragg angle which may be estimated by the formula

$$\left| \Delta\theta_m \right| \leqq \delta_m^2 (3 + 4 \sin^2\theta) \qquad (2.13)$$

which is obtained from equations 2.11 and 2.12 by assuming that $|\delta_1|$ and $|\delta_2|$ are both less than some maximum uncertainty, δ_m.

The remaining correction term in equation 2.11, namely $\phi^2\tan\theta$, is more troublesome. Its effect is both to broaden and displace the antiparallel profile, assuming again a continuous distribution of intensity with ϕ. To analyze the effect accurately, it is necessary to find the sum of a number of antiparallel windows as shown in figure 7, each displaced by $\phi^2\tan\theta$ and with an appropriate intensity for its value of ϕ, and then to fold the resulting window into the spectral line to be analyzed. Shacklett (2) has derived the appropriate integrals and evaluated them numerically using an electronic digital computer. The results of his work indicate that for a uniform source the line is displaced by an amount

$$\Delta\theta_v = \frac{\phi_m^2}{12} \tan\theta \ , \qquad (2.14)$$

where ϕ_m is the maximum angle of vertical divergence, and that for the lines investigated in the present work the increase in width is less than 1/2 percent.

In addition to the corrections already discussed, the absorption of the beam as it traverses the spectrometer will introduce a displacement due to the fact that the absorption coefficient is a function of wavelength. Assuming a cubic dependence of absorption with wavelength, Shacklett has estimated the shift to be

$$\Delta\theta_r \approx 0.6\ \mu\ x\ \left(\frac{a}{\lambda}\right)^2 \tan\theta \text{ seconds} \qquad (2.15)$$

where μ is the linear absorption coefficient of an absorber of length x which is placed in the beam, λ is the wavelength of the center of the line in angstroms, and a is the half-width at half maximum in milliangstroms.

In the present instance, the air path of the spectrometer and the various windows, such as the beryllium cover for the NaI crystal, contribute a μx of about 1.0 at 1.0 A°. To this must be added an estimate of the self absorption in the source. For plutonium, where the incident and fluorescent radiation are on the same side of the source, as shown in figure 11 of Part III, Shacklett has estimated μx to be less than 2.5. For the uranium target tube, it is about 0.3, and for the americium and neptunium fluorescent sources, mounted as shown in figure 12 of Part III, it is less than 1.5. This latter value is the absorption coefficient actually measured at the longest wavelength encountered using these sources. Tanθ for this wavelength is about 0.15

and $(\frac{a}{L})^2$ is approximately a constant equal to 0.2 for most L lines.

Thus, for the most pessimistic case encountered in this investigation,

$$\Delta \theta_r \leq 0.06 \text{ seconds.} \qquad (2.16)$$

This value is on the borderline of being significant, and Shacklett's estimate of μx for the Pu source is considered pessimistic enough so that this correction can be neglected for the purposes of the present investigation.

PART III

DESCRIPTION OF EXPERIMENTAL APPARATUS

The major components of experimental apparatus used in this investigation were the two-crystal spectrometer, the X-ray detector and the X-ray source. Each of these will be described in some detail together with some of the techniques used to ensure the highest accuracy in the measurement of spectral lines. Since this work is a continuation of the work begun by R. S. Shacklett in the same laboratory, much of the material contained in Parts III-A and III-B can be found in references 1 and 2, and is included here in the interest of unity and completeness. However, some of this work, particularly the method of aligning the crystal planes, is believed to be unique in the present research.

A. The Two-Crystal Spectrometer

The spectrometer used in this work was designed and built by DuMond and Marlow and is described in complete detail in reference 3. The instrument is unique in that it couples high precision with a high degree of versatility. It is provided with four independent rotations which may be coupled together or used separately. In addition to the two rotating crystal tables, provision is made for rotation of the entire instrument about the axis of crystal A and for the rotation of the detector arm about the axis of crystal B. These permit the central ray to be automatically kept near

the center of the crystals as the Bragg angle is varied over rather large angles. The crystal tables are provided with mechanisms for adjusting the tilt of the crystals and for translating the crystals in order to place the crystal face directly above the axis of rotation. One of the crystal axes may be made vertical by the use of leveling screws provided on the base of the instrument, and the second axis may then be made parallel to it by an independent adjustment. The entire instrument may then be translated, without disturbing any of the previous adjustments, in order to allow the center of crystal A to intersect the center of the X-ray beam.

The precision worm wheels upon which the crystal tables are mounted have been specially lapped and optically calibrated using techniques invented by Professor DuMond. The error curve is shown in figure 9. These wheels are driven by worm gears matched to the wheels. The gear ratio is such that one revolution of the worm produces a 1° rotation of the crystal table. Attached to the worm gear is a five inch diameter control wheel, the rim of which is divided into divisions representing 10" of arc rotation of the crystal table. The position of this wheel can be read to 1" by using a vernier provided on the instrument or, as in the present work, to a fraction of a second by using a low power microscope mounted on the instrument housing. Backlash is eliminated by weights hung from a cord passing around the precision worm wheels.

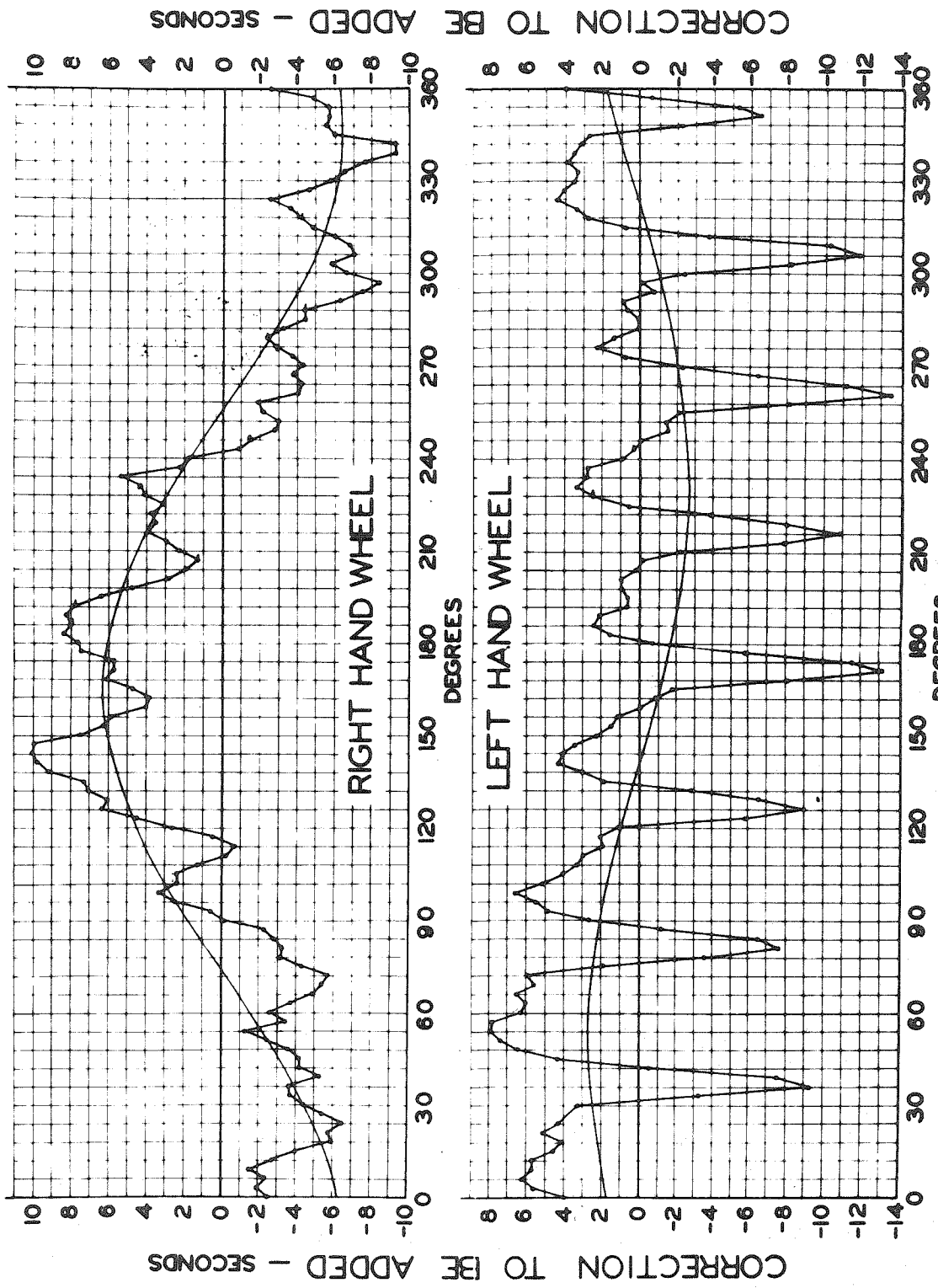

Figure 9. Error graphs obtained by optical calibration of the two worm wheels in the two-crystal X-ray spectrometer (copied from reference 4).

The crystals were rather large (2-3/4" x 2-3/4" x 1") specimens of calcite originally split from a single crystal, with the two faces of the cleavage plane used as the reflecting faces of the two crystals. The crystals were ground and polished to remove the cleavage steps on the reflecting surfaces, and then etched to remove the debris left by the grinding process. In this way, the widths of the parallel rocking curves obtained with these crystals were made comparable to those obtained by other investigators and those predicted for perfect crystals, as shown in figure 10.

A brief description of the procedure followed in aligning the instrument will next be given. In the course of this experiment this procedure was carried out on three different occasions: first, by Shacklett and the present author just prior to Shacklett's investigation, then again when Shacklett's work was completed and prior to the present work, and finally when the equipment was moved from one room to another about half-way through this experiment. The lines of uranium and plutonium were measured before this move, and the americium and neptunium lines and all the edges were done in the new location.

In aligning the instrument, the axis of crystal B is first made vertical by adjusting the leveling screws on the base of the instrument. The verticality of the axis is easily checked by placing a precision spirit level on the crystal table and rotating the table by 180°. Any change in the position of the bubble indicates the angle to be

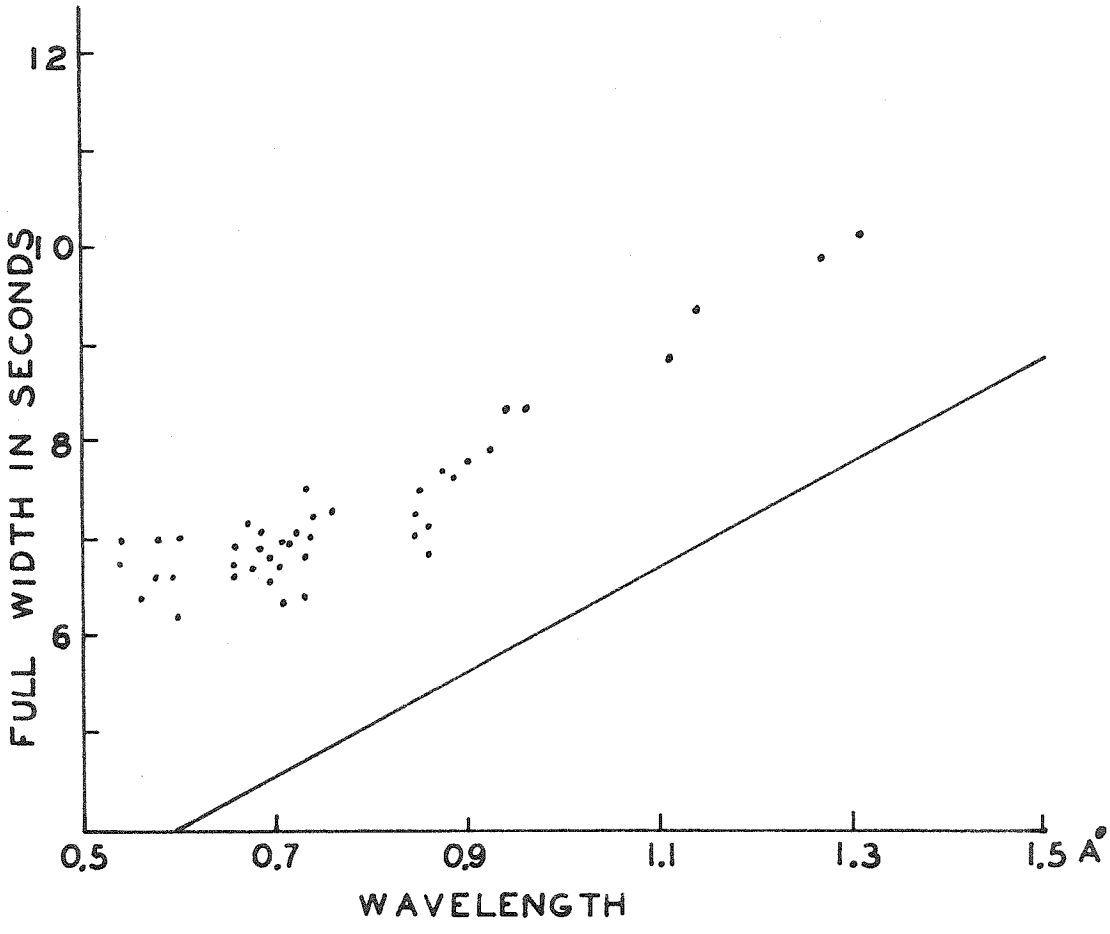

Figure 10. Measured widths of parallel rocking curves plotted against wavelength. The straight line is the theoretical width obtained from the Prins diffraction pattern formula.

corrected. By this method, it was possible to bring this axis to within 15 seconds of arc of a vertical position. Crystal table A is next aligned in the same manner using the independent adjustment inside the instrument dust cover. Fortunately, the two axes remained parallel from the time of the first alignment mentioned above, so that it was not necessary to remove the dust cover for subsequent adjustments.

A surveying level was used for the alignment of the crystals. It was placed on a line roughly perpendicular to a line between the centers of the two crystals and in the same horizontal plane about 4 meters from the spectrometer. The position of the reflecting face of the crystal relative to the axis of rotation was observed by placing the crystal face parallel to the line of sight from the level, adjusting the level so that the vertical crosshair and the crystal face coincided, and then rotating the crystal by 180°. The crystal was translated by an amount given by half the displacement of the face as observed in the telescope, the telescope readjusted onto this new position, and the procedure repeated until no displacement could be observed.

For the angular alignment of the crystals, a meter stick was placed in a vertical position next to the telescope. A thin layer of silver had previously been deposited on the back side of the crystals, and these mirrored surfaces were visible through holes in the crystal mountings. Thus, the angular position of the crystals could be monitored by observing the meter stick as reflected by the crystals to the

telescope. The height of the line of sight was observed by looking directly at the meter stick with the telescope. Next, a series of runs was made over both the parallel and antiparallel profiles of a convenient spectral line, in this case MoKα_1 ($\theta \approx 6°43'$), varying the meter stick scale reading as observed after reflection from crystal B by rotating the crystal about a horizontal axis. The widths of these profiles were next measured and plotted as a function of the scale reading, and the reading corresponding to the minimum width determined from the graph. These were found to be separated by some 0.3 mm, the value for the parallel profiles being the higher of the two. From equations 2.11 and 2.12 it can be seen that the minimum width for the parallel case occurs when

$$\delta_1 + \delta_2 = 0 \qquad (3.1)$$

and for the antiparallel case when

$$\delta_1 - \delta_2 - 4\delta_1 \sin^2\theta = 0. \qquad (3.2)$$

Putting in the appropriate value of $\sin\theta$ and the difference between δ_2 for the two cases,* the value of the scale reading for $\delta_2 = 0$ may be determined as well as a value for

---

*Obtained from the difference between the two meter stick readings corresponding to minimum profile width.

$\delta_1 = 0$. Thus, both crystals may be aligned with an uncertainty in the scale reading of less than 1 mm in 8m corresponding to a maximum misalignment of about 1.3×10^{-4} radians. Using this technique it was possible to reduce the full width of the parallel rocking curve to 6.3 seconds and that of the antiparallel to 24.5 seconds, compared to 7.0 seconds and 25 seconds obtained by the usual method which utilizes only the parallel position (2). Using equation 2.13 and the estimated maximum misalignment angle, the error due to crystal misalignment of a measured spectral line can be estimated with the result

$$|\Delta\theta_m| \leqq .01\ (1 + 1.3\ \sin^2\theta) \text{ seconds.} \qquad (3.3)$$

This is completely negligible for values of θ used in the present investigation ($\sin\theta < .2$).

The temperature of the crystals was controlled in two different ways. Before the instrument was moved, it was possible to control the temperature of the entire room by means of fairly large heaters controlled through a series of relays by a Fenwal thermoswitch placed on the spectrometer. It was found necessary to minimize temperature fluctuations from air convection near the crystal faces which, because of the small penetration distance of X-rays into the crystals, can seriously modify the grating constant close to the surface while a profile is being explored, and so an aluminum cover with thin mylar windows was installed around

the crystals. After moving the instrument to its new location, a few coils of resistance wire were placed around this cover. These coils were heated in response to the thermoswitch, which was then inserted inside the cover, and the temperature of the air bath around the crystals measured by a thermometer with its bulb inside the cover. Temperature gradients inside the air bath were prevented by inserting a small fan to mix the air thoroughly around the crystals.

The two methods of control were equally acceptable, each reducing the temperature variation during a fairly long period of time (several days) to less than $\pm$ .3°C, and even smaller variations during most runs. The second method has the advantage that the room in which the experiment is performed may be kept at a fairly comfortable temperature, while the room temperature using the first method must be kept several degrees higher than normal to achieve effective control.

B. The X-Ray Detector

The X-ray detector consisted of a thin NaI crystal mounted directly on the face of a photomultiplier tube in a holder with a 1 mil beryllium window for the X-rays and a glass window for the light output. The output of the DuMont 6292 photomultiplier was fed into a pre-amplifier mounted on the detector arm, the output pulses of which were amplified by a high-gain linear amplifier and then discriminated by a pulse-height analyzer before reaching the scaler. The main advantages of such a system are that it provides

uniform response over the entire area of the detector, fairly high efficiency in the spectral range under consideration, and a comparatively low background. This latter feature is due to the fact that both cosmic ray pulses and photo-tube noise are eliminated by the pulse-height analyzer.

All of the electronic circuits, including the stabilized high voltage supply for the photomultiplier, were powered through a Sorensen regulator in order to minimize electronic drift. The window of the pulse height analyzer was opened as wide as possible without unduly increasing the background, and its position with respect to the height of the incoming pulses was chosen so that any drift would have a minimum effect. No run was begun until all the electronic equipment had been running continuously for several days, in order to ensure thermal equilibrium of all components.

In order to investigate the resolving time of this system, the spectrometer was placed in the parallel position near the peak of the profile. The intensity was then varied by changing the X-ray tube current while holding the voltage fixed. In this way it was determined that the resolving time was such that no correction is necessary for counting rates less than about 9000 counts per minute, a value seldom exceeded in this investigation. The counting rate was down by about 2 percent at 12,000 counts per minute, assuming a linear relationship between intensity and X-ray tube current, as determined using the meters on the X-ray power supply.

The input window of the detector was fitted with hori-

zontal and vertical slits used to define the geometrical extent of the beam. These were chosen in most instances to provide the highest intensity attainable with due respect for crystal size, source dimensions, detector configuration, and the other geometrical restraints of the apparatus.

C. The X-Ray Sources

Three source configurations were used in this investigation. The plutonium source was the same used by Shacklett (2), the uranium lines were produced in a uranium target X-ray tube, and the americium and neptunium sources were specially prepared for this work.

The plutonium source was a 5.86 gram sample of plutonium metal enclosed in a sealed aluminum sandwich with a thin aluminum window on one side. This was mounted at an angle of 30° with the horizontal and irradiated by a high intensity X-ray tube from a direction perpendicular to the plane of the source. The resulting fluorescent radiation then passed through this same window to the spectrometer, as shown in figure 11. The entire assembly--source, holder and tube--was mounted in a shielded box whose exit portal was provided with slits used to define the beam. This arrangement provided a source which was found to be fairly uniform and of sufficient intensity to permit the measurement of twelve L-lines of plutonium.

The study of the uranium spectrum was greatly enhanced by the availability of two excellently stable uranium target

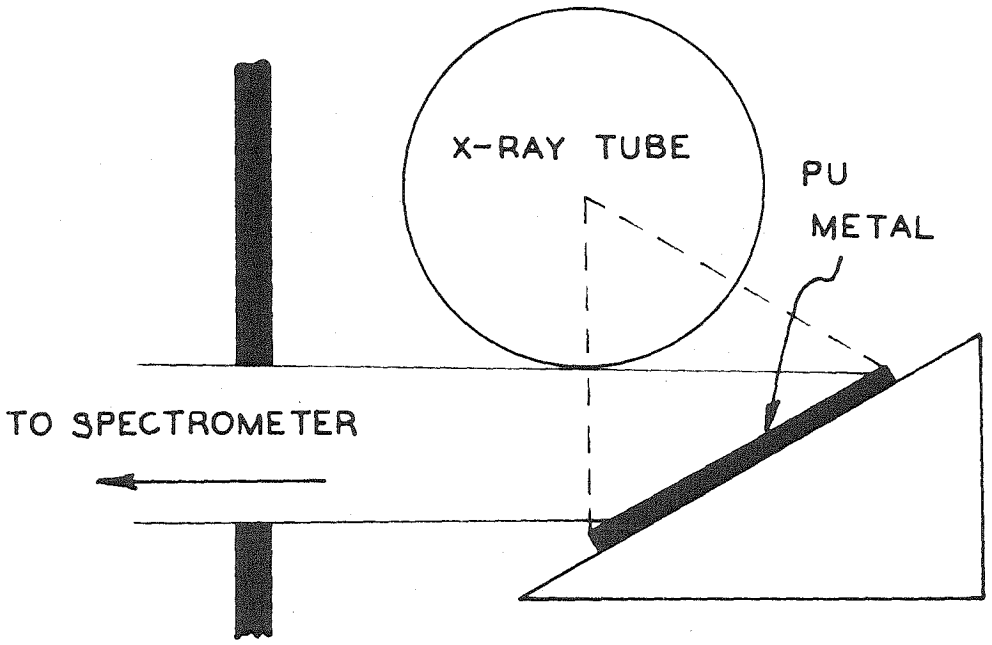

Figure 11. Source configuration for Pu.

X-ray tubes which were produced for this laboratory by Machlett Laboratories, Inc., and believed to be the only such tubes in existence. The high intensity available from this source permitted the measurement of twenty lines of the uranium L-spectrum. The tube was placed in the source box with its target in the same horizontal plane as the center of the detector slit, and pointed directly into the spectrometer. With this source, the slits defining the vertical divergence of the beam could be placed close enough together so that the vertical divergence correction became negligible. As will be described shortly, this permitted a check on the accuracy of this correction for the entire investigation.

Until recently the study of other transuranic elements had been impractical because of the unavailability of suitable samples. A little research revealed that samples of Am and Np could be obtained on loan from the AEC in oxide form, but only in amounts considerably smaller than those previously considered essential for work with this instrument. A preliminary experiment with U_2O_3 demonstrated that satisfactory intensity could be obtained by placing 50 mg of material between two pieces of aluminum foil with about a 3/4 in. diameter (the "sandwich" being held together with Duco cement) and by placing this assembly directly on the window of the high intensity Machlett tube. Thus, the sample was irradiated from one side and the fluorescent radiation passed through the sample and out the other side

to the spectrometer. The direct beam was directed away from the spectrometer by turning the tube through an appropriate angle. This arrangement is shown in figure 12.

After some negotiation, 50 mg samples of Np_2O_3, Pu_2O_3 and Am_2O_3 were obtained on loan and sent to the University of California Radiation Laboratory in Berkeley, California. Here they were encapsulated under the direction of Dr. J. C. Wallman in small aluminum holders with 5 mil windows which would permit them to be handled safely. These could be placed quickly and accurately in a holder which was fabricated to fit on the X-ray tube. This holder also provided slits to define the source size as seen by the spectrometer. A special support was made for the X-ray tube itself. This was designed to permit rotation of the tube about an axis through the position of these sources, and thus to provide a means of studying absorption edges as well as emission spectra.

Pinhole photographs of these sources showed them to be distinctly non-uniform. This causes some uncertainty as to the appropriate vertical divergence correction to be applied as well as some decrease in intensity. The intensity of the Np source was particularly poor, being only about half that of the Am sample, which in turn was considerably weaker than that from the large Pu sample used in measuring the Pu spectrum. However, several lines from each element could be observed, and the small Pu sample, which was obtained with the Am and Np and prepared in similar fashion, was used to

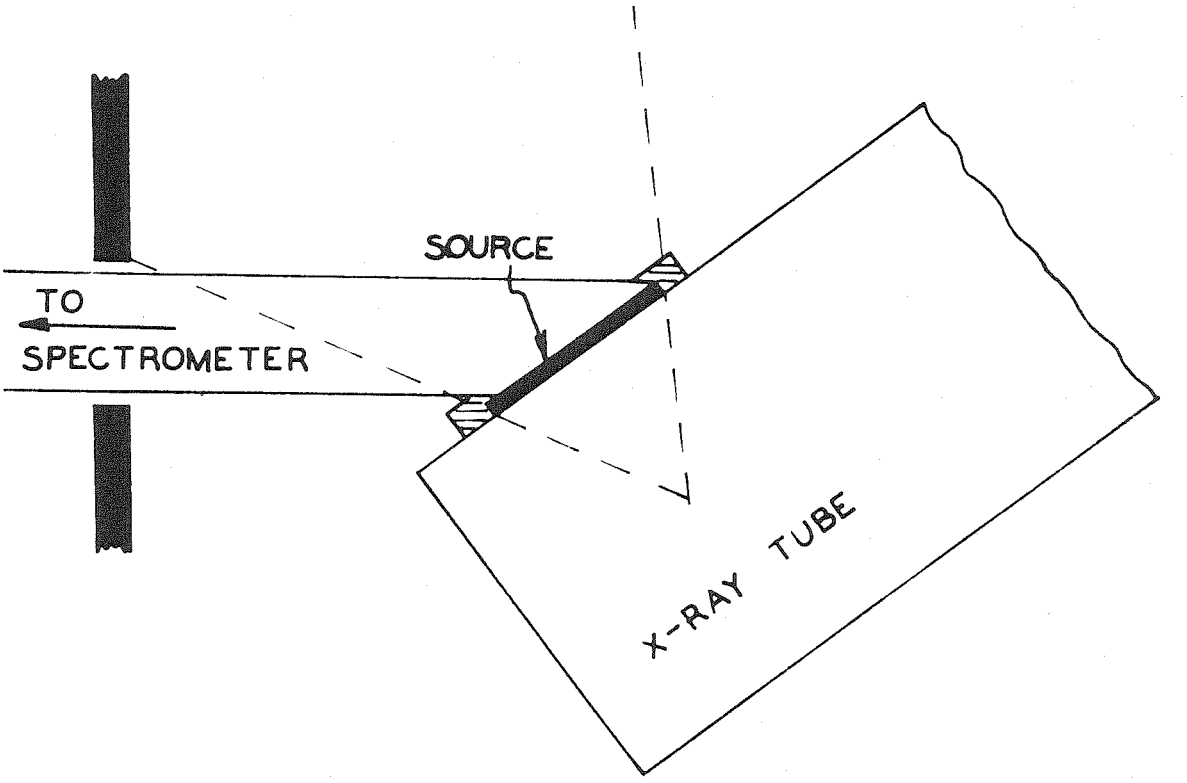

Figure 12. Source configuration for small samples (Np and Am).

check the accuracy of these measurements and the appropriateness of certain assumptions made in estimating the vertical divergence correction, as described in Part IV.

The high intensity X-ray tube used to irradiate the fluorescent samples was a Tungsten target, water-cooled Machlett OEG-50T, which could run continuously at 50 KVP full-wave rectified plate voltage and 50 ma current. All X-ray tubes were powered by a Phillips water cooled diffraction unit fitted with a current stabilizer provided by the manufacturer. To achieve the greatest possible stability of operation, the input of this unit was taken through a 2.5 KVA Sorensen regulator, which was designed to reduce variations of the input voltage to less than 0.1%. With this arrangement it was possible to reduce variations of the source intensity to about 1% over a 24-hour period.

PART IV

EXPERIMENTAL PROCEDURES AND RESULTS

A. Experimental Measurements

The entire spectrum of each element was scanned before any precision measurements were attempted. This was done by locking all the controls of the spectrometer together after the best position for each was found using the strongest line of the spectrum, the $L\alpha_1$, in the antiparallel position. This line could be located approximately by using estimates of its wavelength obtained by extrapolating existing data to the higher atomic numbers. As discussed in Part III-A, the spectrometer automatically maintains the appropriate geometrical relationships between source, crystals, and detector--once they have been achieved for one line--when the spectrometer is used in this fashion. In this way it was possible to locate and identify all the lines of the spectrum with sufficient intensity to be detected above the ever-present background. Identification was achieved by comparing the observed lines with extrapolated data concerning wavelength, intensity, and width.

Each line was then taken in turn for a precision measurement. The spectrometer was returned to the peak of the line, as determined by the search run, where crystal A and the table control were fixed. A preliminary run over the line rotating only crystal B yielded more accurate data concern-

ing its center and width. After setting crystal B at the peak of the line, the table, detector arm and electronic controls could be set to give the maximum peak line intensity. With the information then available, it was possible to schedule a step by step program of points over the line profile moving crystal B 5 or 10 seconds of arc per step while holding crystal A fixed. The direction of rotation was chosen so as to raise the weight provided for the elimination of backlash effects, and thus ensured a constant contact between the gears of the spectrometer.

The time during which counts were accumulated was the same for all the points and was calculated to yield about 6,000 counts at the peak of the line. It was considered impractical to accumulate counts for more than one hour, and so some of the weaker lines had somewhat fewer counts than did the stronger ones. The required counts were obtained in a single run over the line profile in most instances, although all the Pu lines except the PuLα_1 were scanned several times, using proportionately shorter accumulation times, and the sum of all runs used in reducing the data. Except for the U lines, most of these antiparallel runs were quite long, some taking as long as 30 hours or more. The 60 cycle line frequency was used as a time base in controlling the counting interval at each point.

The background was estimated by accumulating counts at a point some five full line-widths from the center of the line in a region uninfluenced by the presence of neighboring

lines. A small correction was made for the influence at this point of the line under investigation (about 1% of the peak line intensity). Thus, the background measurement included all appropriate effects, including incoherent scattering off the crystals and off the slit system. In some instances, particularly in the case of weak lines in the vicinity of stronger ones, the background effects of neighboring lines could not be neglected, nor could it be assumed constant over the line profile. These effects were estimated for each experimental point from information regarding the center, width, and intensity of neighboring lines. The total estimated background was then subtracted from the number of accumulated counts at each point before the data were analyzed.

Crystal B was then moved to the parallel position, where it was advanced over the profile in steps of one second of arc. The intensity in this position was considerably greater due to the fact that the spectrometer passes all wavelengths at the parallel condition, and so sufficient counts could be accumulated in one or two minutes at each point. The centers of the parallel rocking curves were determined by plotting the intensity as a function of the angular setting of crystal B, connecting adjacent points by straight lines, and finally by drawing horizontal chords across the profile at different heights and finding the midpoints of these chords. The angular positions of these central points at different heights never differed from each other on one and

the same profile by more than one tenth of a second of arc for chords higher than one-quarter of the peak intensity. Each determination was repeated by making a second run over the rocking curve and finding its center in the same manner. In most cases the agreement between the two runs was within the desired precision. It was found, however, that a short time had to be allowed between changing crystal B from the antiparallel to the parallel position and the actual initiation of the parallel run. If sufficient time were not allowed, the first run would show a center point at too low an angle. On subsequent runs the central position would occur at a slightly higher angle, in a few cases as much as six-tenths of a second above the first. This second value was then reproducible within one-tenth of a second of arc. It is believed that this shift, which was always in the same direction, was due to a stabilizing in the contact between the precision worm wheel and the worm gear which drives it. In such cases, which occurred quite infrequently, only the stable value of the central position was used in computing the Bragg angle. Figure 13 shows a typical rocking curve. The width of the parallel rocking curve was taken as the full width of the profile at half maximum intensity.

The centers of the antiparallel curves were determined by drawing a smooth curve through the experimental points and again finding points midway between the two sides. For most of the lines these points did not vary by more than

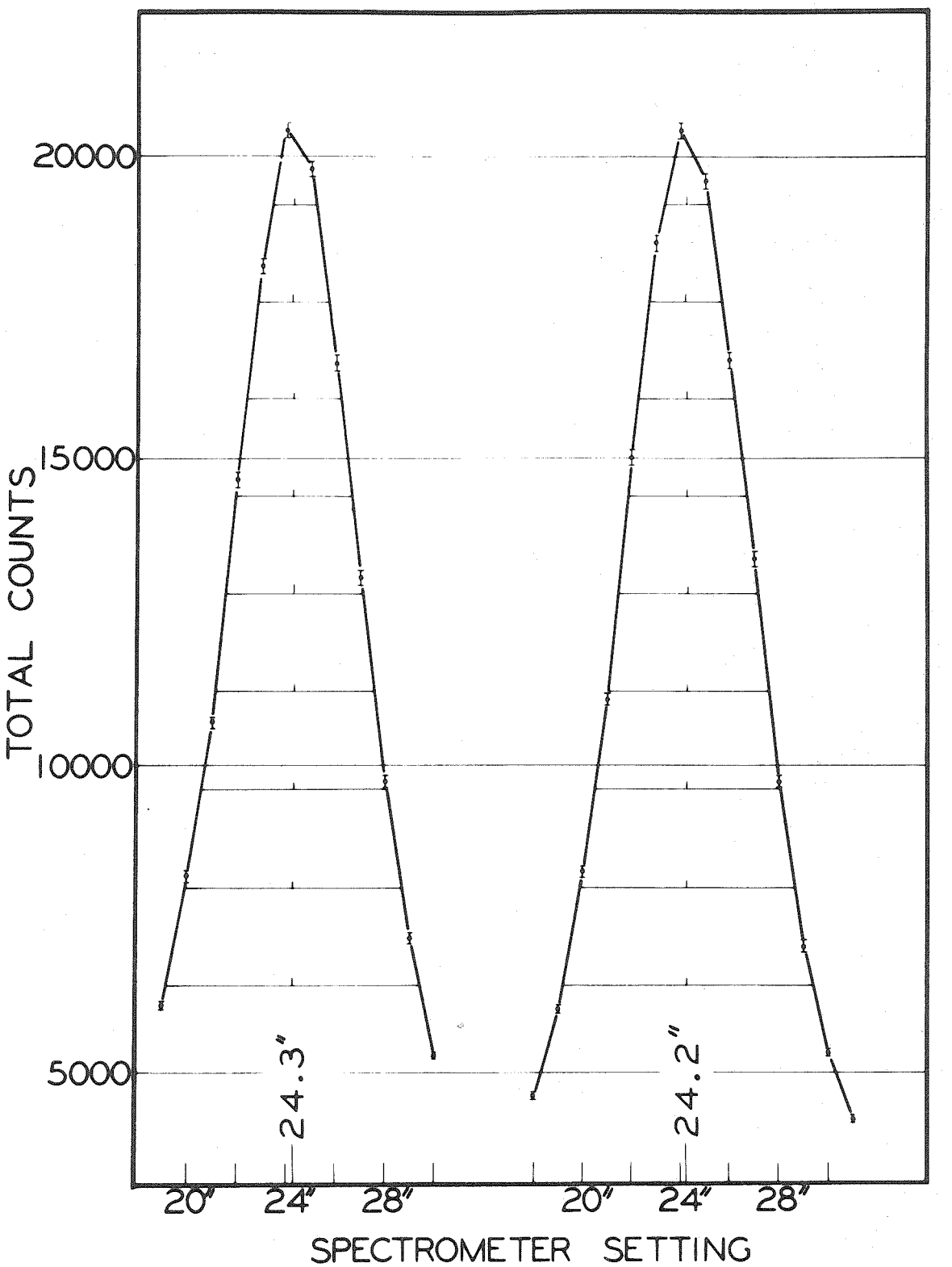

Figure 13. A typical parallel rocking curve (the Pu $L\beta_3$) showing the two runs over the curve.

five-tenths of a second of arc from their mean. In a few cases the spread was greater, and larger probable errors have been assigned to these exceptions. Again, the width was taken as the full width at half maximum intensity after subtraction of the estimated background. The U $L\gamma_4$ line is worthy of special note. The shape of this line indicates that there may be a weaker line of unknown origin on its long wavelength side, perhaps 0.5 x-units or less away. This together with its weakness and the presence of some slight but unexplained background distortion made it impossible to determine the center of this line with high precision. Figure 14 shows an example of one of the better antiparallel curves (the U $L\alpha_1$), while Figure 15 shows one of the poorer ones (the Pu $L\beta_4$).

As a check on the graphical procedure described above, an analytical method of fitting a witch to the experimental data was applied to some of the lines. The method used requires estimation of the background and the peak intensity of the line, both of which are available from the experimental data, and then treats the line center and width as variables in a least-squares adjustment to the experimental data. The points are weighted according to their statistical uncertainty and their effect on the location of the center of the line. Appropriate formulae are derived in Appendix C. This analytical method yielded results in all cases which agreed, within the limits of probable error, with those obtained by the graphical method. For this reason, the

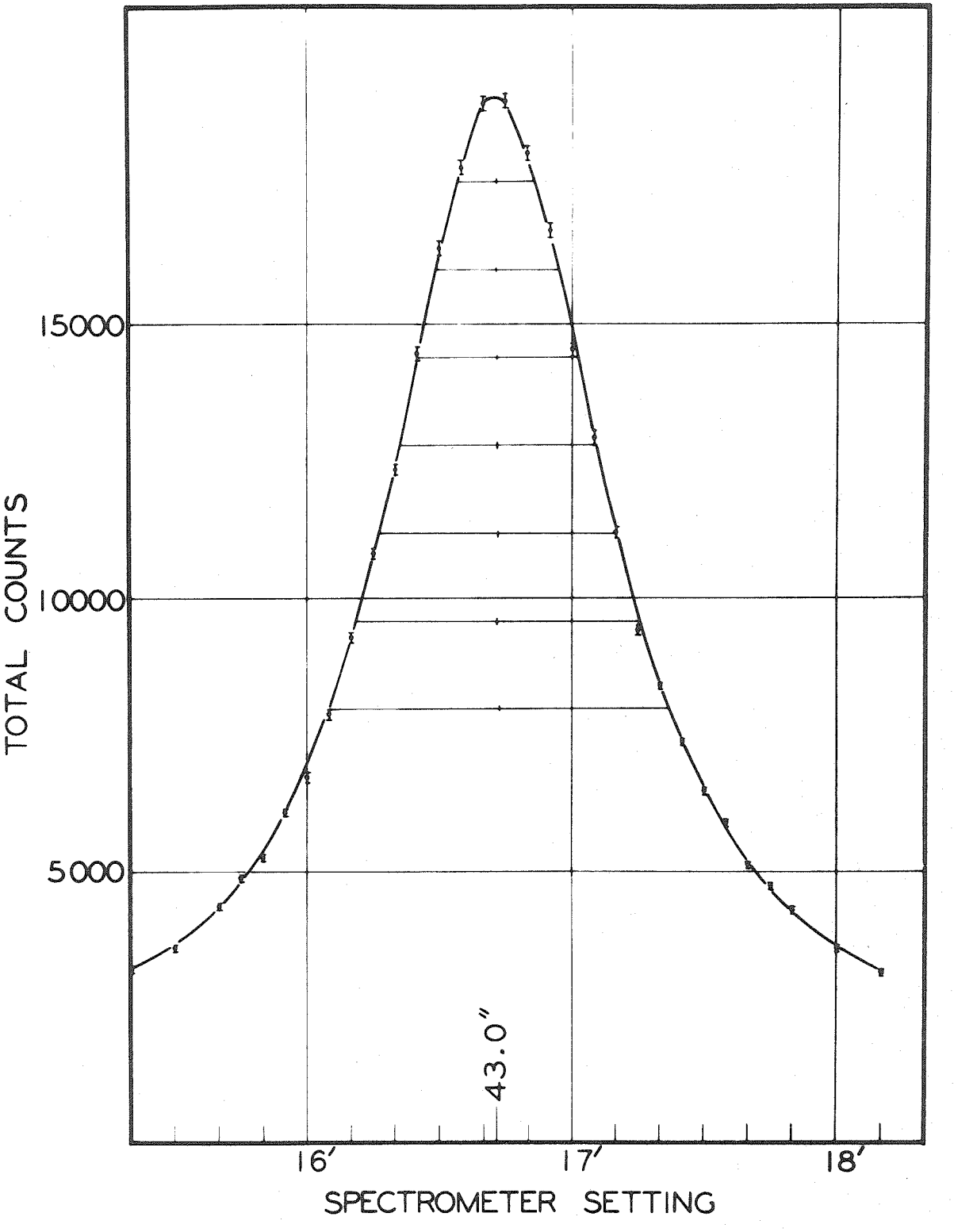

Figure 14. A typical good antiparallel curve (the U $L\alpha_1$).

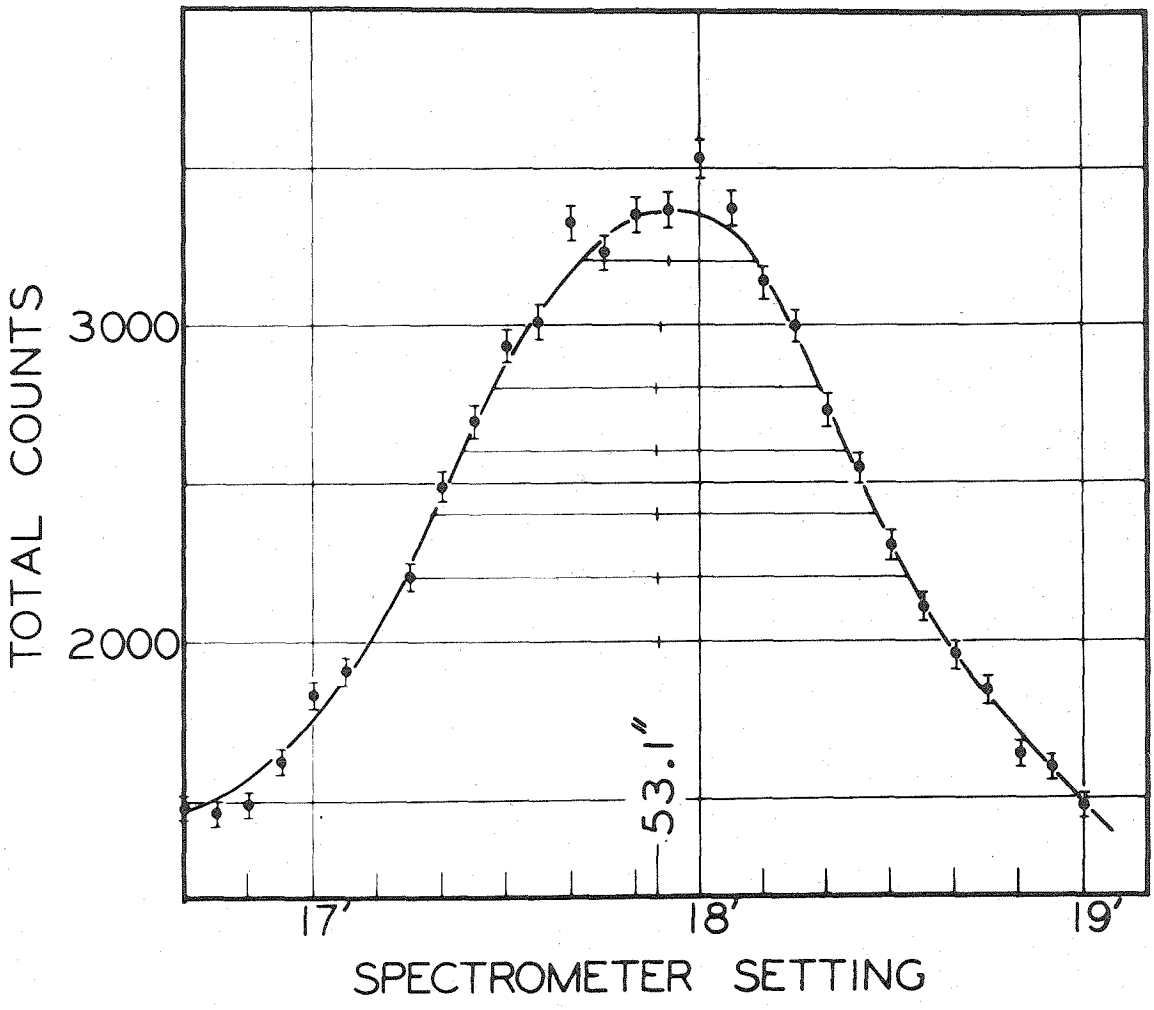

Figure 15. A typical antiparallel curve of a weaker line (the Pu $L\beta_4$).

graphical method was used for most of the lines, since it required considerably less computation and produced results of comparable reproducibility.

At least two independent determinations of the Bragg angle and width were made for each of the lines, and the reproducibility of these measurements was another verification of the accuracy of the methods of analysis used in reducing the data.

The absorption edges were examined in similar fashion, keeping crystal A fixed while examining the parallel and antiparallel profiles. Two runs were taken over the antiparallel curve--one with the source in place and a second with the source removed. This second run was necessitated by the fact that the X-ray tube output was not constant over the range involved. The ratio of the intensities with and without the absorbers was then computed and plotted as a function of the angular position of crystal B. The "center" of the edge was taken as the point halfway between the maximum and minimum values of this curve, and the width was taken as the width between positions of 1/4 and 3/4 of the total jump. Figure 16 shows a typical absorption curve.

Unfortunately, the absorption discontinuity was so small compared to the total transmitted intensity that the statistics of the experimental points were very poor. As a result, none of the structure usually associated with such edges could be observed and, perhaps more important, the center of the profile could not be located with precision comparable to

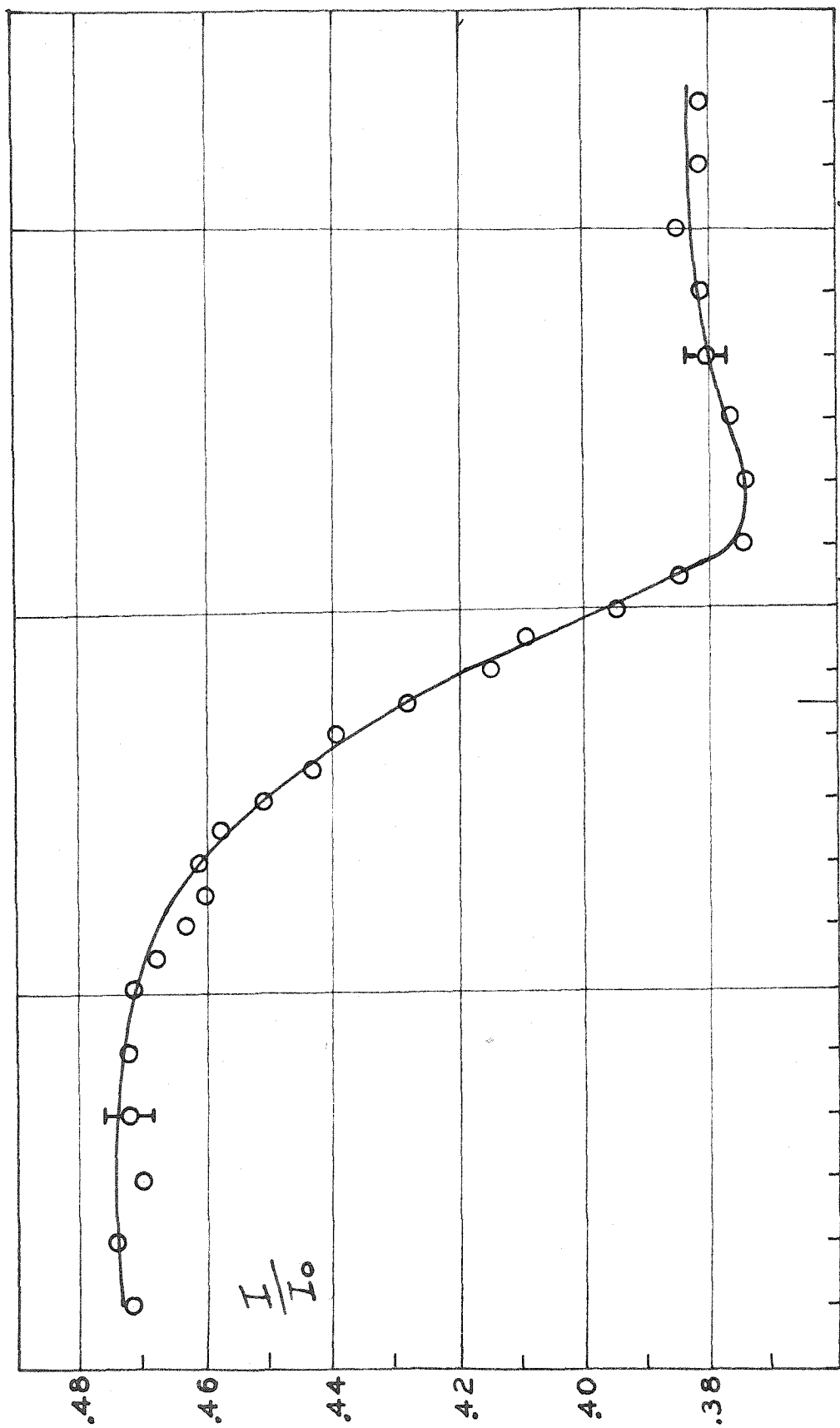

Figure 16. A typical absorption edge (the U L_{III}).

that attained for the spectral lines. Furthermore, the L_I and L_{II} edges could not be observed at all. Since the distribution of the absorbing material was found to be non-uniform, resulting in an uncertainty in the amount of material actually in the absorbed beam, no attempt was made to compute absolute absorption coefficients.

B. Corrections

The angular positions of the centers of the parallel and antiparallel curves were first corrected for the errors in the worm wheel as described in Part III. The difference between the two corrected positions gives then $180° + 2\theta$, where θ is the Bragg angle of the line under consideration. The resulting Bragg angle was then corrected for vertical divergence, the effect of temperature on the grating constant of the crystal, and the effect of crystal diffraction pattern asymmetry.

The vertical divergence correction for the uniform Pu source was given in equation 2.14, namely

$$\Delta\theta_v = -\frac{\phi_m^2}{12}\tan\theta \quad . \tag{4.1}$$

The formula is expected to be different for a point source, such as the focus of the U target X-ray tube. By taking several runs over the U $L\beta_1$ with different maximum angles of vertical divergence, including one so small that $\phi_m^2 \tan\theta$, and hence the correction itself, was less than

.01 seconds, it was determined that the appropriate correction would be

$$\Delta\theta_v' = -\frac{\phi_m^2}{4}\tan\theta \quad . \qquad (4.2)$$

In most cases where this formula was used, the correction was negligible due to the small angles of divergence possible with the intensity of the U target tube.

In the case of the Am and Np lines the correction was more difficult since, as previously stated, the source distribution was found to be non-uniform, and the low intensity necessitated large angles of vertical divergence. An estimate was obtained by placing a collimator between the source and crystal A, and examining the antiparallel profile of the $L\alpha_1$ line both with and without the collimator. The collimator spacing was sufficiently narrow that the correction could be neglected when it was placed in the beam, and so the correction for this line was taken as the difference between the centers of the profiles with and without the collimator. The divergence angles for other lines of the same element were held constant so that the corrections for them could be taken as linear functions of $\tan\theta$, in accordance with equation 2.11. For Np the applied correction was

$$\Delta\theta_v = -10.3\ \tan\theta \text{ seconds (Np)} , \qquad (4.3)$$

and for Am

$$\Delta\theta_v = -3.58 \tan\theta \text{ seconds (Am)} . \qquad (4.4)$$

In order to check the accuracy of these corrections, the Pu $L\alpha_1$ and $L\beta_1$ were measured using both the "transmission" and "reflection source" configurations (see figures 11 and 12, Part III). Since the Pu transmission source was found to be the most non-uniform of the entire group, the agreement of these two measurements showed that the corrections as given by the more complicated method leading to equations 4.3 and 4.4 are at least as good as that of equation 4.1 applied to a uniform source.

This experiment also verified the equivalence of the two systems of temperature controls, since the reflection experiments were done prior to the change in location discussed in Part III and the transmission measurements were done with the new temperature control after the spectrometer had been realigned in the second laboratory. It was also possible to check the accuracy of equation 4.1, since the U $L\beta_1$ could be measured with negligible vertical divergence (as described above) and also using the same source configuration as applied to Pu in this investigation. Again, the two measurements agreed to within the standard deviations of the two measurements (actually, within 0.1 second), demonstrating the accuracy of equation 4.1 and hence equations 4.3 and 4.4.

The Bragg angles were reduced to their values at 18°C by applying the correction given by equation 2.9, namely

$$\Delta\theta_t = +2.1(t-18°)\tan\theta \text{ seconds.} \qquad (4.5)$$

The shift of the observed lines due to crystal pattern asymmetry was corrected by applying the correction

$$\Delta\theta_a = \frac{\varepsilon}{2} = 3.67 \sin^2\theta \text{ seconds,} \qquad (4.6)$$

which was obtained by substituting the Bragg law into equation 2.10, using $2d = 6.058$ Å for the cleavage planes of calcite.

Typical angle calculations are shown in Table I for the U $L\alpha_1$ and the Pu$L\beta_4$ lines.

Parratt (12) has shown that the position and structure of absorption edges is dependent on the thickness of the absorber. This effect is apparently due to the tails of the monochromatic response curve of the spectrometer, and has been estimated to be negligible for the thin samples used in this investigation.

C. Errors

(a) The most important random error in determining the Bragg angle of a spectral line is the uncertainty of the location of the center of the antiparallel curve, $\delta\theta_{ap}$. This uncertainty varies from about 0.2 to 5 seconds of arc, usually being less than 0.5 second. Other statistical

TABLE I. Typical Bragg angle calculations for U $L\alpha_1$ and Pu $L\beta_4$ lines.

Run	Parallel position	Antiparallel position	Worm-wheel correction $-\Delta\theta_w$	2θ (uncorrected)	$\Delta\theta_t+\Delta\theta_v+\varepsilon/2$	Bragg angle θ(corrected)
			(a) U $L\alpha_1$			
1	294°17'14.15"	97° 1'54.9"±0.1"	-6.15"	17°15'13.1"	2.8"	8°37'39.35"
2	97° 1'23.7"	294°16'43.0"±0.1"	-6.15"	17°15'13.15"	2.7"	8°37'39.23"
			(b) Pu $L\beta_4$			
1	292°20'28.8"	98°58'46.5"±0.8"	-6.36"	13°21'35.9"	+1.54"	6°40'49.5"
2	98°56' 9.1"	292°17'53.1"±0.8"	-6.36"	13°21'37.6"	+1.50"	6°40'50.3"

errors are listed below, with their assigned uncertainties:

(b) Uncertainty in the location of the center of the parallel curve, $\delta\theta_p \cong 0.1"$.

(c) Uncertainty in the applied worm wheel correction, $\delta\theta_w \cong 0.1"$.

(d) Uncertainty in the ambient temperature of the reflecting crystals, resulting in an uncertainty in the temperature correction, $\delta\theta_t \cong 0.05"$.

(e) Uncertainty in the applied correction for vertical divergence, $\delta\theta_v < 0.05"$.

(f) Uncertainty in the applied correction for crystal diffraction pattern asymmetry (Darwin dynamical theory), $\delta\theta_c < 0.01"$.

Since the required Bragg angle was computed by subtracting the parallel and antiparallel readings after the worm wheel correction had been applied, and by dividing the result minus 180° by two before applying the other corrections, the uncertainty in the Bragg angle is

$$\delta\theta B_1 = [(\delta\theta p_1^2 + \delta\theta ap_1^2 + 2\,\delta\theta_w^2/4 + 2\,\delta\theta_t^2 + \delta\theta_v^2 + \delta\theta_c^2]^{1/2} .$$

Since two independent measurements of each line are averaged to obtain the final Bragg angle, its uncertainty is

$$\begin{aligned}\delta\theta_B &= 1/2[\,(\delta\theta B_1)^2 + (\delta\theta B_2)^2]^{1/2} \\ &= 1/2[1/2(\delta\theta_p^2 + \delta\theta_{ap}^2) + \delta\theta_w^2 + 2\,\delta\theta_t^2 + 2\,\delta\theta_v^2 + 2\,\delta\theta_c^2]^{1/2} \\ &= 1/2[1/2\,\delta\theta_{ap}^2 + 0.040]^{1/2} ,\end{aligned}$$

if one assumes that the same uncertainty is assigned to the position of the centers of the line profiles in the two cases.

D. Results

The corrected Bragg angles are shown in Table II. The angles for $UL\alpha_2$ and $PuL\alpha_2$ were measured in Shacklett's work (1) and are included for completeness. The wavelengths given in the table were calculated by using the effective first order grating space $2d_1 = 6058.09 \pm 0.03$ x-units. This value was obtained by defining, for the purposes of this work, one x-unit as such that the Mo $K\alpha_1$ lines central wavelength is $\lambda \equiv 707.8490$ x-units. This line was measured in the calibration of our crystals* and its Bragg angle was found to be

$$\Theta = 6°42'35.9'' \pm 0.1'' \quad .$$

The uncertainty in the measurement of this line was included as an additional independent uncertainty in the calculation of the wavelengths of the various lines. This choice for the wavelength of $MoK\alpha_1$ is discussed further in the Appendix to the paper included here as Appendix D.

The widths of the lines are also included in Table II. These values were obtained from the experimental data by subtracting from the observed widths an amount determined by figure 8 in order to correct for the effect of the

---

*See Reference 1.

TABLE II. Experimental results. Uncertainties in values of ν/R due to Bragg angle uncertainty alone are included in parentheses.

X-ray line	Transition	Bragg angle (calcite)	Wavelength (x-units)	ν/R	Corrected width ($\Delta\nu/R$)
Uranium					
$L\alpha_1$	L_{III}-M_V	8°37'39.3" ±0.1"	908.782±.007	1000.693±.016(.006)	0.82±.02
$L\alpha_2$	L_{III}-M_{IV}	8°44'29.0" ±0.2"	920.676±.008	987.767±.016(.006)	0.92±.02
$L\beta_1$	L_{II} -M_{IV}	6°48'41.4" ±0.1"	718.509±.007	1265.701±.020(.005)	0.90±.02
$L\beta_2$	L_{III}-N_V	7° 8'29.3" ±0.15"	753.140±.008	1207.494±.019(.007)	0.88±.03
$L\beta_3$	L_I -M_{III}	6°43' 9.6" ±0.3"	708.832±.011	1282.973±.024(.015)	1.65±.08
$L\beta_4$	L_I -M_{II}	7° 4'40.1" ±0.2"	746.460±.008	1218.300±.021(.010)	1.81±.07
$L\beta_5$	L_{III}-O_V	6°52'18.56"±0.1	724.814±.007	1254.684±.024(.005)	0.85±.05
$L\beta_6$	L_{III}-N_I	7°27'43.5" ±0.4	786.763±.013	1155.897±.019(.017)	1.45±.04
$L\beta_{7'}$	L_{III}-N_{VI},N_{VII}	6°59'18.7" ±0.3	737.091±.011	1233.785±.025(.015)	0.61±.04
$L\beta_7$	L_{III}-O_I	6°57'49.8" ±2"	734.500±.060	1238.139±.100(.100)	
$L\beta_9$	L_I -M_V	6°26'28.4" ±0.1	679.620±.007	1338.119±.021(.005)	1.82±.12
$L\beta_{15}$	L_{III}-N_{IV}	7° 9'36.2" ±0.2"	755.090±.008	1204.376±.021(.010)	0.96±.03
$L\eta$	L_{II} -M_I	7°37'16.1" ±0.4"	803.436±.013	1131.903±.024(.017)	1.36±.04
$L\ell$	L_{III}-M_I	10° 7'28.3" ±0.5"	1064.941±.016	853.946±.017(.015)	1.56±.06
$L\nu_1$	L_{II} -N_{IV}	5°48'44.3" ±0.1	613.503±.007	1482.329±.024(.007)	1.15±.04

TABLE II (continued)

X-ray line	Transition	Bragg angle (calcite)	Wavelength (x-units)	ν/R	Corrected width ($\Delta\nu$/R)
$L\nu_2$	$L_I - N_{II}$	5°43'19.1" ±0.2	604.000±.008	1505.651±.027(.015)	1.96±.04
$L\nu_3$	$L_I - N_{III}$	5°39'31.7" ±0.1	597.354±.007	1522.402±.024(.007)	1.80±.08
$L\gamma_4$	$L_I - O_{III}$	5°26' 6.0" ±3"	573.801±.090	1584.892±.240(.240)	
$L\gamma_{4'}$	$L_I - O_{II}$	5°27' 5.0" ±0.2"	575.526±.008	1580.142±.028(.016)	
$L\gamma_5$	$L_{II} - N_I$	6° 0'35.6" ±0.15	634.276±.013	1433.780±.036(.028)	1.41±.07
$L\gamma_6$	$L_{II} - O_{IV}$	5°37'24.3" ±0.1	593.630±.007	1531.952±.025(.008)	0.96±.04
L_{III} edge		6°49'57.5" ±1"	720.727±.029	1261.799±.054(.050)	
Neptunium					
$L\alpha_1$	$L_{III} - M_V$	8°25'27.5" ±0.2"	887.555±.007	1024.627±.016(.006)	0.91±.01
$L\alpha_2$	$L_{III} - M_{IV}$	8°32' 9.4" ±0.2"	899.201±.007	1011.356±.016(.006)	0.93±.01
$L\beta_1$	$L_{II} - M_{IV}$	6°36'25.7" ±0.2"	697.049±.007	1304.661±.022(.011)	1.09±.02
$L\beta_2$	$L_{III} - N_V$	6°57'57.5" ±0.2"	734.724±.007	1237.761±.021(.010)	0.96±.02
$L\beta_4$	$L_I - M_{II}$	6°52'31.6" ±0.5"	725.222±.014	1253.978±.030(.024)	1.90±.08
$L\beta_5$	$L_{III} - O_V$	6°41'56.1" ±0.3"	706.688±.009	1286.866±.024(.015)	0.83±.03
$L\gamma_1$	$L_{II} - N_{IV}$	5°38'20.8" ±0.15"	595.277±.006	1527.713±.026(.012)	1.28±.02

TABLE II (continued)

X-ray line	Transition	Bragg angle (calcite)	Wavelength (x-units)	ν/R	Corrected width ($\Delta\nu/R$)
$L\gamma_6$	L_{II} -O_{IV}	5°27'17.1" ±1.5"	575.806±.043	1579.373±.106(.106)	1.44±.08
L_{III} edge		6°39'41.0" ±1"	702.747±.028	1294.082±.055(.050)	
Plutonium					
$L\alpha_1$	L_{III}-M_V	8°13'23.7" ±0.2"	866.492±.008	1049.534+.017(.007)	0.93±.01
$L\alpha_2$	L_{III}-M_{IV}	8°20'16.2" ±0.1"	878.480±.007	1035.212±.017(.004)	1.00±.03
$L\beta_1$	L_{II} -M_{IV}	6°24'35.4" ±0.1"	676.321±.008	1344.647±.023(.011)	1.05±.03
$L\beta_2$	L_{III}-N_V	6°47'50.8" ±0.2"	717.034±.008	1268.298±.022(.010)	1.07±.02
$L\beta_3$	L_I -M_{III}	6°19'27.4" ±0.7"	667.332±.021	1362.759±.047(.041)	1.76±.03
$L\beta_4$	L_I -M_{II}	6°40'49.9" ±0.5"	704.757±.016	1290.392±.032(.026)	2.11±.15
$L\beta_5$	L_{III}-O_V	6°31'58.9" ±0.2"	689.265±.008	1319.394±.022(.011)	0.84±.03
$L\beta_6$	L_{III}-N_I	7° 6'39.4" ±0.5"	749.937±.016	1212.652±.030(.024)	1.25±.05
$L\gamma_1$	L_{II} -N_{IV}	5°28'19.3" ±0.15"	577.698±.008	1574.200±.027(.013)	1.18±.04
$L\gamma_2$	L_I -N_{II}	5°23'39.3" ±0.5"	569.511±.016	1596.830±.048(.040)	1.92±.05
$L\gamma_3$	L_I -N_{III}	5°19'51.6" ±0.2"	562.847±.008	1615.737±.029(.018)	1.78±.06
$L\gamma_6$	L_{II} -O_{IV}	5°17'25.5" ±0.6"	558.580±.018	1628.078±.055(.052)	1.47±.22
L_{III} edge		6°29'44.5" ±1"	685.343±.029	1326.945±.060(.056)	

TABLE II (continued)

X-ray line	Transition	Bragg angle (calcite)	Wavelength (x-units)	ν/R	Corrected width ($\Delta\nu/R$)
Americium					
$L\alpha_1$	$L_{III}-M_V$	8° 1'54.45"±0.15"	846.452±.006	1074.382±.018(.005)	1.00±.01
$L\alpha_2$	$L_{III}-M_{IV}$	8° 8'49.0" ±0.2"	858.506±.007	1059.296±.018(.007)	0.99±.01
$L\beta_1$	$L_{II}-M_V$	6°13' 9.9" ±0.2"	656.310±.007	1385.644±.022(.012)	1.16±.03
$L\beta_2$	$L_{III}-N_V$	6°38' 5.3" ±0.2"	699.955±.007	1299.244±.022(.010)	1.07±.03
$L\beta_3$	L_I-M_{III}	6° 8'11.2" ±0.4"	647.589±.012	1404.305±.032(.025)	1.80±.15
$L\beta_4$	L_I-M_{II}	6°29'32.3" ±0.5"	684.987±.015	1327.635±.035(.028)	2.16±.08
$L\beta_5$	$L_{III}-O_V$	6°22'23.1" ±0.3"	672.448±.009	1352.391±.026(.016)	0.91±.02
$L\beta_6$	$L_{III}-N_I$	6°56'47.2" ±0.5"	732.675±.014	1241.222±.030(.024)	1.41±.04
$L\beta_{15}$	$L_{III}-N_{IV}$	6°39'14.4" ±0.4"	701.971±.012	1295.513±.033(.030)	
$L\gamma_1$	$L_{II}-N_{IV}$	5°18'39.2" ±0.2"	560.736±.006	1621.819±.029(.016)	1.27±.02
$L\gamma_6$	$L_{II}-O_{IV}$	5° 7'58.6" ±0.4"	541.999±.012	1677.886±.045(.037)	1.80±.14
L_{III} edge		6°20'12.5" ±1"	668.648±.028	1360.077±.061(.057)	

monochromatic profile of the spectrometer. The width of the monochromatic profile at half maximum height was taken as the same as the parallel rocking curves, since these were shown in Part IV-B to be identical in the case of negligible absorption, a condition which is closely approached in the work of this investigation.

The transition energies and widths are given in units of the Rydberg, and the transitions in terms of Kev using constants from the least-squares analysis of Cohen and DuMond (13), namely: $\lambda_g/\lambda_s = 1.002039$ and $R = 109737.309\ cm^{-1}$.*

*The constant λ_g/λ_s is at present being redetermined in at least two laboratories and the entire data of the least squares analysis of 1955 cited in reference 13 are subject to revision because of more refined subsequent work so that a more accurate least-square analysis will probably be forthcoming in the near future. The changes from the 1955 values are expected to be of the order of no more than a few parts per hundred thousand at most.

PART V

DISCUSSION OF EXPERIMENTAL RESULTS

A. Electron Binding Energies

Using the data of table II it is possible to compute the binding energies of electrons in the various shells and sub-shells of these atoms. The results, converted to electron volts using the constant $E\lambda_s = 12372.44 \pm 0.16$ K.V. x units (14), are shown in table III. Since the L_{III} edge is the only level measured directly, all binding energies computed with these data must be interpreted as the energy necessary to remove an electron from its inner shell to the energy level corresponding to the final state of the electron involved in the L_{III} absorption edge. This last may differ slightly with the physical state and state of chemical combination of the atom with other atoms. Thus, each energy is in the present instance referred to a common level, which may or may not, however, correspond to the so-called Fermi level. As a matter of fact, this common level may not even be available as a possible final state for an electron removed from another shell. This is evidenced by the fact that measured spectral lines do not always correspond exactly to the differences between experimental absorption edges (14). This discrepancy apparently is caused by the symmetry properties of the valance electron states surrounding an atom. Transitions between an inner level and an unoccupied outer level or band must satisfy the same selection rules as for

TABLE III. Electron binding energies of U, Np, Pu and Am expressed in electron volts. Uncertainties are ± 1 ev unless otherwise noted. Values in parentheses are derived from estimated splittings as discussed in the text, and are believed significant to ± 3 ev.

Level	U	Np	Pu	Am
L_I	21,757	(22,414)	(23,095)	(23,792)
L_{II}	20,948	21,596	22,263	22,943
L_{III}	17,167	17,606	18,053	18,503
M_I	5,549	5,724	5,914	6,114
M_{II}	5,183	(5,354)	(5,540)	(5,730)
M_{III}	4,303	(4,422)	(4,555)	(4,687)
M_{IV}	3,728	3,847	3,969	4,092
M_V	3,552	3,666	3,774	3,886
N_I	1,441	(1,490)	1,555	1,617
N_{II}	1,273	(1,318)	(1,371)	(1,429)
N_{III}	1,045	(1,076)	(1,114)	(1,154)
N_{IV}	781	812	846	879
N_V	739	768	798	827
O_I	322±2	(340)	(360)	(378)
O_{II}	260	(275)	(292)	(309)
O_{III}	195±4	(196)	(202)	(207)
O_{IV}	106	108±2	113	116
O_V	97	98	103	105

transitions between inner levels. Thus, the final states available to an s-electron, for example, may be quite different from those for a p- or d-electron. Parratt (15) has suggested that the electron states involved in transitions very close to the absorption edge are those of the ionized atom caused by the removal of the electron involved in the transition. Thus, these are states which do not even exist in the normal, un-ionized atom. All of this introduces an uncertainty, of the order of a few electron volts, into the zero point of energy for levels computed by the present method.

Nordling and Hagström (16) have measured the binding energies of the L_{III}, L_{II} to L_V inclusive and N_I to N_V inclusive levels of uranium using the photo electron method, in which the energy of the photo electron ejected by a photon of known energy is measured. After correcting for the work function of the source, this method yields binding energies referred to the Fermi level. Their results agree with those of the present investigation within experimental error (about 1 ev).

Chemical bonds are known to affect measured values of absorption edges, again due to changes in the energy levels available to the ejected electron. Changes as large as 10-20 ev have been observed. Again, the agreement of the present results with those of Nordling and Hagström, who used a metallic U source, suggest that the oxides used in this investigation do not shift the levels by more than 1 ev.

Using the transitions included in table II it is possible to compute binding energies for all the levels listed in table III, but only for the case of uranium. Indeed, even this would not be possible if it were not for the presence of the forbidden (for dipole transitions) line $L\beta_9$ which, together with the $L\alpha_1$, permits the calculation of the L_I level, and hence of all levels for which there is a transition involving L_I.

Since the $L\beta_9$ and several other lines were not measurable in the other spectra, the other levels for these elements had to be estimated. These estimated values are included in table III enclosed in parentheses. Fortunately, at least two sub-levels in each major shell (L, M, N, O) could be computed directly, so that the values for the other sub-shells could be estimated by using well known splitting formulas based on the Dirac relativistic eigenvalues for the hydrogen atom.

The binding energy of an electron in a hydrogen-like atom, as derived using the Dirac equation (17), may be written in terms of the Rydberg as

$$\frac{\nu}{R} = \frac{2}{\alpha^2}\left\{\left[1 + \left(\frac{\alpha Z}{n-k+\sqrt{k^2-\alpha^2Z^2}}\right)^2\right]^{-1/2} - 1\right\}, \qquad (5.1)$$

where n is the principal quantum number and $k = j+1/2$, j being the usual total angular momentum quantum number. It

has been found* that the energy levels of more complicated atoms may be estimated from this formula if Z is replaced by an effective nuclear charge Z-s, where s represents the screening effects of the other electrons in the atom and is, in general, different for each sub-level of the atom but a very slowly varying function of Z. Since the binding energy depends only on j and not on ℓ, it can be seen that the energy difference between adjacent levels with the same j must be due to the difference in the screening constant, s, for the two levels. Indeed, it can be shown that, to first order, the difference in the square roots of the energy of such a "screening doublet" is given by

$$\sqrt{\frac{\nu}{R}} - \sqrt{\frac{\nu'}{R}} \approx \frac{s'-s}{n} \quad . \tag{5.2}$$

This formula was used to compute the splitting of the following levels using values of s'-s obtained from existing data (18): M_I-M_{II}, M_{III}-M_{IV}, N_I-N_{II}, N_{III}-N_{IV}, O_I-O_{II} and O_{III}-O_{IV}. In each case it was found that for $Z > 80$, s'-s can be considered to be a constant within the required precision.

The splitting of spin-doublets (levels with the same ℓ but different j) cannot be accurately represented by expansions of equation 5.1, and so the entire expression must be

---

*Compton and Allison, op. cit., p. 583.

used. It has been found, however, that satisfactory agreement with experiment may be obtained by assigning, for splitting computations only, the same screening constant to the two levels involved. In practice, the splitting was computed as a function of Z using equation 5.1 with s = 0. The result was plotted on translucent graph paper using a suitable scale. This was then placed over a second graph on which the presently available data were plotted, and the ordinates of the two graphs moved with respect to one another until the two curves coincided. The theoretical curve was then used to extrapolate the experimental data. This technique was used for the M_{II}-M_{III} splitting in Np and the N_{II}-N_{III} splitting of Np, Pu and Am. A splitting constant of 8.04 for M_{II}-M_{III} and 17.5 for N_{II}-N_{III} was found to give satisfactory agreement with the experimental data. The O_{II}-O_{III} splitting was estimated from a Moseley plot.

None of the splitting estimates discussed above are believed to introduce errors of greater than 1 ev. Since the L_{III} levels were measured to an accuracy of 1 ev, it is believed that all energies obtained directly from appropriate emission lines are accurate to $\pm$ 1 ev, and that those obtained by using one or more splitting estimates, are accurate to about $\pm$ 3 ev.

It is interesting to compare the present results with values obtained by extrapolating previously available results to higher atomic numbers using the Moseley extrapolation (19). In general the values are within 20 ev of one

another, although occasional discrepancies as high as 40 ev can be found.

S. Cohen (20) has recently attempted a relativistic self-consistent calculation of the wave functions and eigenvalues for heavy atoms. His results for uranium agree with the present experimental values only to about 1 part in 200, the computed values being consistently lower than the experimental ones.

B. The Theory of the L_{II}-L_{III} Energy Level Difference

The L_{II}-L_{III} energy level difference has attracted considerable attention for some time. Binge (21) suggested that equation 5.1 could be used to evaluate the constant $\alpha = e^2/(\hbar c)$. For this splitting the equation becomes the well known Sommerfeld formula

$$\frac{\Delta\nu}{R} = \frac{1}{\alpha^2}\left\{\sqrt{4-\alpha^2Z^2} - [2+2\sqrt{1-\alpha^2Z^2}]^{1/2}\right\} = \frac{2}{\alpha^2}\, S(\alpha Z) \ . \qquad (5.3)$$

As discussed in Part V-A, satisfactory agreement with theory could be obtained only by introducing a screening constant s defined in such a way that the level splitting is given by $S[\alpha(Z-s)]$. It was found that the value of the screening constant calculated from the experiments was about 3.5 for the heaviest atoms and did not vary appreciably with atomic number above Z = 60. However, the value of s and its Z dependence were found to be altered when different values of α were used in the computations.

Christy and Keller (22) pointed out that the field which acts on an electron in a heavy atom is certainly not a pure coulomb field, and that this circumstance could not be corrected for by introducing an uncalculable screening constant into a formula derived assuming a coulomb field. Furthermore, they pointed out, an increase in nuclear charge itself produces distortions in the wave functions of the electrons, and not just a change of scale as in the non-relativistic theory even in the case of a pure coulomb field. Thus, the screening constant approach could not be expected to be useful in obtaining a value of α from experimental data.

In order to correct the Sommerfeld formula for the effects of the other electrons in an atom, Christy and Keller estimated these effects by a perturbation computation using Dirac wave functions for a coulomb field of charge Ze as the unperturbed wave functions. Their computation included electrons in the K-, L- and M-shells and the result can be expressed in the form

$$\frac{\Delta\nu}{R} = \frac{2}{\alpha^2} S(\alpha Z) - 2\alpha^2 Z^3 f(\alpha Z) - 2(0.0178)\alpha^4 Z^5 + BZ^2 = \phi(\alpha Z) + BZ^2, \quad (5.4)$$

where $f(\alpha Z)$ can be obtained from table II of their paper and B is a small constant to be determined from experimental data. $f(\alpha Z)$ is estimated by Christy and Keller to be accurate to better than 1%, and Shacklett (1,2) has shown that it can be computed with precision consistent with its

estimated accuracy by Lagrange interpolation of log $f(\alpha Z)$ expressed as a function of $1-(1-\alpha^2Z^2)^{1/2}$. The interpolation formula, as derived by Shacklett, is

$$\log[10f(\alpha Z)]\ C_o + C_1X+C_2X^2-C_3X^3+C_4X^4 \qquad (5.5)$$

with

$$C_o = 6.794690 \times 10^{-1}$$
$$C_1 = 6.83439 \times 10^{-3}$$
$$C_2 = 2.648 \times 10^{-5}$$
$$C_3 = 5.26 \times 10^{-7}$$
$$C_4 = 1.09 \times 10^{-8}$$

and with

$$X = 100[1-(1-\alpha^2Z^2)^{1/2}] \ .$$

Although the value of α obtained from the L_{II}-L_{III} difference is not sufficiently precise to affect the presently accepted value from the highly precise atomic beam measurements of Triebwasser, Dayhoff, and Lamb on deuterium (23), the Christy-Keller corrections have served as a valuable approximation to be compared with experimental data, as will be discussed shortly.

Since the $2p_{1/2}$ and $2p_{3/2}$ electronic wave functions differ in their behavior in the vicinity of the nucleus, the finite nuclear size may be expected to affect these wave functions in different amounts, and thus to affect the

L_{II}-L_{III} energy difference. Schawlow and Townes (24) have considered this effect and computed its contribution to the splitting. Their purpose was to estimate the nuclear radius by comparing existing X-ray data with the Christy-Keller formulas discussed above, and by choosing a nuclear radius which could account for the observed discrepancies. For $R = r_o A^{1/3}$, where R is the nuclear radius and A the atomic mass number, Schawlow and Townes concluded that $r_o = (2.1 \pm 0.2) \times 10^{-13}$ cm, which is to be compared with the value of $r_o \cong 1.2 \times 10^{-13}$ cm obtained from other experiments (25). In an attempt to improve the X-ray data which was used to arrive at this seemingly anomalous result, Shacklett initiated the research described in references 1 and 2. Using the same assumptions as Schawlow and Townes, Shacklett arrived at the value $r_o = 1.08 \times 10^{-13}$ cm using his values of the L_{II}-L_{III} difference as computed from the $L\alpha_2$ and $L\beta_1$ lines of six elements from Z = 74 to Z = 94. However, other factors affecting this splitting have been pointed out so that even this value of r_o cannot be considered significant. The work of Schawlow and Townes is sufficiently comprehensive so that an estimate of the contribution to the L_{II}-L_{III} splitting caused by finite nuclear size may be obtained from their paper. Shacklett has shown that the result may be written in the form

$$\Delta E/h\Delta\nu = -De^{b(Z-60)} , \qquad (5.6)$$

where, for $r_o = 1.2 \times 10^{-13}$ cm, $D = 0.54 \times 10^{-4}$ and $b = 0.0878$. In this expression, $h\Delta\nu$ is the splitting without nuclear size and ΔE is the contribution caused by nuclear size.

Three corrections from quantum electrodynamics contribute to the splitting, and must be included before comparison with experiment is meaningful. The first of these is due to the anomolous magnetic moment of the electron. If μ_e is the electron moment and μ_o the Bohr magneton the theory (26) until recently has given

$$\mu_e/\mu_o = (1 + \frac{\alpha}{2} - 2.973 \frac{\alpha^2}{2}) \quad . \tag{5.7}$$

This has recently been corrected by Petermann (27), by Sommerfield (28) and finally also by Kroll to yield a value some 14 ppm larger than this value. Using $\alpha^{-1} = 137.037$, we have

$$\mu_e/\mu_o = 1.001159 \quad . \tag{5.8}$$

Now the splitting of the $2p_{1/2}$ and $2p_{3/2}$ levels may be thought of as being due to two effects (neglecting for the moment the small corrections due to nuclear size and the other quantum electrodynamical effects), (1) the magnetic interaction between the anomolous electron magnetic moment, μ, and the orbital magnetic moment, resulting in a splitting proportional to 2μ; (2) the Thomas precession resulting in

a splitting proportional to $-\mu_o$ (the Bohr magneton without anomolous correction). Thus, the theoretical splitting values must be multiplied by a factor

$$2\mu_e/\mu_o - 1 = 1.002318 \ . \qquad (5.9)$$

The second correction from quantum electrodynamics is due to the effect of vacuum polarization. Wichmann and Kroll (29) have made an accurate determination of this contribution to the L_{II}-L_{III} splitting, and present the results as $\delta_p^{(1)}$ in table I of their paper. Shacklett found that the fraction $\delta_p^{(1)}/(\Delta\nu/R)$ could be represented accurately by the formula

$$\delta_p^{(1)}/(\Delta\nu/R) = Ve^{c(Z-60)} \ , \qquad (5.10)$$

with $V = 1.73 \times 10^{-4}$ and $c = 0.0462$.

The last known correction is due to the so-called "Lamb Shift." Unfortunately, this contribution has not yet been evaluated for the region of interest, due mainly to the difficulty in the computations for $\alpha Z \approx 1$. It is, however, expected to cause a decrease in the splitting.

C. The L_{II}-L_{III} Energy Level Difference--Comparison of Theory with Experiment

The measured values of the fine structure splitting as found from the data of table II are shown in table IV. The

TABLE IV. Experimental values of the fine structure splitting

Element	$\Delta\nu/R$	Relative error (ppm)
$_{74}W$	98.275 ± 0.004	± 37
$_{78}Pt$	125.599 ± 0.008	± 64
$_{83}Bi$	168.511 ± 0.007	± 42
$_{90}Th$	249.364 ± 0.009	± 34
$_{92}U$	277.936 ± 0.006	± 17
$_{93}Np$	293.305 ± 0.012	± 41
$_{94}Pu$	309.435 ± 0.012	± 39
$_{95}Am$	326.335 ± 0.019	± 58

values obtained by Shacklett (1,2) for Z = 74, 78, 83 and 90 are also included, since the present investigation is a continuation of his work. The values for W, Pt, Bi, Th, Np and Pu were obtained from a single pair of spectral lines in each spectrum, namely the $L\beta_1$-$L\alpha_2$ difference. The value for U was derived from four pairs, namely the $L\beta_1$-$L\alpha_2$, $L\gamma_1$-$L\beta_{15}$, $L\gamma_5$-$L\beta_6$ and the $L\eta$-$L\ell$ differences, each value being weighted inversely as its probable error. The Am difference was obtained from the $L\beta_1$-$L\alpha_2$ and the $L\gamma_1$-$L\beta_{15}$ differences.

Values involved in the computation of the splitting are shown in table V. Included in the table are values of $\phi(\alpha Z)$, computed using equations 5.3, 5.4 and 5.5 and corrected for the anomolous moment, together with $\Delta E/h\Delta\nu$ and $\delta p^{(1)}/(\Delta\nu/R)$, each expressed in terms of relative parts per million. Now, the only calculable term in the theoretical value of the fine structure not included in table V is the term BZ^2 in equation 5.4. If B is now adjusted by a least-squares adjustment to minimize the differences between theory and experiment using only the data in table IV it is found that $B = 4.671 \times 10^{-4}$. Using this value of B, the remaining discrepancies between theory and experiment may be computed, with the results shown in figure 17. In drawing any conclusions from such a computation, it must be remembered that the quantity $f(\alpha Z)$ in equation 5.4 is only considered to be accurate within 1%. The solid curves of figure 17 are roughly the values which would have been

TABLE V. Theoretical values entering into the computation of the fine structure splitting.

Atomic number	$\phi(\alpha Z)$ (Rydbergs)	$\Delta E/h\Delta\nu$ (ppm)	$\delta_p^{(1)}/(\Delta\nu/R)$ (ppm)
74	95.651	-184	+330
78	122.689	-264	+396
83	165.224	-409	+500
90	245.588	-750	+689
92	274.066	-890	+760
93	289.377	-980	+790
94	305.447	-1060	+830
95	322.330	-1160	+870

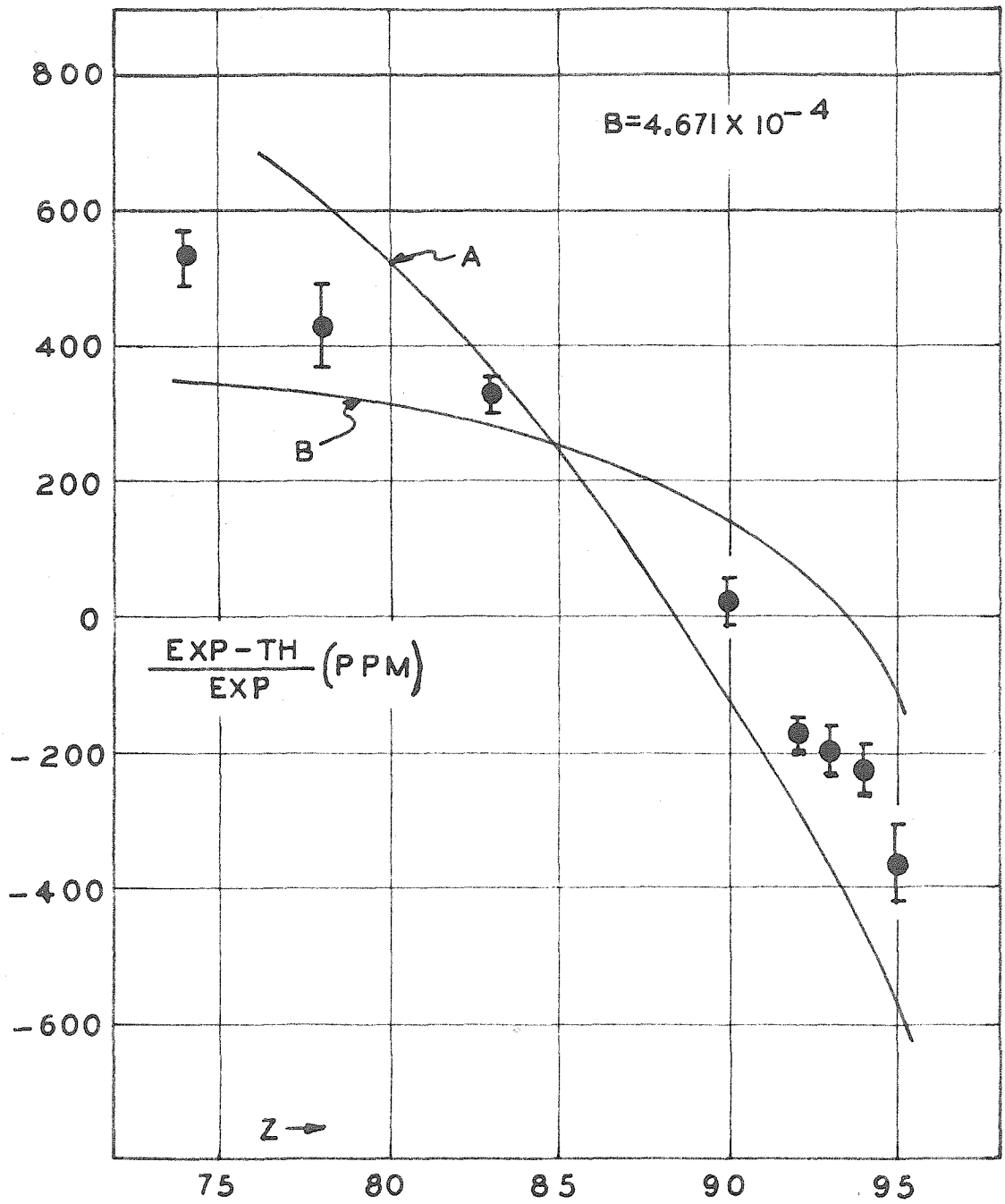

Figure 17. Deviation between theory and experiment using only the data of Shacklett and Merrill. The solid curves A and B are roughly the values which would have been obtained if f were 1/2% higher or lower, respectively.

obtained if f were changed by $\pm$ 1/2% — + 1/2% for curve A and - 1/2% for curve B. It appears from figure 17 as if there were an additional term needed in the theory which would cause a relative decrease in the splitting for high atomic numbers, which at least may qualitatively be due to the Lamb shift. The magnitude of this term, however, is highly uncertain, due to the uncertainties in $f(\alpha Z)$.

All of the above considerations do not take into account the work of other investigators. Bergvall and Hagström (30) have recently concluded a measurement of the atomic level energies in the rare earth elements using the photo electron method. Their results for the L_{II}-L_{III} difference are claimed to be accurate within $\pm$ 0.05%. For the elements included in their study (Z = 57 to 71) the effects of nuclear size, vacuum polarization and Lamb shift should be negligible, so that the splitting should be given accurately by equation 5.4, corrected only for the effect of the anomolous electron moment. Thus we should be able to adjust the Christy-Keller formula to agree with the data in this range, and then to use this value of B to gain a meaningful estimate of these other corrections using the data of the present investigation.

It was found, however, that an adjustment of the Christy-Keller formula to their experimental data was possible only within $\pm$ 0.3% on the assumption of a constant value of B. By calculating the value of B needed to give exact agreement between theory and experiment for each

element, they arrived at the results shown in figure 18, where the results of the present investigation, uncorrected for vacuum polarization or nuclear size, are included. From figure 18 it is tempting to assume that B varies linearly with Z, the deviation from this rule for high Z being due to the neglected correction terms due to vacuum polarization, nuclear size, and Lamb shift. Fitting the data of figure 18 for $Z < 73$ with a straight line, weighting each point proportional to Z^2, yields

$$B = (2.85 + 0.028Z) \times 10^{-4} . \qquad (5.11)$$

This is the straight line plotted on figure 18. If these values of B are then used in equation 5.4, the resulting deviations between theory and experiment are shown in figure 19.

It was found that the data of Bergvall and Hagström could be represented, within the limits of experimental error, by assuming a constant B, and an error in $f(\alpha Z)$ of -2.5%. This was discovered by adding to equation 5.4 a term given by $\beta f(\alpha Z)$, and then adjusting β and B by least squares. The value of B obtained in this manner was 3.69×10^{-4} and β turned out to be .025. There was very little latitude in the choice of β if B were not allowed to be a function of Z. For example, $\beta = .013$ gave a root mean square deviation between theory and experiment some two times as large as the experimental errors. Figure 19 also shows the results

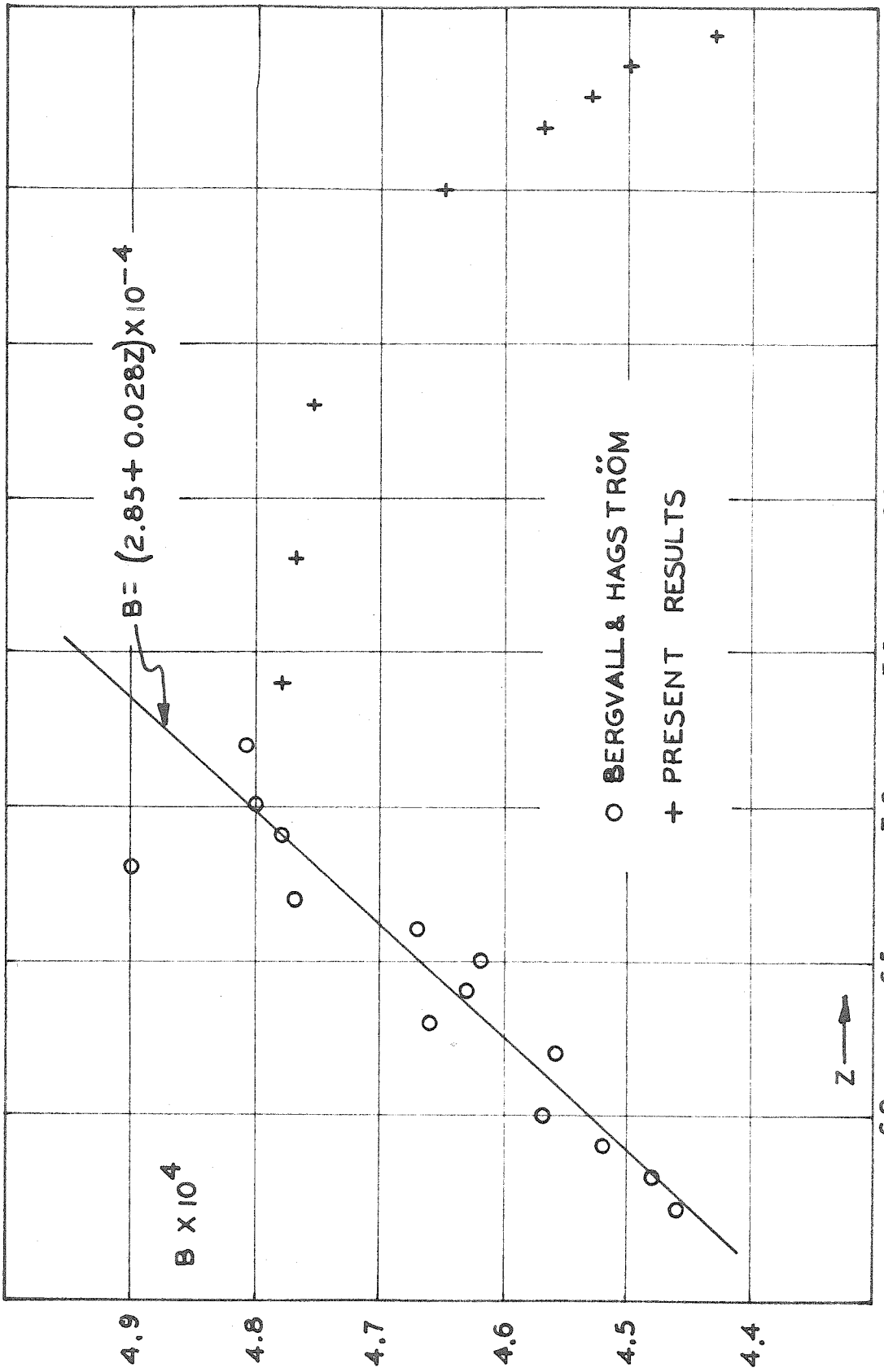

Figure 18. B vs Z according to the results of Bergvall and Hagström and the present investigation.

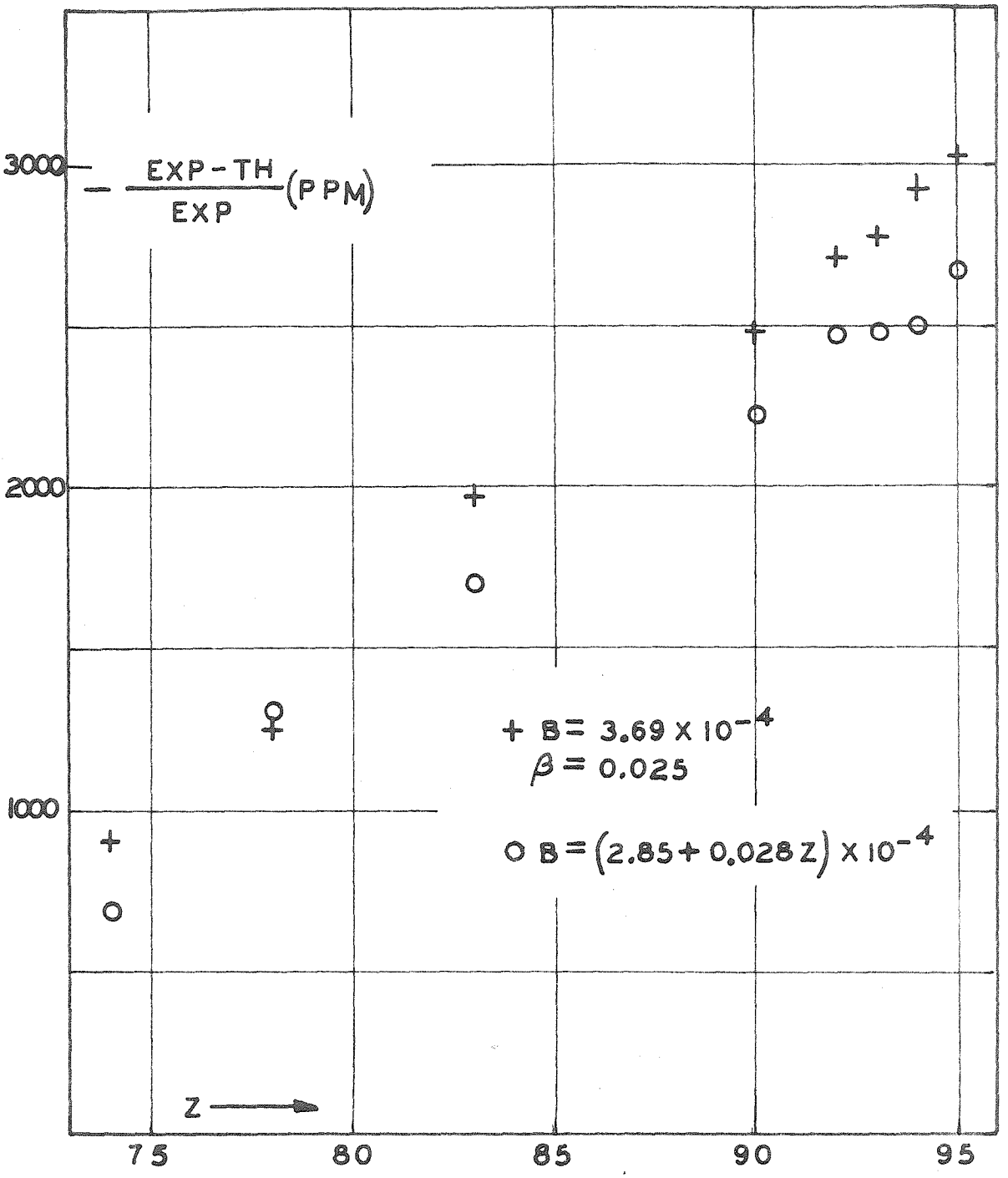

Figure 19. Deviations between theory and experiment using extrapolations from the data of Bergvall and Hagström. Note that the experimental values are consistently below the theoretical.

of extrapolating the theory to higher atomic number using these values of B and β.

Both sets of data shown in figure 19 show considerably larger deviations than were obtained using the present measurements alone, and demonstrate that there are still deviations between theory and experiment which are of the order of 0.1% to 0.3%, and which hopefully could be removed or at least reduced by further refinements of the theory.

Professor L. C. Biedenharn of Rice Institute hopes to attempt such a theoretical refinement in the near future, possibly with the help of the new electronic digital computer at present under construction there.

D. Line Widths

Theoretical estimates of X-ray line widths have been accomplished for only a very few transitions in isolated atoms, none of which are included in the present investigation. Such calculations are extremely tedious, since the width of a particular state depends upon the total transition probability involving the state, including both radiative and non-radiative transitions. The line width is then the resultant of the widths of the two states involved in the transition.

However, some features of the experimental widths included in table II are worthy of special note. These will be described in the following material. Qualitative explanations will be offered which could account for the observed features. These, however, should be regarded only as tentative suggestions pending a more complete theoretical treatment of the problem.

In addition to the data included in table II, the author had at his disposal the experimental data of Shacklett (2), from which the line widths of the $L\beta_1$ and $L\alpha_2$ lines of W, Pt, Bi and Th were obtained. These data, together with the widths of the same lines taken from table II, are shown in figure 20, where $(\Delta\nu/R)^{1/2}$ is plotted as a function of atomic number for these two lines. Note that the $L\alpha_2$ widths lie, within experimental accuracy, on a straight line. The $L\beta_1$ widths, however, are best represented

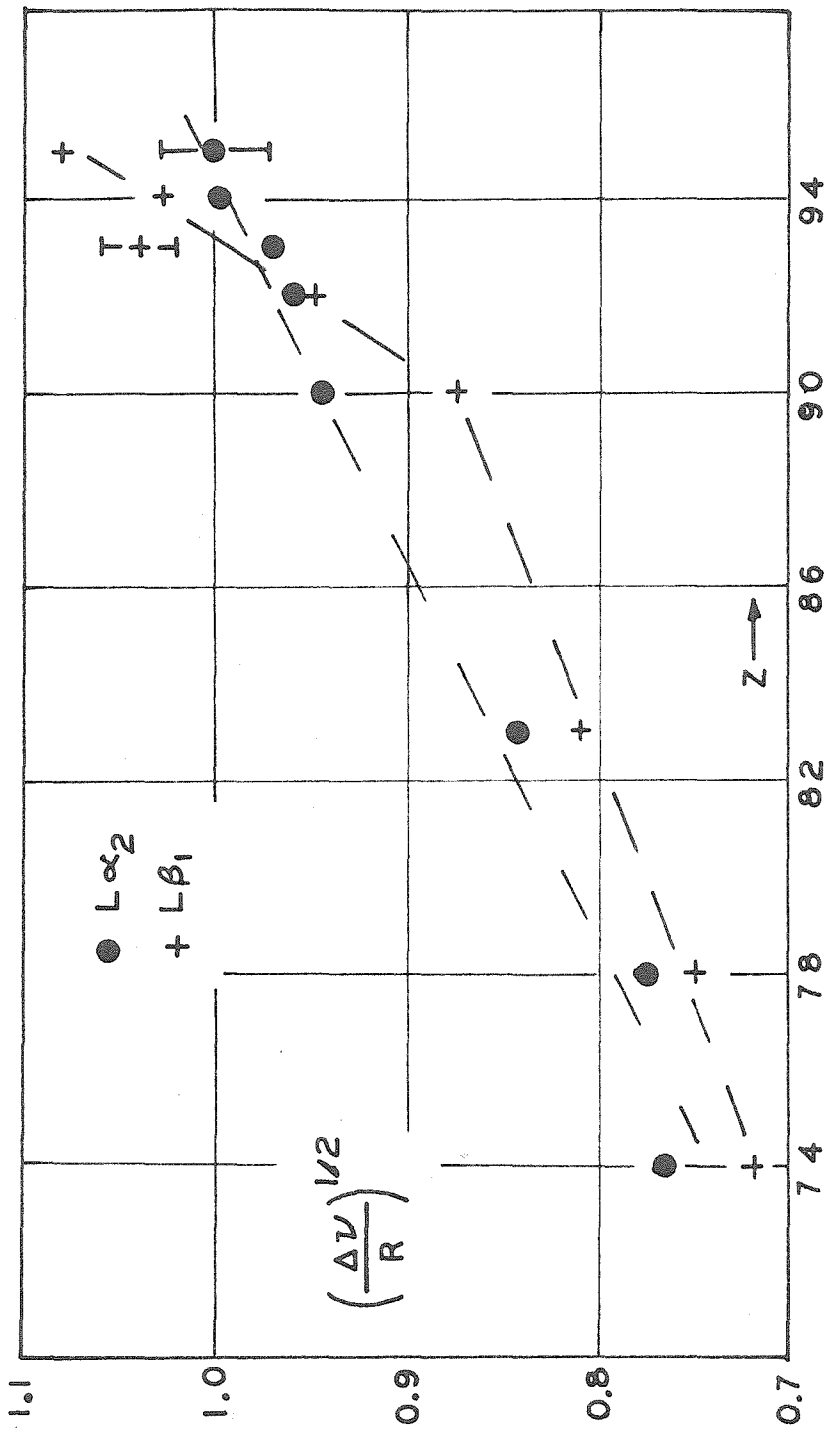

Figure 20. Widths of the $L\beta_1$ and $L\alpha_2$ lines as a function of atomic number.

by a broken line, the slope for $Z \geq 90$ being considerably greater than the slope for $74 \leq Z \leq 90$. Finally, note that the Np $L\beta_1$ line is considerably broader than one would expect by interpolation of nearby values. All of these differences between the behavior of these lines must be due to differences in the L_{II} and L_{III} levels, since the final state involved in the two transitions is in both cases the same, namely the M_{IV} level.

The dramatic increase in the width of the $L\beta_1$ line relative to the $L\alpha_2$ for high atomic number may be explained by considering Auger transitions of the Coster-Kronig type; that is, transitions in which, for example, an L_{II} excited state decays to an L_{III} excited state with the emission of an electron from the M_V level ($L_{II} \rightarrow L_{III}M_V$). The result, in this example, is the same as if an M_V electron had dropped to the L_{II} level with the resulting energy being absorbed by an electron in the L_{III} shell. Such transitions furnish an additional mode of decay for the excited atom, and thus they will increase the transition probability, and hence the width, of the state and will be observed as an increase in width of any line involving this state. Coster-Kronig transitions are energetically possible only for certain elements. The transition $L_I \rightarrow L_{III}M_V$; for example, is possible only if the L_I-L_{III} energy difference is greater than the binding energy of an M_V electron in the ionized atom, which can be estimated by assuming it to be equal to the

binding energy of the M_V electron in the atom of atomic number Z+1.

If energy calculations are made, it is found that the transition $L_{II} \rightarrow L_{III}M_V$ is energetically possible only for $Z < 30$ or $Z > 90$. Outside the range $30 < Z < 90$ therefore the possibility of this Coster-Kronig transition would cause an increase in width for lines involving the L_{II} level and, in particular, would increase the width of the $L\beta_1$ and thus explain the sudden increase in slope of the $L\beta_1$ width curve of figure 20. This explanation is enhanced by the observation that the increase of the $L\beta_1$ width seems to be quite abrupt, indicating that something new is added to the situation at about Z = 90. A more gradual change would be expected if the observed increase were due, for example, to the finite nuclear size or to distortions of the electronic wave functions from increased nuclear charge.*

This does not account, however, for the extremely large value of the Np $L\beta_1$ width. This same result is obtained from other lines involving the L_{II} level, as shown in figure 21. In each case the data may be represented by a smooth curve except for the case of Np. In each case, the

---

*For large atomic numbers, $s_{1/2}$ and $p_{1/2}$ level wave functions behave more and more alike. Now the $2s_{1/2}$ level is considerably broader than the $2p_{1/2}$, mainly due to the effects of Auger transitions. Thus, we would expect the L_{II} level to become broader, relative to the L_{III}, as Z increases. This should, however, be more gradual than observed in the present research.

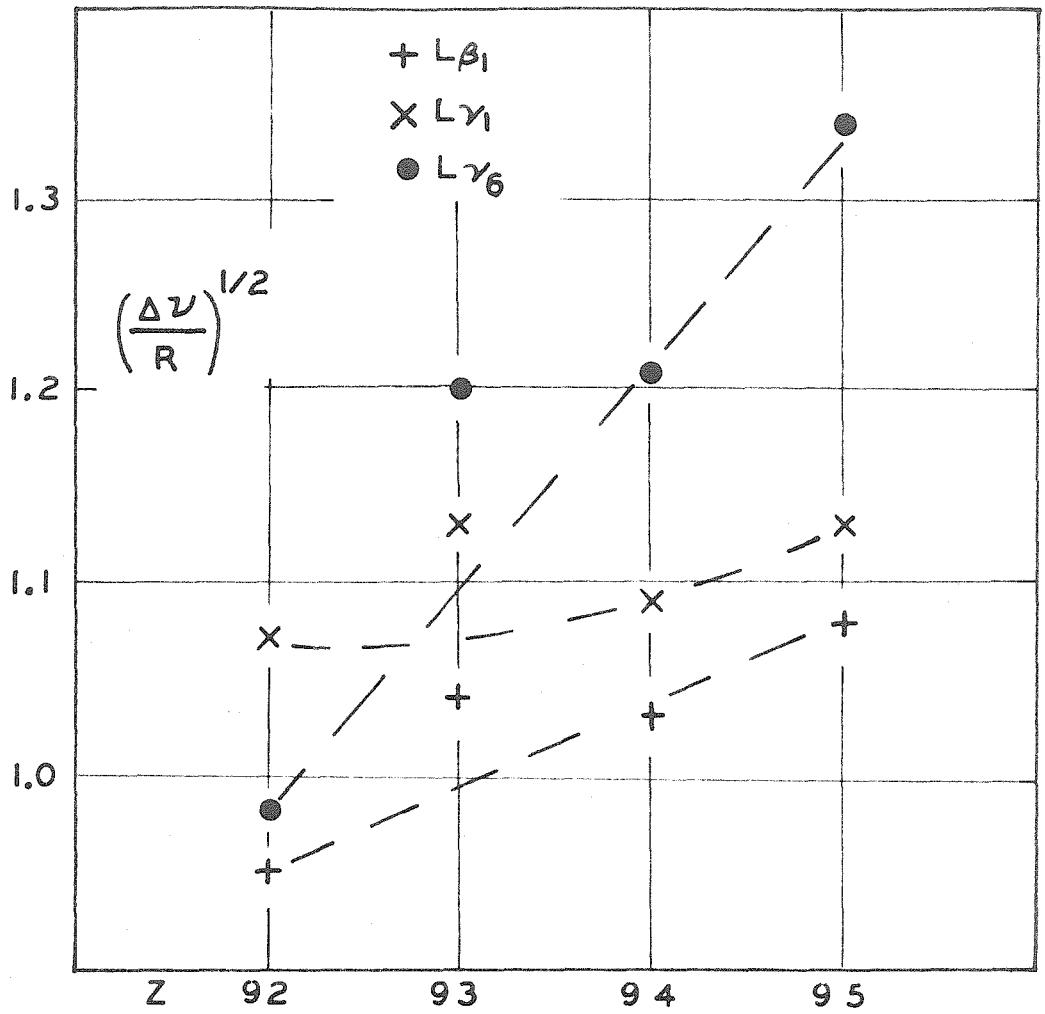

Figure 21. Widths of three lines involving the L_{II} level as a function of atomic number.

deviation between the smooth curve and the Np result is several times the estimated experimental error. Furthermore, this result is not obtained for lines involving the L_{III} level, for which the Np results lie on the smooth curve passed through the other points. Unfortunately, the experimental uncertainties in the widths of lines involving the L_I level are so large as to mask any deviations of comparable magnitude.

A possible explanation of this phenomenon is that the additional width of the Np lines is due to hyperfine splitting of the L_{II} level, caused by the interaction of the electron magnetic moment with the nuclear magnetic moment. The Np sample used in this investigation was mainly Np^{237} which has a nuclear magnetic moment of about 6.0 nuclear magnetons (31). The other samples were mainly U^{238} with $\mu=0$, Pu^{239} with $\mu=0.4$ (31), and Am^{241} with $\mu=1.4$ (32). Thus the Np moment is considerably larger than that of its immediate neighbors in the data of this research.

Unfortunately, a theoretical treatment of hyperfine splitting for relativistic atomic electrons is not available. Nonrelativistic theory* yields the following value for the maximum splitting of hyperfine levels for $\ell \neq 0$ and $j < I$, where I is the nuclear spin:

$$E = 2\alpha^2 \frac{m}{M_p} g \frac{\ell(\ell+1)}{j+1} \left(I+\frac{1}{2}\right) a_o^3 \overline{\frac{1}{r^3}} \text{ Ry} . \qquad (5.12)$$

If relativistic hydrogen-like wave functions are used to esti-

*Bethe and Salpeter, loc. cit., pg. 110.

mate the expectation value of $1/r^3$, a rough value of the expected splitting may be obtained. For the $2p_{3/2}$ (L_{III}) level the integration is straightforward and yields $\Delta E \approx$ .016 Ry, assuming I = 5/2 and g = 12/5. The corresponding value for the $2p_{1/2}$ (L_{II}) level is, however, divergent, due to the behavior of the wave function near the origin. If the nuclear radius is used as the lower integration limit, the computation yields $\Delta E \simeq 0.74$ Ry. This latter value was computed by integrating the "large" component of the wave function analytically and the "small" component numerically. It is interesting to note that the contribution to $\overline{1/r^3}$ of the small component is about 80% of the total value.

In view of the uncertainties in the theoretical estimates, the agreement with the data of this investigation is most remarkable. The calculated splitting for the L_{III} level is too small to be detected and none is observed. The calculated splitting for the L_{II} level is about six times the observed value, but 4/5 of this comes from the small component of the relativistic wave function. It is expected that the parts of equation 5.12 which are derived from expected values of angular momentum and spin operators should be modified to treat more realistically the relativistic wave functions, and that this modification would be especially significant for the contribution of the small component.

It is believed that this is the first experimental observation of the hyperfine splitting of X-ray lines.

APPENDIX A

THE EFFECT OF THE MONOCHROMATIC ANTIPARALLEL PROFILE ON THE OBSERVED WIDTHS OF SPECTRAL LINES

Neglecting the effects of vertical divergence and crystal misalignment, the monochromatic profile of the two-crystal spectrometer in the antiparallel position can be shown to be

$$P(t) = \int_{-\infty}^{\infty} I(\ell)\, I\,(t-\ell)\, d\ell \qquad \text{(A-1)}$$

where $I(\ell)$ is the single crystal diffraction pattern given by equation 2.1 and $t = (\beta - 2\theta)\,\frac{\sin 2\theta}{\delta}$. For $t >> F/Z$ we may write approximately

$$P(t) \approx \int_{-\infty}^{\infty} I(\ell) I(t)\, d\ell + \int_{-\infty}^{\infty} I(t) I(\ell)\, d\ell = 2I(t) \int_{-\infty}^{\infty} I(\ell)\, d\ell \qquad \text{(A-2)}$$

using the fact that $I(\ell)$ is roughly a constant over the range that $I(t-\ell)$ has appreciable area, and vice versa. Now $\int I(\ell)\, d\ell$ is a constant equal to $4/3$ for the Darwin pattern, which neglects absorption. Furthermore, $I(t) \approx \frac{a^2}{2t^2}$ under the same assumptions, where $a = \frac{F}{Z}\sqrt{2}$. Thus we may write

$$P(t) \approx \frac{4a^2}{3t^2} \qquad \text{(A-3)}$$

for $t >> a$.

In order to analyze the effects of the monochromatic profile on a spectral line, it is convenient to divide $P(t)$

into two parts, namely

$$P(t) = W(t) + \Delta P(t) \quad . \tag{A-4}$$

In this expression W(t) is a "witch" chosen to have the same asymptotic behavior as P(t) for large values of t. That is

$$W(t) = A\left(1 + \frac{t^2}{w^2}\right)^{-1} \tag{A-5}$$

where

$$Aw^2 = \frac{4}{3} a^2 \quad . \tag{A-6}$$

$\Delta P(t)$ is the difference between P(t) and W(t) and will have significant values only within a relatively small region around t = 0. The constants A and w may be chosen, within the restriction of equation A-6, to make P(t) as small as possible even in this region.

Assuming a spectral line in the form of a witch, namely

$$L(\lambda) = B\left(1 + \frac{(\lambda-\lambda_o)^2}{\Delta\lambda^2}\right)^{-1} \tag{A-7}$$

The spectrometer output becomes

$$E(t) = \int_{-\infty}^{\infty} P(t-x)\, L^*(x)\, dx \quad , \tag{A-8}$$

where $L^*(x)$ is the witch $L(\lambda)$ expressed in terms of angular variables, namely

$$L^*(x) = B^* \left[1 + \frac{x^2}{b^2}\right]^{-1} \qquad \text{(A-9)}$$

where $B^* = \frac{Bd\delta}{2\sin\theta}$ and $b = \frac{d\delta}{2\sin\theta}\Delta\lambda$

In terms of $W(t)$ and $\Delta P(t)$ equation A-8 becomes

$$E(t) = \int_{-\infty}^{\infty} W(t-x)L^*(x)dx + \int_{-\infty}^{\infty} \Delta P(t-x)L^*(x)dx \ . \qquad \text{(A-10)}$$

The first integral in equation A-10 may be done exactly, and the second may be adequately estimated by a numerical integration which need only extend over the region in which $\Delta P(t-x)$ is significant. Thus

$$E(t) = \pi AB^*\left(\frac{bw}{b+w}\right)\left[1 + \frac{t^2}{(b+w)^2}\right]^{-1} + \sum \frac{B^*}{1+\frac{x^2}{b^2}} \Delta P(t-x)\Delta x. \qquad \text{(A-11)}$$

The advantage of this method over a complete numerical integration is that the main contributions may be done exactly, including the tails of all functions, and the less precise numerical work used only for a correction term.

In the present analysis, the values of $P(t)$ for $t \leq 2.13$ were taken from reference 7. $E(t)$ was evaluated, using equation A-11 for several different values of b. The procedure was checked by using three different choices of

A and w, and two values of Δx, namely 0.1 and 0.05. The full widths at half maximum height of these profiles were measured, with results as shown in figure 8 of Part II. In this figure the difference between the widths at half maximum of the observed profile and the spectral line, ΔW_e, expressed in terms of the width of the monochromatic profile, W_m, is plotted as a function of the width of the observed profile, W_{obs}, again normalized to W_m.

APPENDIX B

THE EFFECT OF HORIZONTAL AND VERTICAL DIVERGENCE AND IMPERFECT CRYSTAL ALIGNMENT[1]

Assume monochromatic incoming radiation of wavelength λ which is to be reflected in the first order by identical perfect crystals. In figure B-1, AB and CD are traces on the horizontal plane of two idealized Bragg reflectors mounted so that the angle β may be varied. The vector $\underline{r}$ is the unit vector along the incoming ray, $\underline{R}$ the unit vector in the direction of this ray after the first reflection. The vectors $\underline{n}_1$ and $\underline{n}_2$ are the unit vectors normal to the two reflecting planes. In the figure, only the projections of vectors and angles in the horizontal x-y plane are shown. The x axis makes the angle Θ with AB and the line EF makes the angle Θ with CD, where Θ is the Bragg angle corresponding to λ . The angle α is the angle between the horizontal projection of $\underline{r}$ and the x-axis (the measure of horizontal divergence). The angle ε is the angle between $\underline{R}$ and EF. Angles not shown in the figure are as follows: the angle ϕ between $\underline{r}$ and its horizontal projection (the measure of vertical divergence) and the angles δ_1 and δ_2 between $\underline{n}_1$ and $\underline{n}_2$ and their horizontal projections.

If d is the effective crystal spacing, the conditions

---

[1]This approach was suggested by work done by M. Shwarzchild in reference 33.

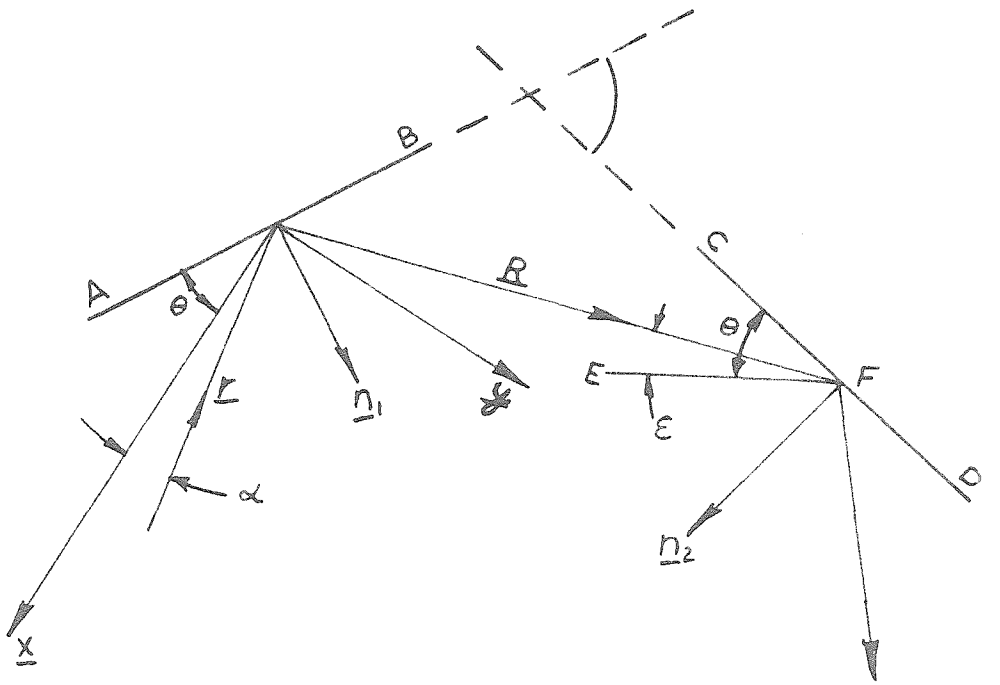

Figure B-1. Variables used in analyzing the effect of horizontal and vertical divergence and imperfect crystal alignment.

for first order reflection are

$$\underline{r} \cdot \underline{n}_1 = -\sin\theta = \frac{-\lambda}{2d} \qquad \text{(B-1)}$$

$$\underline{r} \cdot \underline{n}_1 = -\underline{R} \cdot \underline{n}_1 \qquad \text{(B-2)}$$

$$\underline{r} \times \underline{n}_1 = \underline{R} \times \underline{n}_1 \qquad \text{(B-3)}$$

and

$$\underline{R} \cdot \underline{n}_2 = -\sin\theta = \frac{-\lambda}{2d} = \underline{r} \cdot \underline{n}_1 \ . \qquad \text{(B-4)}$$

Operating on both sides of equation B-3 with $\underline{n}_1 x$ and substituting from equation B-2, we obtain

$$\underline{R} = \underline{r} - 2\underline{n}_1(\underline{n}_1 \cdot \underline{r}) \ . \qquad \text{(B-5)}$$

By operating on both sides of equation B-5 with $n_2 \cdot$, and using equation B-4 we derive

$$\underline{r} \cdot \underline{n}_1 = \underline{r} \cdot \underline{n}_2 - 2(\underline{n}_1 \cdot \underline{n}_2)(\underline{n}_1 \cdot \underline{r}_1) \ . \qquad \text{(B-6)}$$

To make these equations useful, we must write them in terms of the direction coordinates of the vectors involved. Thus

$$\underline{r} = -\cos\phi\cos\alpha\,\underline{i} - \cos\phi\sin\alpha\,\underline{j} - \sin\phi\,\underline{k} \qquad \text{(B-7a)}$$

$$\underline{n}_1 = \sin\theta\cos\delta_1\,\underline{i} + \cos\theta\cos\delta_1\,\underline{j} + \sin\delta_1\,\underline{k} \qquad \text{(B-7b)}$$

$$\underline{n}_2 = \sin(\theta+\beta)\cos\delta_2\underline{i} + \cos(\theta+\beta)\cos\delta_2\underline{j} + \sin\delta_2\underline{k} \qquad \text{(B-7c)}$$

Rewriting equation B-6 with the help of equations B-1 and B-7, we have

$$-\sin\theta = -[\cos\phi\cos\delta_1(\cos\alpha\,\sin(\theta+\beta)+\cos(\theta+\beta)\sin\alpha)+\sin\delta_2\sin\phi]$$
$$+ 2\sin\theta[\cos\delta_1\cos\delta_2(\sin\theta\sin(\theta+\beta)+\cos\theta\cos(\theta+\beta))+\sin\delta_1\sin\delta_2]$$

or

$$\sin\theta = [\cos\phi\cos\delta_1\sin(\theta+\alpha+\beta)+\sin\delta_2\sin\phi]$$
$$- 2\sin\theta[\cos\delta_1\cos\delta_2\cos\beta+\sin\delta_1\sin\delta_2]. \qquad \text{(B-8)}$$

Equation B-1 may be written as

$$\cos\phi\sin(\alpha+\theta)\cos\delta_1 = \sin\theta-\sin\delta_1\sin\phi \triangleq A' \qquad \text{(B-9)}$$

and from this we can deduce

$$\cos\phi\cos(\alpha+\theta)\cos\delta_1 =$$
$$\left\{\cos^2\phi\cos^2\delta_1-\sin^2\theta-\sin^2\delta_1\sin^2\phi + 2\sin\theta\sin\delta_1\sin\phi\right\}^{1/2} \triangleq B. \qquad \text{(B-10)}$$

Noting that

$$\sin(\alpha+\theta+\beta) = \sin\beta\cos(\alpha+\theta)+\cos\beta\sin(\alpha+\theta)$$

$$= \frac{B\sin\beta}{\cos\phi\cos\delta_1} + \frac{A' \cos\beta}{\cos\phi\cos\delta_1}$$

equation B-8 becomes

$$\sin\theta(1+2\sin\delta_1\sin\delta_2)-\sin\delta_2\sin\phi = B\sin\beta-A\cos\beta \triangleq C \qquad \text{(B-11)}$$

where

$$A = 2\sin\theta\cos\delta_1\cos\delta_2-A' = \sin\theta[2\cos\delta_1\cos\delta_2-1]+\sin\delta_1\sin\phi.$$

Dividing equation B-11 through by $(A^2+B^2)^{1/2}$ we obtain an expression of the form

$$\sin\beta\cos\nu -\cos\beta\sin\nu = \sin\eta \qquad \text{(B-12)}$$

where

$$\nu = \sin^{-1}\frac{A}{(A^2+B^2)^{1/2}} \quad \text{and} \quad \eta = \sin^{-1}\frac{C}{(A^2+B^2)^{1/2}} \qquad \text{(B-13)}$$

equation B-12 can be written as

$$\sin(\beta-\nu) = \sin\eta \qquad \text{(B-14)}$$

from which we may deduce

$$\beta - \nu - \eta = 0 \qquad \text{(B-15a)}$$

or

$$\beta - \pi + \eta - \nu = 0 \qquad \text{(B-15b)}$$

If we let

$$\sin \nu = \frac{A}{(A^2+B^2)^{1/2}} = \sin\theta + h_1 \qquad \text{(B-16a)}$$

and

$$\sin \eta = \frac{C}{(A^2+B^2)^{1/2}} = \sin\theta + h_2 \qquad \text{(B-16b)}$$

then

$$h_1 \approx \left(\frac{\phi^2}{2} + \frac{\delta_1^2}{2}\right) \sin\theta + \delta_1\phi(1-2\sin^2\theta) - \delta^2\sin\theta(1-\sin^2\theta) \qquad \text{(B-17a)}$$

and

$$h_2 \approx \frac{\phi^2}{2} \sin\theta - \phi(\delta_2 + 2\delta_1\sin^2\theta) + \sin\theta(2\delta_1\delta_2 + \frac{\delta_1^2}{2} + \delta^2\sin^2\theta) \qquad \text{(B-17b)}$$

neglecting terms higher than second order in the small angles ϕ, δ_1 and δ_2, and where $\delta^2 = \delta_1^2 + \delta_2^2$. Using equation B-16 to expand equation B-13 to second order by Taylor's Theorem, we get

$$\nu \cong \theta + \frac{h_1}{\cos\theta} \qquad \text{(B-18a)}$$

and

$$\eta \cong \theta + \frac{h_2}{\cos\theta} \qquad \text{(B-18b)}$$

Substituting these values in equation B-15 with the help of equation B-17 we get, finally, for the dihedral angles at which successive reflection can occur,

$$\beta_1 = 2\theta+\phi^2\tan\theta+\phi\left[\frac{\delta_1-\delta_2-4\delta_1\sin^2\theta}{\cos\theta}\right]+\tan\theta\left[2\delta_1\delta_2-\delta_2^2+2\delta^2\sin^2\theta\right] \qquad \text{(B-19a)}$$

$$\beta_2 = \pi + \frac{(\delta_1+\delta_2)}{\cos\theta}\,\phi - \tan\theta(\delta_1+\delta_2)^2 \quad . \qquad \text{(B-19b)}$$

APPENDIX C

LEAST SQUARES ANALYSIS OF EXPERIMENTAL LINE PROFILES

It is desired to find the "witch" which "best" fits the experimental data obtained in studying an antiparallel line profile. In actual practice, the spectrometer is set at an angular position, Θ_i, where a number of counts, say C_i, are accumulated. It is assumed that the background, B, and the peak intensity, P, are known and that the profile is in actuality a witch as observed experimentally, namely of the form

$$C_i = \frac{A}{1+\left(\frac{\Theta_c-\Theta_i}{a}\right)^2} + B \ , \qquad \text{(C-1)}$$

where $A = P-B$, Θ_c is the central angle and a is the half-width at half maximum intensity. Using equation C-1 it would be possible to estimate the central angle for each Θ_i using an arbitrary value of a. That is

$$\Theta_{ci} = \Theta_i \pm a\left(\frac{A}{y_i} - 1\right)^{1/2} \ , \qquad \text{(C-2)}$$

where $y_i = C_i - B$. If the i^{th} estimate is assigned a weight w_i, the weighted mean for the central angle would be

$$\overline{\Theta_c} = \frac{\sum_i w_i \Theta_{ci}}{\sum_i w_i} = \frac{\sum_i w_i[\Theta_i - a t_i]}{\sum_i w_i} = \frac{\sum_i w_i \Theta_i}{\sum_i w_i} - \frac{a\sum_i w_i t_i}{\sum_i w_i} \qquad \text{(C-3)}$$

where $t_i = \pm \left(\frac{A}{y_i} - 1\right)^{1/2}$. If there are n experimental points, the probable standard deviation of the weighted mean could be computed from the formula

$$\sigma_n = \left\{ \frac{\sum w_i(\theta_{ci} - \bar{\theta}_c)^2}{(n-1)\sum w_i} \right\}^{1/2} . \qquad (C\text{-}4)$$

Now it is possible to adjust the half-width, a, so that σ_n will be a minimum, thus yielding the most precise estimate of the central angle of the profile. The appropriate value of a can be shown to be

$$a = \frac{\sum w_i(\theta_i - \theta_o)(t_i - t_o)}{\sum w_i(t_i - t_o)^2} , \qquad (C\text{-}5)$$

where $\theta_o = \frac{\sum w_i \theta_i}{\sum w_i}$ and $t_o = \frac{\sum w_i t_i}{\sum t_i}$. θ_c can then be found from equation C-3 which may be written as

$$\bar{\theta}_c = \theta_o - a t_o , \qquad (C\text{-}6)$$

and finally, the standard deviation may be computed from equation C-4.

The only remaining concern is to assign appropriate weights to the experimental observations. Again assuming that the observed line has the shape of a witch, $y = A(1+t^2)^{-1}$, we may calculate the uncertainty, dt, in the horizontal position of a point due to an uncertainty, dy, in the value of y.

We have

$$t^2 = \frac{A}{y_i} - 1 \quad \text{and} \quad 2tdt = -\frac{A}{y^2}\,dy$$

$$\text{so that} \qquad dt = -\frac{A}{2ty^2}\,dy \ . \tag{C-7}$$

Now the weight attached to a given point will be taken to be inversely proportional to the square of the uncertainty in the measurement of t_i (and hence of θ_{ci}), namely

$$w_i = \frac{k'}{(dt)_i^2} = \frac{k\,t_i^2 y_i^4}{A^2 (dy_i)^2} \ . \tag{C-8}$$

The value of y_i is determined by the accumulation of c_i counts from which a background B has been subtracted. Therefore

$$dy_i = (c_i + B)^{1/2} = (y_i + 2B)^{1/2} \ , \tag{C-9}$$

and finally

$$w_i = k\left(\frac{A}{y_i} - 1\right)\left(\frac{y_i}{A}\right)^3 \left(\frac{y_i}{y_i + 2B}\right) \ . \tag{C-10}$$

It is interesting to note that in the case B = 0 the highest weight is given a point for which $A/y_i \approx 1.5$ ($t_i \approx .71$) and that the weight is down by a factor of 4

for $A/y_i \approx 4.6$ ($t_i \approx 1.9$). Thus, the important experimental points are within two half-widths of the center, and points farther out on the profile do not contribute significantly to our estimate of the central angle.

APPENDIX D

In the original copy of this thesis the pages indicated above contain the text of a published article:

"Precision Measurement of the L X-Ray Spectra of Uranium and Plutonium:

by John J. Merrill and Jesse W. M. DuMond

The Physical Review, vol. 110, No. 1, pp. 79-84 (1958)

Precision Measurement of the L X-Ray Spectra of Uranium and Plutonium*

JOHN J. MERRILL† AND JESSE W. M. DUMOND
California Institute of Technology, Pasadena, California
(Received November 20, 1957)

Twenty uranium L x-ray transitions have been measured using a commercial, sealed off, uranium target x-ray tube. Twelve plutonium L x-ray transitions have been measured in conventional x-ray fluorescence from a 5.86-g sample. All lines were measured with high precision using the two-crystal spectrometer, and corrected for the effects of temperature on the grating space of calcite, the effects of vertical divergence, and the effects of crystal diffraction pattern asymmetry. The wavelengths corresponding to these transitions are given in terms of the x-unit (where the latter is so defined that the wavelength of the Mo K_{α_1} line is 707.8490 x-units) with relative errors of less than 15 ppm (parts per million) in the case of U, and less than 30 ppm in the case of Pu.

I. INTRODUCTION

THE precision of recent measurements of the L spectrum of plutonium has been limited by the low available source intensities. Thus, Cauchois, Manescu, and Le Berquier[1] studied this spectrum using 10 mg of Pu, and Rogosa and Peed[2] used approximately 200 mg. The low intensities available from these samples using conventional x-ray fluorescence would not permit the use of the 2-crystal spectrometer. Both of these investigations were performed with curved crystal transmission spectrometers of the Cauchois type, an instrument with significantly less resolving power. The availability in this laboratory of a fairly large (5.860 g) sample of Pu permitted the measurement of this spectrum using the two-crystal spectrometer. Twelve lines have been measured, with relative errors of less than 30 ppm (parts per million).

Similarly, the most recent investigation of the L spectrum of U was performed by using a Cauchois type photographic spectrometer.[3] Again, the availability of a commercial, sealed-off x-ray tube with a uranium target has permitted us to use the two-crystal spectrometer. Twenty lines of this spectrum have been measured, with relative errors in most cases less than 15 ppm.

II. EXPERIMENTAL

The two-crystal spectrometer used in these investigations was designed by one of us and, together with the procedure for preparing and calibrating its precision worm wheels for the angular measurements, is described in some detail elsewhere.[4] The adjustment and calibration of the instrument for these measurements, as well as the scintillation crystal x-ray detector, have also been described in a previous article.[5] The same article describes the Pu source and its excitation.

The U radiation was obtained from a Machlett Type A-2 Uranium Target X-Ray Tube,[6] while the fluorescent Pu lines were excited by radiation from an OEG-50T high-intensity tungsten target x-ray tube. X-ray tube power was obtained from a Phillips water-cooled diffraction unit. The primary voltage of this unit was regulated by an electronic Sorenson regulator, and the x-ray tube current was stabilized by an electronic stabilizer added to the diffraction unit. Neither primary voltage nor tube current varied by more than 0.1% during the course of a measurement.

In the present investigation, two independent determinations of the Bragg angle were made for each of the lines. Measurements were made in the usual way with crystal number 1 fixed by advancing crystal number 2 one second of arc at a time over the parallel rocking curve and five or ten seconds at a time over the antiparallel curve. At each setting the x-ray intensity would be determined by accumulating counts over a sufficient time interval to obtain good counting statistics. The time interval was the same for all points on a given curve, and was controlled by the 60-cycle power-line frequency.

For all the Pu lines except the Pu L_{α_1} the intensity was too low to get the desired number of counts at the peak (about 6000) in just one run over the line. Therefore, several runs were necessary in order to make the time per run of reasonable length. For example, a total of thirty hours were required for the seven runs over the Pu L_{β_3} line. The precision claimed for locating the center of a weak line in this manner is justified by the agreement between the two independent measurements, which was always of comparable

* Work supported by U. S. Atomic Energy Commission.
† Howard Hughes Fellow.
[1] Cauchois, Manescu, and Le Berquier, Compt. rend. **239**, 1780 (1954).
[2] G. L. Rogosa and W. F. Peed, Phys. Rev. **101**, 591 (1956).
[3] H. Claëson, Z. Physik **101**, 499 (1936).
[4] J. W. M. DuMond and D. Marlow, Rev. Sci. Instr. **8**, 112 (1937).
[5] R. L. Shacklett and J. W. M. DuMond, Phys. Rev. **106**, 501 (1957).
[6] We are much indebted to the Machlett Laboratories, Inc., and especially to their engineer, Mr. T. H. Rogers, for their courtesy, patience, and cooperation in producing for us, without additional charge for development, two excellently stable uranium target x-ray tubes, probably the only such in existence. We are also much indebted to Robert A. Noland and D. E. Walker, metallurgists of the Argonne National Laboratory, and to the administration of that laboratory, for furnishing us with the normal uranium target disks appropriately bonded to the Machlett Laboratories' copper backings for incorporation into the Machlett tube structure.

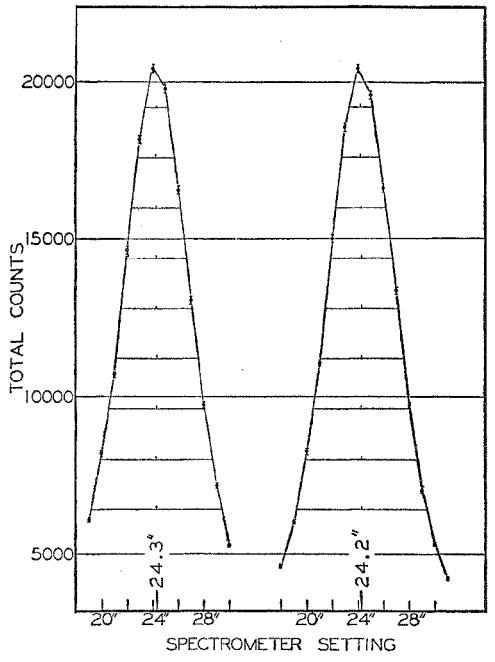

FIG. 1. A typical parallel rocking curve (the Pu $L\beta_3$), showing the two runs over the curve.

magnitude. The temperature[7] was thermostatically maintained at a constant value to within one or two-tenths of a degree during the course of each series of runs.

The centers of the parallel rocking curves were determined by drawing horizontal chords across the profile between the observed points at different heights and finding the midpoints of these chords. These central points at different heights never differed from each other on one and the same profile by more than one tenth of a second of arc. Each determination was repeated by making a second run over the rocking curve and finding its center in the same manner. In most cases the agreement between the two runs was within the desired precision. It was found, however, that a short time had to be allowed between changing crystal number two from the antiparallel to the parallel position and the actual initiation of the parallel run. If sufficient time were not allowed, the first run would show a center point at too low an angle. On subsequent runs the central position would occur at a slightly higher angle, in a few cases as much as six-tenths of a second above the first. This second value was then reproducible within one-tenth of a second of arc. It is believed that this shift, which was always in the same direction, was due to a stabilizing in the contact between the precision worm wheel and the worm gear which drives it. In such cases, which occurred quite infrequently, only the stable value of the central position was used in computing the Bragg angle. Figure 1 shows a typical rocking curve.

The centers of the antiparallel curves were determined by drawing a smooth curve through the experimental points and again finding points midway between the two sides. For most of the lines these points did not vary by more than five-tenths of a second of arc from their mean. In a few cases the spread was greater, and larger probable errors have been assigned to these exceptions. The U $L_{\gamma 4}$ line is worthy of special note. The shape of this line indicates that there may be a weaker line of unknown origin on its long wavelength side, perhaps 0.5 x-units or less away. This together with its weakness and the presence of some slight but unexplained background distortion made it impossible to determine the center of this line with high precision. Figure 2 shows an example of one of the better antiparallel curves (the U L_{α_1}), while Fig. 3 shows one of the poorer ones (the Pu $L\beta_4$).

III. CORRECTIONS

The angular positions of the centers of the parallel and anti-parallel curves were first corrected for the errors in the worm wheel as described elsewhere.[4] The

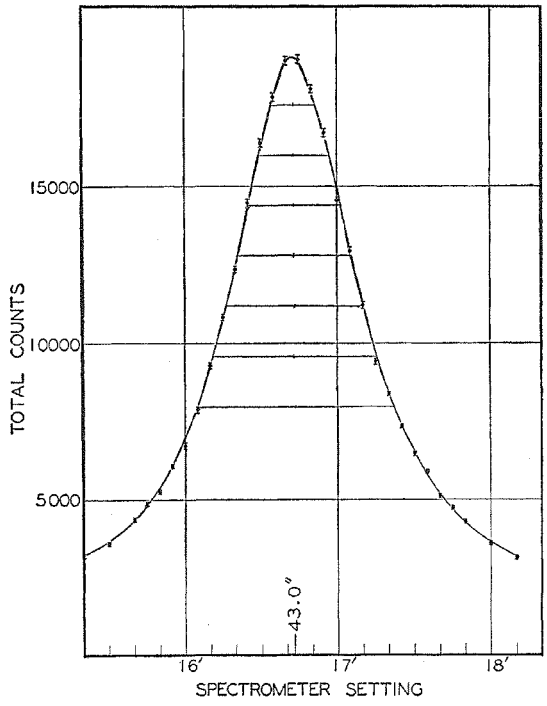

FIG. 2. A typical good antiparallel curve (the U L_{α_1}).

[7] As in the article of reference 5, this temperature was read on a thermometer immersed in an oil-filled well in good thermal contact with an aluminum heat shield which completely covered both crystals. This shield was provided with thin Mylar windows for entry and exit of the x-ray beam and it served the important purpose of minimizing air convection near the reflecting surfaces of the calcite crystals. The layer of the crystal surface participating in selective x-ray reflection is so thin that convective heating and cooling of crystal planes near the surface can prove quite troublesome, particularly in the parallel rocking curve case.

TABLE I. Typical Bragg angle calculations for U $L\alpha_1$ and Pu $L\beta_4$ lines.

Run	Parallel position	Antiparallel position	Worm-wheel correction $-\Delta\theta_w$	2θ (uncorrected)	$\Delta\theta_t+\Delta\theta_v+\epsilon/2$	Bragg angle θ (corrected)
			(a) U $L\alpha_1$			
1	294° 17′ 14.15″	97° 1′ 54.9″±0.1″	−6.15″	17° 15′ 13.1″	2.8″	8° 37′ 39.35″
2	97° 1′ 23.7″	294° 16′ 43.0″±0.1″	−6.15″	17° 15′ 13.15″	2.7″	8° 37′ 39.23″
			(b) Pu $L\beta_4$			
1	292° 20′ 28.8″	98° 58′ 46.5″±0.8″	−6.36″	13° 21′ 35.9″	+1.54″	6° 40′ 49.5″
2	98° 56′ 9.1″	292° 17′ 53.1″±0.8″	−6.36″	13° 21′ 37.6″	+1.50″	6° 40′ 50.3″

difference between the two corrected positions gives then $180°+2\theta$, where θ is the Bragg angle of the line under consideration. The resulting Bragg angle was then corrected for vertical divergence, the effect of temperature on the grating constant of the crystal, and the effect of crystal diffraction pattern asymmetry. The vertical divergence correction is given by

$$\Delta\theta_v=-(1/12)\phi_m^2\tan\theta, \quad (1)$$

where ϕ_m is the maximum angle of vertical divergence. This formula was developed in a previous paper.[5] The Bragg angles were all reduced to their values at 18°C by applying the correction, $\Delta\theta_t$, given by the following working formula in seconds of arc:

$$\Delta\theta_t=+2.1(t-18°)\tan\theta. \quad (2)$$

The shift of the observed lines due to crystal pattern asymmetry was corrected by applying the correction

$$\tfrac{1}{2}\epsilon=0.2\lambda^2 \text{ second } (\lambda \text{ in A}). \quad (3)$$

This correction is also justified elsewhere.[5]

Typical angle calculations are shown in Table I for the U $L\alpha_1$ and Pu $L\beta_4$ lines.

IV. ERRORS

(a) The most important random error in determining the Bragg angle of a spectral line is the uncertainty of the location of the center of the antiparallel curve, $\delta\theta_{ap}$. This uncertainty varies from about 0.2 to 5 seconds of arc, usually being less than 0.5 second. Other statistical errors are listed below, with their assigned uncertainties:

(b) Uncertainty in the location of the center of the parallel curve, $\delta\theta_p\cong 0.1''$.

(c) Uncertainty in the applied worm wheel correction, $\delta\theta_w\cong 0.1''$.

(d) Uncertainty in the ambient temperature of the reflecting crystals, resulting in an uncertainty in the temperature correction, $\delta\theta_t\cong 0.05''$.

(e) Uncertainty in the applied correction for vertical divergence, $\delta\theta_v<0.05''$.

(f) Uncertainty in the applied correction for crystal diffraction pattern asymmetry (Darwin dynamical theory), $\delta\theta_c<0.01''$.

Since the required Bragg angle was computed by subtracting the parallel and antiparallel readings after the worm wheel correction had been applied, and by dividing the result minus 180° by two before applying the other corrections, the uncertainty in the Bragg angle is

$$\delta\theta_{B1}=[(\delta\theta_{p1}^2+\delta\theta_{ap1}^2+2\delta\theta_w^2)/4+2\delta\theta_t^2+\delta\theta_v^2+\delta\theta_c^2]^{\frac{1}{2}}.$$

Since two independent measurements of each line are averaged to obtain the final Bragg angle, its uncertainty is

$$\begin{aligned}\delta\theta_B&=\tfrac{1}{2}[(\delta\theta_{B1})^2+(\delta\theta_{B2})^2]^{\frac{1}{2}}\\&=\tfrac{1}{2}[\tfrac{1}{2}(\delta\theta_p^2+\delta\theta_{ap}^2)+\delta\theta_w^2+2\delta\theta_t^2+2\delta\theta_v^2+2\delta\theta_c^2]^{\frac{1}{2}}\\&=\tfrac{1}{2}[\tfrac{1}{2}\delta\theta_{ap}^2+0.040]^{\frac{1}{2}},\end{aligned}$$

if one assumes that the same uncertainty is assigned to the position of the centers of the line profiles in the two cases.

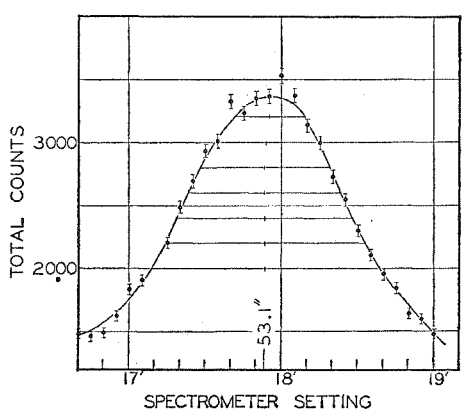

FIG. 3. A typical antiparallel curve of a weaker line (the Pu $L\beta_4$).

V. RESULTS

The corrected Bragg angles are shown in Table II, where the angles for U $L\alpha_2$, Pu $L\alpha_2$, and Pu $L\beta_1$ are included for completeness. These lines were measured in a previous study[5] and were not remeasured. The U $L\beta_1$ line was remeasured, however, since the higher intensity made possible by the U target permitted the use of extremely small angles of vertical divergence. The vertical divergence correction was made quite negligible in this way, and the formula and method of correction used by R. L. Shacklett and one of us[5] could thus be

TABLE II. Experimental results.

X-ray line	Transition	Bragg angle (calcite)	Wavelength (x-units)	Previous results	
Uranium				Claëson[a]	
$L\alpha_1$	$L_{III}-M_V$	8° 37′ 39.3″ ±0.1″	908.782±0.007	908.69	
$L\alpha_2$[b]	$L_{III}-M_{IV}$	8° 44′ 29.0″ ±0.2″	920.676±0.008	920.56	
$L\beta_1$	$L_{II}-M_{IV}$	6° 48′ 41.4″ ±0.1″	718.509±0.007	718.54	
$L\beta_2$	$L_{III}-N_V$	7° 8′ 29.3″ ±0.15″	753.140±0.008	753.14	
$L\beta_3$	L_I-M_{III}	6° 43′ 9.6″ ±0.3″	708.832±0.011	708.81	
$L\beta_4$	L_I-M_{II}	7° 4′ 40.1″ ±0.2″	746.460±0.008	746.39	
$L\beta_5$	$L_{III}-O_{IV}, O_V$	6° 52′ 18.56″±0.1″	724.814±0.007	724.84	
$L\beta_6$	$L_{III}-N_I$	7° 27′ 43.3″ ±0.2″	786.759±0.008	786.78	
$L\beta_{7'}$	$L_{III}-N_{VI}, N_{VII}$	6° 59′ 18.7″ ±0.3″	737.091±0.011	737.07	
$L\beta_7$	$L_{III}-O_I$	6° 57′ 49.8″ ±2″	734.500±0.060	734.64	
$L\beta_9$	L_I-M_V	6° 26′ 28.4″ ±0.1″	679.620±0.007	679.6	
$L\eta$	$L_{II}-M_I$	7° 37′ 16.1″ ±0.4″	803.436±0.013	803.59	
L_1	$L_{III}-M_I$	10° 7′ 28.3″ ±0.5″	1064.941±0.016	1064.89	
$L\gamma_1$	$L_{II}-N_{IV}$	5° 48′ 44.3″ ±0.1″	613.503±0.007	613.50	
$L\gamma_2$	L_I-N_{II}	5° 43′ 19.1″ ±0.2″	604.000±0.008	603.99	
$L\gamma_3$	L_I-N_{III}	5° 39′ 31.7″ ±0.1″	597.354±0.007	597.30	
$L\gamma_4$	L_I-O_{III}	5° 26′ 6.0″ ±3″	573.801±0.090	573.90	
$L\gamma_{4'}$	L_I-O_{II}	5° 27′ 5.0″ ±0.2″	575.526±0.008	575.45	
$L\gamma_5$	$L_{II}-N_I$	6° 0′ 35.6″ ±0.15″	637.283±0.008	634.23	
$L\gamma_6$	$L_{II}-O_{IV}$	5° 37′ 24.3″ ±0.1″	593.630±0.007	593.61	
Plutonium				Cauchois *et al.*[c]	Rogosa and Peed[d]
$L\alpha_1$	$L_{III}-M_{II}$	8° 13′ 23.7″ ±0.2″	866.492±0.008	866.8	866.52±0.18
$L\alpha_2$[b]	$L_{III}-M_{IV}$	8° 20′ 16.2″ ±0.1″	878.480±0.007	878.4	878.52±0.25
$L\beta_1$[b]	$L_{II}-M_{IV}$	6° 24′ 35.4″ ±0.2″	676.321±0.008	676.5	676.45±0.22
$L\beta_2$	$L_{III}-N_V$	6° 47′ 50.8″ ±0.2″	717.034±0.008	717.0	717.15±0.22
$L\beta_3$	L_I-M_{III}	6° 19′ 27.4″ ±0.7″	667.332±0.021		667.50±0.29
$L\beta_4$	L_I-M_{II}	6° 40′ 49.9″ ±0.5″	704.757±0.016		704.93±0.20
$L\beta_5$	$L_{III}-O_{IV}, O_V$	6° 31′ 58.9″ ±0.2″	689.265±0.008		689.41±0.19
$L\beta_6$	$L_{III}-N_I$	7° 6′ 39.4″ ±0.5″	749.937±0.016		
$L\gamma_1$	$L_{II}-N_{IV}$	5° 28′ 19.3″ ±0.15″	577.698±0.008		577.87±0.22
$L\gamma_2$	L_I-N_{II}	5° 23′ 39.3″ ±0.5″	569.511±0.016		
$L\gamma_3$	L_I-N_{III}	5° 19′ 51.6″ ±0.2″	562.847±0.008		
$L\gamma_6$	$L_{II}-O_{IV}$	5° 17′ 25.5″ ±0.6″	558.580±0.018		

[a] See reference 3. [b] See reference 5. [c] See reference 1. [d] See reference 2.

checked. The difference between the two determinations was less than one-tenth of a second of arc (6 ppm).

The wavelengths given in Table II were calculated from the Bragg law by using the effective first order grating space $2d_1=6058.09\pm0.03$ x-units. This value was obtained by defining, for the purposes of this article, one x-unit[8] as such that the Mo $K\alpha_1$ line's central wavelength is $\lambda\equiv707.8490$ x-units. This line was measured in the calibration of our crystals,[5] and its Bragg angle was found to be

$$\theta=6°\ 42'\ 35.9''\pm0.1''.$$

The uncertainty in the measurement of this line was included as an additional independent uncertainty in the calculation of the wavelengths of the various lines.

The results of the most recent previous measurements of these spectra are included for comparison in Table II.

VI. CONCLUSION

The L spectrum of Pu has been measured by using conventional x-ray fluorescence with relative errors of less than 30 ppm. The L spectrum of U has been investigated using the direct beam from a U-target x-ray tube, with relative errors in most cases of less than 15 ppm. The high intensity available from this source permitted measurements to be made with small angles of vertical divergence, so that the formulas and methods of correcting for the errors introduced by larger divergences could be verified. The results agree with those of previous work in the same laboratory to one-tenth of a second of arc.

APPENDIX I. DEFINITION OF THE x-UNIT AS USED IN THIS ARTICLE

Relative to each other the wavelengths of x-ray spectrum lines, as measured by the high precision methods employing crystal diffraction, are known in many cases with a precision from a part in 10^4 to a part in 10^5. Somewhat over 5000 of these lines have been observed in the spectral region (from about 0.1 to 400 angstrom units) characteristic of different electronic transitions in atoms of the atomic table from Li to U. These lines constitute therefore a very reliable and reproducible set of fixed points in our scale of lengths in this region of length magnitudes. Unfortunately the *unit* in terms of which we express these wavelengths is, even today, not known in absolute value (e.g., in angstroms) with as much accuracy as the accuracy with which the x-ray line wavelengths can be measured relative to each other. The unit, in terms of which they are expressed, known as the x-unit, was originally

[8] It seems to us preferable, when highest precision is involved, to base the definition of the x-unit *on a well-known, oft-measured, and highly reproducible x-ray emission line* (such as Mo $K\alpha_1$) rather than on the grating constant of calcite. We have no test whereby the grating space of a sample of calcite can be proven to have the standard value other than by measuring such a line with it. The defining wavelength here tentatively selected is discussed in the appendix.

chosen by Siegbahn[9] with the intention that one x-unit would be as closely as possible equal to a milliangstrom. To do this, Siegbahn and others endeavored to calculate the grating constants in angstroms of the crystals they used, such as rock salt or calcite, employing a value of the Avogadro number, N, the bulk density of the crystal, ρ, the molecular weight of the molecule of which the crystal was composed, M, and a constant, ϕ, depending upon the geometry of its unit cell. They took for the Avogadro number, N, a value computed by dividing the electrochemically determined Faraday, F, by the electronic charge, $e=4.774\times10^{-10}$ esu as determined by Millikan using his famous "oil drop" method. By such methods the "effective" value in first order reflection of the grating constant of the cleavage planes of calcite at 18°C came to be accepted as

$$d_{18}''=3029.04 \text{ x-units.}$$

The true grating space (after correction for refractive index) corresponding to this was

$$d_{18}'=3029.494 \text{ x-units.}$$

When at a later date, however, a method was developed for measuring certain soft x-ray lines with artificially ruled gratings, calibrated using known optical wavelengths, it was found that a discrepancy existed between the "grating scale" of x-ray wavelengths and the "crystal scale" of Siegbahn. Many hypotheses for this discrepancy were carefully examined and rejected one by one[10] until it was shown that the principal source of the discrepancy came from the fact that Millikan's oil drop value of e was in error chiefly by reason of his having used an erroneous value of the viscosity of air in his calculations. In fact, the discrepancy indicated that the value of e was more nearly 4.802×10^{-10} esu.

Thus Siegbahn's "x-unit" (in terms of which the calcite grating constant has the value given above), *is not* exactly a milliangstrom as he intended. In Siegbahn's calculation of d, other numerical factors, more accurately known today, also require small revisions. In view of these errors it has come to be regarded as preferable to treat Siegbahn's system of measure for x-ray wavelengths as a purely arbitrary system. It is fortunate that Siegbahn very wisely chose to call his unit by a distinctive name, the x-unit. We therefore can no longer take one x-unit as equal to a milliangstrom, but because of the much greater *relative* accuracy with which the x-ray line wavelengths are known relative to each other we continue to express them in terms of x-units. It has become customary, on the contrary, to *define* the x-unit as such a unit that the "effective" grating space of calcite for first order reflection at 18°C is

$$d_{18}''=3029.04 \text{ x-units.}$$

The true experimental datum of observation is, of course, the angle, θ, at which an x-ray line of wavelength, λ x-units, is reflected from the cleavage planes of a calcite crystal in the first order at 18°C and this will be related to λ expressed in x-units by the Bragg equation:

$$\lambda=2d_{18}''\sin\theta.$$

The ratio of the x-unit to the milliangstrom unit, $\Lambda=\lambda_0/\lambda_s$, is probably somewhere between 1.00202 and 1.00204. With the improvement in the level of precision with which most of the constants and conversion factors of physics are now known, it is highly desirable to improve our knowledge of Λ.[11] As a first step in this direction the authors of this paper believe that the *definition* of the x-unit as it is presently accepted, based on the grating constant of calcite, should be abandoned in favor of a more reliably reproducible definition in terms of a well-known x-ray line. Different samples of calcite from different parts of the world have been shown by J. A. Bearden[12] to reflect one and the same x-ray line at slightly different Bragg angles in the first order, for example, ranging over a variation of some 0.3 second of arc and in the fourth order, 0.7 second of arc. If calcite were taken as the conventional standard to define the x-unit it would therefore strictly be necessary for the International Bureau of Weights and Measures at Sèvres to keep in a desiccator under extremely carefully controlled conditions one standard calcite crystal, or perhaps a pair of them for use in a two-crystal spectrometer, against which all other crystals for use by x-ray spectroscopists could be compared. Such a cumbersome procedure is clearly not in the spirit of modern physics where every effort is made to relate our standards to the most fundamentally reproducible natural units or constants obtainable. Just as the meter is, for the most accurate purposes, defined in terms of the wavelength of a spectral line in the optical region so the x-unit should be also defined in terms of an x-ray line. For this purpose we must select an x-ray line whose wavelength can readily and precisely be compared, by crystal diffraction or other methods, with the wavelengths of most of the other some 5000 x-ray lines (using single or successive multiple steps of comparison).

For this standard reference line we tentatively propose the Mo $K\alpha_1$ line because of the great care and attention which has already been given to its study. There is every reason to believe that a wavelength definition based on this line can be considerably more reproducible[13] than any definition in terms of a crystal grating constant. What then shall we adopt as the conventional numerical value in x-units of the Mo $K\alpha_1$ line wavelength for the purpose of more precisely defining the x-unit? It is clearly desirable to improve the precision of our definition without shifting the magnitude of the unit outside the general range of uncertainty or irreproducibility within which it was formerly defined in terms of the calcite grating constant and in fact it would perhaps be desirable and most convenient to fix it in accord with the most representative value among many samples of calcite if such a dominant value could be established. All this must be done by a general conventional agreement which as yet does not exist. To tie down the precision results of the present article in the most definite possible way we therefore *adopt*, for the purpose of defining what we mean in this paper by the term one "x-unit," the convention that the central wavelength value of the Mo $K\alpha_1$ line

---

[9] Manne Siegbahn, *Spektroskopie der Roentgenstrahlen* (Verlag Julius Springer, Berlin, 1931).

[10] For a brief account of the history in this connection, see the article by E. R. Cohen and J. W. M. DuMond, in *Handbuch der Physik* (Springer-Verlag, Berlin, 1957), Vol. 35, p. 1.

[11] Work on Λ has been of two kinds, (1) measurements of the absolute angles of incidence and diffraction of x-ray lines using plane gratings of which the best example is the work of J. A. Bearden and (2) comparisons of soft x-ray line positions, recorded with a grazing incidence concave grating vacuum spectrometer, with the positions of calibrating spark line spectra from one-electron hydrogen-like atoms whose wavelengths can be theoretically computed from our very precise knowledge of the Rydberg constant. The best example of the latter method developed in Sweden has undoubtedly been the work of Folke Tyrén in his dissertation, 1940. Tyrén's results are, unfortunately, now rendered invalid by the fact that the discovery of the Lamb shift in 1950 necessitates that all his calibrating wavelengths be recomputed. It seems likely that the discrepancy between Tyrén's $\Lambda=1.00199$ and the higher average value arrived at by J. A. Bearden, $\Lambda=1.00203$, is to be explained in this way. J. W. M. DuMond and E. R. Cohen, Phys. Rev. **103**, 1583 (1956); J. W. M. DuMond and E. R. Cohen, in *Handbuch der Physik* (Springer-Verlag, Berlin, 1957), Vol. 35, pp. 10–16. Folke Tyrén, dissertation, Uppsala, 1940 (unpublished); J. A. Bearden, Phys. Rev. **37**, 1210 (1931); **48**, 385 (1935). W. E. Lamb, Jr., and R. C. Retherford, Phys. Rev. **79**, 549 (1950).

[12] J. A. Bearden, Phys. Rev. **38**, 2089 (1931).

[13] That the wavelengths of x-ray lines can be very slightly shifted by effects of chemical combination has been known for many years. In the case of the Mo $K\alpha_1$ line from a pure metallic molybdenum target in a well-evacuated outgassed and permanently sealed off tube however there is no evidence to show any relative irreproducibility comparable to the small fluctuations in crystal grating constants. The line wavelength is almost surely reproducible to ±10 ppm.

profile (determined by means of the median points of chords[14] across it as explained in this paper) shall be 707.8490 "x-units." Should a later change in the convention modify this number it will be a simple matter for anyone to modify all our observed tabular wavelengths herein reported by the same proportional amount to suit the change in definition of the unit. We are aware, of course, that the conventional number we have here adopted for Mo $K\alpha_1$ differs slightly from the value in x-units (707.831) frequently quoted and tabulated for this line. The difference is in fact 25.4 parts per million. Our primary reason for our particular numerical choice is because it is consistent with assigning the conventional value of the effective grating space in the first order, $d_1=3029.040$ x-units to the pair of calcite crystals we have used in this research. Since our particular pair of crystals might well be exceptional rather than representative, this alone is insufficient justification for such a choice, however.

The value of the wavelength of the Mo $K\alpha_1$ line defined in this article, namely 707.8490 x-units, is however also consistent with the conventional first order grating space of calcite, $d_1=3029.04$ x-units, and the Bragg angle as found by other investigators in first order reflections using the two-crystal spectrometer. When the vertical divergence correction of Williams[15] (whose validity Shacklett's careful work[5] has completely verified) is applied, the resultant Bragg angle as obtained by Compton[16] from the natural cleavage planes of calcite is

$$\theta_1=6^\circ\,42'\,35.9_5''.$$

Tu,[17] using the same formula for the vertical divergence correction, obtained the value

$$\theta_1=6^\circ\,42'\,35.5''\pm0.1''$$

from a natural cleavage face, and a value

$$\theta_1=6^\circ\,42'\,36.0''\pm0.1''$$

after he had polished and etched the faces of his crystals. Bearden,[18] using an incorrect formula for the vertical divergence correction, obtained various values ranging from

$$\theta_1=6^\circ\,42'\,35.3''\quad\text{to}\quad\theta_1=6^\circ\,42'\,35.6''$$

from four different samples of calcite, which he obtained from different parts of the world. Williams' formula for the vertical divergence correction would raise this value slightly. The result of the present investigators and Shacklett[5] is

$$\theta_1=6^\circ\,42'\,35.9''\pm0.2''.$$

The value chosen for the present definition of the x-unit is

$$\theta_1=6^\circ\,42'\,36.0''.$$

The authors recognize that this is an arbitrary definition. It was made in this manner because it agrees with work done in this laboratory and with the work of other investigators using similar methods (i.e., the two-crystal spectrometer in the first order).

Other investigations[15,16,18–20] have yielded different values for this wavelength. These results are indicated in Table III. It is the discrepancy in these results, as well as the differences in the Bragg angle as measured by Bearden[12] using different samples of calcite, which has prompted the present authors to propose a definition of the x-unit in terms of a spectral line, rather than one based on the grating space of calcite.

TABLE III. Results of other investigations.

Method	λ (x-units)	Investigator
Bragg ionization spectrometer	707.862	Allison and Armstrong[a]
Photographic tube spectrometer	707.833	Larsson[b]
Double crystal spectrometer (fourth order)	707.843	Williams,[c] Compton[d]
Double crystal spectrometer (fourth order)	707.833	Bearden[e]

[a] See reference 19.
[b] See reference 20.
[c] See reference 15.
[d] See reference 16.
[e] See reference 18.

From an examination of such work as that of Larsson and others by photographic methods and a comparison with the two-crystal spectrometer method in which precise angular measurements of crystal rotation are alone involved and the spectral profile of the line is quantitatively delineated by statistical counting of photons with a very definitely calculable statistical precision, we feel that more reliability can certainly be attached to the two-crystal spectrometer results than to the photographic results. The "tube spectrometer" work of Larsson, in which the cross hair of a micrometer comparator is simply centered by subjective estimation on the photographically recorded line image (see Plate 18 of the Larsson article for comparison with the line profile in our Fig. 2, for example), is nevertheless the basis for the tabular value, 707.831 x-units, given in the Cauchois-Hulubei tables. The estimated standard deviation of the mean value, $\langle\Delta\phi\rangle_{Av}$, of Larsson's seven comparator measurements (the first seven in his Table II, our reference 20) computed by accepted statistical formulas from the squares of the deviations of his individual measurements from their mean is ±0.246 second of arc corresponding to about ±10 ppm uncertainty in the Bragg angle and in the wavelength. It is by no means the intention of the authors to make a final decision in this definition, and the wavelengths given in Table II may easily be modified when by general agreement such a definition is adopted.

[14] We are well aware that there is no unanimity of convention as to what feature of the spectral profile of an x-ray line to take as "the" wavelength. The maximum point, the center of gravity or "centroid," the point of intersection of the tangents to the two points of inflection of the profile, and the common position of the median points of horizontal chords, have all been used or proposed. In the case of nearly all the x-ray lines determined with photographic spectrometers, a cross hair in the microscope of a comparator is simply made, by a subjective judgment, to divide the blackened image of the line as nearly in two as can be estimated. We believe that this latter process comes nearer to determining the median point of horizontal chords than to any of the other procedures. There is a real difficulty with adopting the "centroid" of the profile as a definition. This stems from the fact that the line profile both according to theory and observation [the work of Archer Hoyt, Phys. Rev. **40**, 477 (1932)] is a "witch," i.e., $I(\lambda)=A[1+(\lambda-\lambda_0)^2/W^2]^{-1}$, wherein W is the half-width at half maximum height. In a strict mathematical sense this profile has no centroid since all its moments from the first on up diverge. In a practical sense this means that the exact position of the center of gravity is extremely sensitive to our choice of the positions where we chop off the tails of the curve on either side of the maximum for the purpose of determining the center of gravity. To symmetrize these positions appropriately we have to "beg the question" and use some other criterion than the centroid.

We believe that the best choice of convention to fix "the" wavelength of a line will be the one which yields the most reproducible definition. It is our impression that the chord median point method does this. Of course, if the line is not symmetric, the method fails to give a definite answer without further detailed specification of the procedure, but this is true of any of the other proposals too.

[15] J. H. Williams, Phys. Rev. **40**, 636 (1932).
[16] A. H. Compton, Rev. Sci. Instr. **2**, 365 (1931).
[17] Y. Tu, Phys. Rev. **40**, 662 (1932).
[18] J. A. Bearden, Phys. Rev. **38**, 1389 (1931).
[19] S. K. Allison and A. H. Armstrong, Phys. Rev. **26**, 701 (1925).
[20] A. Larson, Phil. Mag. **3**, 1136 (1927).

REFERENCES

1. R. L. Shacklett and J. W. M. DuMond, Phys. Rev. 106, 501 (1957).

2. R. L. Shacklett, Ph.D. Thesis, California Institute of Technology, 1956.

3. J. W. M. DuMond and D. Marlow, Rev. Sci. Inst. 8, 112 (1937).

4. A. H. Compton and S. K. Allison, X-Rays in Theory and Experiment, D. Van Nostrand Co., 1935, pp. 709-740.

5. Prins, Zeits. f. Physik 63, 477 (1930).

6. C. G. Darwin, Phil. Mag. 27, 325; 675 (1914).

7. S. K. Allison, Phys. Rev. 41, 1 (1932).

8. L. G. Parratt, Phys. Rev. 41, 561 (1932).

9. J. W. M. DuMond, Phys. Rev. 52, 872 (1937).

10. S. K. Allison, Phys. Rev. 44, 63 (1933).

11. A. Hoyt, Phys. Rev. 40, 477 (1932); J. H. Williams, Phys. Rev. 40, 791 (1932); G. Brogan, Archiv. f. Fysik 8, 391 (1954).

12. G. Parratt, C. F. Hempstead and E. L. Jossem, Phys. Rev. 105, 1228 (1957).

13. E. R. Cohen, J. W. M. DuMond, T. W. Layton, and J. S. Rollett, Rev. Med. Phys. 27, 363 (1955).

14. L lines. S. Idei, Sci. Rep. Tohoku Imperial University, 19, 559 (1930).

M absorption edges. E. Lindberg, Zs. f. Physik 54, 632 (1929).

L absorption edges. A. Sandstrom, Zs. f. Physik 65, 632 (1930).

15. L. G. Parratt, Rev. Med. Phys. 31, 616 (1959).

16. C. Nordling and S. Hagström, Arkiv. f. Fysik 15, 431 (1959).

17. H. A. Bethe and E. E. Salpeter, Quantum Mechanics of One- and Two-Electron Atoms, Academic Press Inc., 1957, pp. 63-71.

18. Y. Cauchois, J. Phys. Radium, 13, 113 (1952); 16, 253 (1955).

19. A. H. Wapstra, G. J. Nijgh and R. Van Lieshout, Nuclear Spectroscopy Tables, Interscience Publishers Inc., 1959, pp. 78-79.

20. S. Cohen, UCRL-8389 (1958), 8633, 8634, 8635 (1959).

21. R. T. Binge, Phys. Rev. 55, 1119 (1939).

22. R. F. Christy and J. M. Keller, Phys. Rev. 61, 147 (1942).

23. S. Triebwasser, E. S. Dayhoff, and W. E. Lamb, Jr., Phys. Rev. 89, 98 (1953).

24. A. L. Schawlow and C. H. Townes, Phys. Rev. 100, 1273 (1955).

25. L. N. Cooper and E. M. Henley, Phys. Rev. 92, 801 (1953). K. W. Ford and D. L. Hill, Phys. Rev. 94, 1630 (1954).

26. R. Karplus and N. M. Kroll, Phys. Rev. 81, 73 (1951).

27. A. Petermann, Helv. Phys. Acta, 30, 407 (1957).

28. C. M. Sommerfield, Phys. Rev. 107, 328 (1957).

29. E. H. Wichmann and N. M. Kroll, Phys. Rev. 101, 843 (1956).

30. P. Bergvall and S. Hagström, Arkiv. f. Fysik 17, 61 (1960).

31. B. Bleaney, P. M. Llewellyn, H. M. L. Pryce and G. R. Hall, Phil. Mag. 45, 992 (1954).

32. T. E. Manning, M. Fred, and F. S. Tomkins, Phys. Rev. 102, 1108 (1956).

33. Schwarzschild, Phys. Rev. 32, 162-171 (1928).